NUMERICAL MODELING AND FIELD MEASUREMENT OF VEHICLE-GENERATED ROAD DUST TRANSPORT AND REMOVAL NEAR THE ROAD

by

Scott Speckart

A dissertation submitted to the faculty of
The University of Utah
in partial fulfillment of the requirements for the degree of

Doctor of Philosophy

Department of Mechanical Engineering

The University of Utah

December 2013

The University of Utah Graduate School

STATEMENT OF DISSERTATION APPROVAL

The dissertation of **Scott Speckart**

has been approved by the following supervisory committee members:

Eric R. Pardyjak	, Chair	**4/30/2013** Date Approved
John M. Veranth	, Member	**7/17/2013** Date Approved
James R. Stoll	, Member	**5/2/2013** Date Approved
Meredith M. Metzger	, Member	**5/9/2013** Date Approved
Timothy A. Ameel	, Member	**5/9/2013** Date Approved

and by **Timothy A. Ameel** , Chair of the Department of **Mechanical Engineering**

and by David B. Kieda, Dean of The Graduate School.

ABSTRACT

The result of this dissertation enables routine calculation for removal of vehicle-generated particulate matter with a mean aerodynamic diameter less than 10 microns (known as PM_{10}) downwind of unpaved roads given the height and density of vegetation downwind of the road. At present, the calculation of PM_{10} removal given vegetative height and density requires an expensive field study or classifying the vegetation as being one of five very general vegetative types. The estimation of PM_{10} removal downwind of an unpaved road is important in developing net PM_{10} emission inventories for use in regional air-quality models. Current methodologies for estimating PM_{10} removal by downwind roughness elements are based on the results of a small number of field studies measuring removal under limited roughness and atmospheric conditions. To significantly increase the data relating PM_{10} removal rate to site roughness and atmospheric stability, numerical modeling is employed and an additional field study is performed. The simulations utilize Lagrangian dispersion and Atmospheric Diffusion Equation (ADE) techniques. The new field study site features roughness and meteorological conditions distinct from those previously documented in the existing peer-reviewed literature. The PM_{10} removal measured in the field studies compared well, within a relative 10% error, to the numerical simulation predictions of PM_{10} removal for the field study site conditions. The simulation results indicate that PM_{10} removal is related to roughness and atmospheric stability by:

$$(1 - CF) = (1 - \exp(-2.8H^*)) \exp(-2.0T_m^{*0.64}) + \exp(-2.8H^*),$$

where CF is the captured fraction of PM_{10} within the first 100 m and H^* and T_m^* parameterize site roughness and meteorological conditions. Qualitatively, this equation indicates that CF increases with atmospheric stability, canopy height, and canopy density.

Simple transport models for mean horizontal advection and vertical turbulence within downwind roughness are developed for use in numerical simulations. The models are applicable for both canopies (an array of horizontally homogeneous roughness elements with infinite fetch) and windbreaks (an array of nonhorizontally homogeneous roughness elements located in rows with finite fetches). These transport models have simple inputs, such as vegetative mean height, leaf area index (for canopies), and optical porosity (for windbreaks). These models are also applicable for all practical atmospheric stabilities, roughness heights, and most roughness densities (canopies with frontal area indexes greater than 0.075 and windbreaks with optical porosities less than 0.9). For sparsely distributed roughness elements, traditional atmospheric surface layer parameterizations are more appropriate.

CONTENTS

CHAPTER 1

INTRODUCTION

1.1 Motivation

Dust emitted into the atmosphere as a result of vehicle traffic on unpaved roads is referred to as fugitive dust. It contains particulate matter with a mean aerodynamic diameter less than 10 microns (known as PM_{10}). PM_{10} is a pollutant regulated by the United States EPA. Currently, roadside emissions are estimated using the United States EPA AP-42 model (EPA, 2006). Downwind of the road, the dust plume interacts with roughness elements, such as vegetation, which remove particles and effectively filter the plume (Watson and Chow, 2000). Recent efforts have been directed at estimating the fraction of the initial plume that is still airborne after being transported 100 m downwind. This fraction of the initial plume is available for regional transport and is referred to as the transmitted fraction, *TF*. Estimating *TF* is important for developing accurate emissions inventories in regional air quality models such as the Community Multiscale Air Quality (CMAQ). Pace (2005) proposed that *TF* varies with vegetation type surrounding the road and presented an estimated *TF* for five vegetative types. This is shown in Table 1.1 Pace (2005) generalized the results in Table 1.1 by proposing a simple conceptual model that indicated that *TF* decreased with either increasing vegetative height or thickness. This is shown in Figure 1.1.

The result of this dissertation will enable routine calculation of PM_{10} removal at a site with a given vegetative height and density. At present, the calculation of PM_{10} removal given vegetative height and density requires an expensive field study or classifying the downwind vegetation as one of five very broad categories. To develop the methodology for routine calculation, this dissertation develops a simple empirical equation that quantifies the conceptual model proposed by Pace (2005) shown in Figure 1.1. Simple measureable parameters such as the ratio of the characteristic vegetative height to the initial roadside plume are utilized. The effects of atmospheric stability, which the conceptual model neglected, are also incorporated into this simple empirical equation. Such improvements to the conceptual model are suggested by Pace (2005). To develop the quantitative model, this dissertation addresses these specific questions:

1. What are the effects of vegetative height, thickness, atmospheric stability to mean wind and turbulence for vegetation with an infinite fetch depth, such as a forest or fields of sagebrush? Such vegetation is referred to as a canopy. What do simple numerical 1-D models (vertical dimension) suggest?
2. What are the effects of vegetative height and thickness to mean and wind turbulence for vegetation with a small fetch depth, such as rows of trees? Such vegetation is referred to as a windbreak. Can simple 2-D models (vertical and downwind) describe the mean wind and turbulence fields of windbreaks?
3. What does field measurement of PM_{10} transport and under stable meteorological conditions within a desert canopy typical of the arid southwestern United States reveal about PM_{10} removal under such conditions? What do previous field measurements taken under varying site conditions

reveal about the effects of atmospheric stability, vegetative height, and vegetative density?

4. Can transport models, such as an Atmospheric Diffusion Equation (ADE) and Lagrangian dispersion models, account for the variation of *TF* measured under varying roughness and meteorological conditions?
5. What is the dependence of *TF* upon meteorological stability, vegetative height, and vegetative thickness? Can this dependence be quantified?

This dissertation is divided into four peer-reviewed publications. Each chapter is self-contained with its own introduction, motivation, methods, results, and conclusions.

Chapter 2 documents a field study that contributes data pertinent to questions 1 and 3. Chapter 3 introduces an ADE model along with models for mean and turbulent winds within canopies and is relevant to questions 1 and 4. Chapter 4 combines the field study results of Chapter 2 with previous field studies, ADE simulation results from Chapter 3, and Lagrangian dispersion modeling to parameterize a simple analytical function that relates *TF* to canopy density and height along with atmospheric conditions. It also examines if varying experimental methodologies used in the field studies contributed to varying transmitted fractions obtained. Chapter 4 answers questions 4-5. Chapter 5 develops a windbreak model for mean and turbulent winds answering question 2. The model applies for windbreaks of optical porosities from 0 to 0.9, of multiple heights and subject to varying upstream roughness conditions and for all distances up and downwind of windbreaks.

Table 1.1. The estimation of the transmitted fraction, *TF*, of initially suspended road dust, as it is transported downwind through roughness elements. Removal depends upon vegetative height and thickness (Pace, 2005).

Land Cover Type	**Average Height (m)**	**Recommended *TF* (%)**	**Estimated *TF* Range (%)**	**COMMENT**
Forest	18-20	0%	0 to 20%	Forested areas will capture dust effectively
Urban	5 – 50+	50%	25 to 75%	Structures are interspersed with open areas
Sparsely Wooded & Grasses	1 – 2	75%	60 to 90%	Portion of plume is below sparse vegetation
Agricultural	1 - 2	75%	60 to 90%	Portion of plume is below crop (seasonally)
Barren / Water	0	100%	100% to 90%	Impediment-free surfaces are ineffective to capture dust

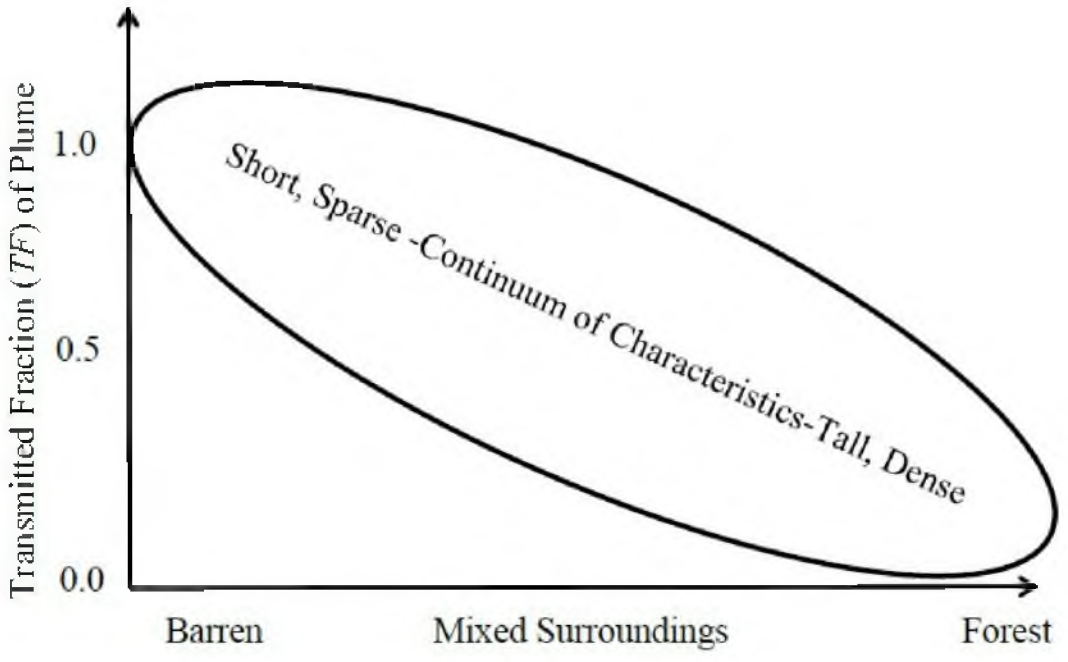

Figure 1.1. The conceptual model proposed by Pace (2005), indicating that the transmitted fraction of a vehicle generated plume is a function of the height and density of downwind roughness elements.

1.2 References

EPA, 2006: AP-42, Compilation of Air Pollutant Emission Factors, Vol. 1. Stationary, Point, and Area Sources, Chapter 13.2.2 Unpaved Roads. US Environmental Protection Agency, Washington, DC. http://www.epa.gov/ttn/chief/ap42/ch13/final/c13s0202.pdf

Pace, T.G., 2005: Methodology to Estimate the Transportable Fraction (*TF*) of Fugitive Dust Emissions for urban Scale Air Quality Analyses. USEPA. http://www.epa.gov/ttnchie1/emch/dustfractions/transportable_fraction_080305_rev.pdf

Watson, J.G., and J. C. Chow, 2000: Reconciling urban fugitive dust emissions inventory and ambient source concentration estimates: summary of current knowledge and needed research, Desert Research Institute, Reno, NV, www.epa.gov/ttn/chief/efdocs/fugitivedust.pdf.

CHAPTER 2

REMOVAL OF PM_{10} IN THE NEAR-SOURCE ZONE DOWNWIND OF UNPAVED ROADS PART 1: LAS CRUCES, NM FIELD STUDY

The content of this chapter is ready for submission to the peer-reviewed journal Atmospheric Environment.

2.1 Abstract

A field study was conducted to examine the removal of PM_{10} emitted by vehicular traffic on unpaved roads as it is transported downwind through surface roughness elements (vegetation). Understanding the relationship between PM_{10} removal and surface roughness is important for improving estimates of net emission for air pollution inventories utilized in regional air quality models. The field study site, near Las Cruces, NM, featured a vegetative canopy typical of conditions in the arid southwest United States and the atmospheric boundary-layer featured stable conditions. The study was conducted in the early spring, during and after sunset. Fugitive PM_{10} emissions were measured at the roadside, 17 and 100 m downwind. The captured fraction, or removed fraction, 100 m downwind was between 35% and 60% (95% confidence.) The captured fraction at about 20 m downwind was less than 30%, (95% confidence). Forty-four distinct trips with a passenger van created the fugitive dust emission. The captured

fraction was calculated for each trip, and the resulting distributions yielded the stated results. Also, a new method for calculating the captured fraction when PM_{10} data near the top of the dust cloud are absent is presented and introduces a relative error of less than 10 %. The meteorological and turbulence conditions within the atmospheric boundary layer and the canopy were measured with fast-response sonic anemometers and were found to be steady throughout the field study. Concentration was found to be insensitive to changes in height within the roughness layer, 1.5 times the canopy height.

2.2 Introduction

Fugitive dust generated from vehicle traffic on unpaved roads is a significant source of the EPA regulated pollutant PM_{10} (Watson and Chow, 2000). At the road, emissions are currently predicted by the EPA AP-42 model (EPA, 2006). Within the first 100 m downwind of the road, the plume interacts with roughness elements that may be present. Watson and Chow (2000) and Countess (2001) proposed that the presence of roughness, typically in the form of vegetation, within the first few hundreds of meters downwind of roads may remove vehicle-generated fugitive PM_{10}. Pace (2005) presented a conceptual model indicating that increasing roughness height or density increased the captured fraction (CF) of fugitive dust as it travels from roadside to 100 m downwind. This model has been compared to two recent field studies, Veranth et al. (2003) and Etyemezian et al. (2004). These two field studies also reported two extremes of aerodynamic roughness height, z_o, which is a measure of surface roughness (Ayra, 2001) and captured fraction. Veranth et al. (2003) measured a captured fraction of 85% within a simulated urban canopy characterized by a z_o value of 0.71 m at Dugway, UT. Etyemezian et al. (2004) measured a negligible captured fraction within a sparse desert

canopy characterized by a z_o value of 0.005 m at Ft. Bliss, TX. The studies hypothesized that differences in roughness and meteorological conditions were the cause of the differing results; however, both field studies concluded that additional field studies were needed to substantiate this claim.

The objective of the current study is to measure the captured fraction of PM_{10} at a desert site with a roughness height and density intermediate of that for the Veranth et al. (2003) (Dugway, UT) and Etyemezian et al. (2004) (Ft. Bliss, TX) sites.

2.3 Methods

2.3.1 Experimental Methods

The field measurement was performed at the flat, straight, nearly north-south running "La Jornada" road northeast of Las Cruces, NM. The site was located at 32° 25.589' N 106° 43.658' W at 1315 m above sea level. The area was a relatively flat vegetative plain with a slope of 3 m km^{-1} rising to the east of the road. The bottom of the plain was a dry stream bed located ~300 m to the west of the road. The predominant wind direction during field measurements was from the southwest. The local soil consisted mostly of sand and the vegetation of various species, which in decreasing abundance were: Ephedra trifurca (Mormon or Mexican, tea/longleaf joint fir), prebloom Prosopis Glandulosa (Honey Mesquite), Pleuraphis Mutica (tobosa grass), and Yucca Elata (Soaptree Yucca). The height of the fir, mesquite, and yucca plants varied from ~0.9 to 1.75 m while the grass varied from ~40 to 60 cm. Equipment was deployed March 14-18, 2005. The wind direction was required to vary less than 45° from orthogonal to the road. Also, the wind speed was required to be sufficiently low so as not to generate soil erosion dust, but sufficiently high to transport the vehicle-generated

fugitive dust plume downwind. The data presented were taken on March 16 from 17:45 to 19:30 Mountain Standard Time when equipment was functioning and the winds were the proper direction and speed (sunset was 18:11). The skies were clear and a mean temperature of 280 K was measured. The Las Cruces airport, about 20 km to the southwest, reported 31% RH and 865 mbar. It was assumed these are close to the site RH and pressure because the airport temperature and wind data agreed well with the field site measurements and the difference in altitude between the airport and field site was only approximately 10 m. A 1994 Dodge RAM van (3000 kg GVW) equipped with standard all-seasonal tires was used to generate a dust plume. The van traveled along a ~1.5 km-long section of road, reaching an average maximum speed of approximately 65 km/hr. Care was taken to insure a constant, smooth speed. The sensors were deployed downwind of the road, as shown in Figure 2.1. A vehicle pass was made about every 2.5 minutes in alternating north and south directions. A total of 44 vehicle trips were made.

Eight DustTrak (Model 8520 TSI, Inc. Shoreview, MN) monitors were utilized to measure PM_{10} concentrations. These monitors' locations are indicated in Figure 2.1. The DustTrak is a portable aerosol monitor with a measurement range from 0.001 to 100 mg/m^3. The DustTrak monitors were calibrated to PM_{10} concentrations by the manufacturer utilizing the respirable fraction of Arizona Road Dust (ISO 12103–1, A1). Etyemezian et al. (2004) note for the DustTrak and other nephelometer sensors, which utilize intensity of light scattering to infer particle concentration, the measured particle concentration depends not only upon the true particle concentration but also upon particle size distribution and composition. However, DustTraks can be utilized for relative measurements if composition and size distribution are assumed constant within a given

plume. Veranth et al. (2003) and Etyemezian et al. (2004) utilized DustTraks in this manner. The DustTraks were collocated to insure consistency from instrument to instrument for identical PM_{10} samples. The duration of the colocation data acquisition was 1 hour and utilized 5-min averages, 1 Hz data recording, and PM_{10} inlets. During the field measurements, the recording frequency remained at 1 Hz and the PM_{10} inlets were utilized.

To characterize the meteorology, four CSAT3 (Campbell Scientific, Inc. Logan, UT) 3-D sonic anemometers were utilized. Their locations are shown in Figure 2.1. Because the roughness conditions at the site were horizontally homogenous, only one tower was needed to characterize the meteorology. The CSAT3 is a robust portable instrument that measures all three components of wind velocity along with virtual temperature at sampling rates up to 60Hz. The current study utilized four CSAT3s sampling at 10 Hz because of manufacturer-recommended operating conditions for four CSAT3 connected to one data logger.

2.3.2 Analysis Methods

The PM_{10} concentration and wind data were analyzed to obtain: time integrated, PM_{10} concentrations, mean wind speed, mean turbulence quantities, horizontal fluxes of PM_{10}, and captured fraction of PM_{10}. A new method for calculating horizontal fluxes of PM_{10} when PM_{10} measurements near the top of the dust plume are absent is presented.

2.3.2.1 Concentration

The PM_{10} data were time integrated to approximate a temporally continuous line source, while using data from discrete vehicle trips. This is described in Eq. 2.1:

$$c_{int}(x,z) = \int_{t=0}^{t=t_{max}} c(x,z,t)dt, \quad (2.1)$$

where c_{int} is the time-integrated concentration, c is the PM_{10} concentration data, t_{max} is the time required for a vehicle-generated plume to travel from roadside to downwind of the sensor array. Veranth et al. (2003) referred to c_{int} as pulse area. c_{int} was calculated at each DustTrak for each of the 44 runs.

2.3.2.2 Roughness and Boundary Layer Wind data

Reynolds averaging (Stull, 1988) was applied to find the mean wind speed and direction at each 3-D sonic anemometer for the entire 1.75-hour field study and for 5-minute periods corresponding to each of the 44 vehicle trips. In the latter, the 5-minute averaging time encompassed the time from roadside emission of the plume to its transport past the sensors located 106 m downwind. The result of Reynolds averaging is shown for streamline velocity, u:

$$u = \bar{u} + u', \quad (2.2)$$

where $\bar{u}$ is the mean wind speed, u the measured wind speed, and u' the turbulent fluctuations. Four mean turbulent quantities were also calculated for the entire field study (1.75 hour averaging time) and for each run (5 minute averaging time). More advanced methods were employed to calculate the four mean turbulent quantities. First, the velocity measured from each of the four 3-D sonic anemometers was rotated into an appropriate streamline coordinate system using the Wilzack et al. (2001) planar fit coordinate

transformation. This transformation was applied once for each averaging period (1.75 hours or 5 minutes) and utilized 10 subaverages of each of the three orthogonal directions to determine the plane where the average vertical velocity is minimized. Subsequently, eddy covariance methods (Aubient et al., 2012) were used to calculate four mean turbulence quantities. The first two of the four mean turbulence quantities, the turbulent velocity scale, u_*, and the turbulent kinetic energy, *tke*, are used to quantify the gustiness of the wind. u_*, is defined as:

$$u_* = [\langle\overline{u'v'}\rangle^2 + \langle\overline{u'w'}\rangle^2]^{1/4}. \tag{2.3}$$

where u', v', and w' indicate the fluctuations of the *u* (stream wise), *v* (span wise), and *w* (vertical) components from the mean during Reynolds averaging, respectively. Theturbulent kinetic energy, *tke,* is defined as:

$$tke = \frac{1}{2}\left(\overline{u'^2} + \overline{v'^2} + \overline{w'^2}\right). \tag{2.4}$$

Vertical mixing of the plume is enhanced by atmospheric instabilities and is inhibited by atmospheric stability. Neutral atmospheric conditions are neither enhancing nor inhibiting to vertical mixing of the plume. The last two of the four mean turbulent quantities, the Monin-Obukhov length scale, L , and the gradient Richardson number, *Ri*, are used to determine atmospheric stability. L is defined as:

$$L = -\frac{\bar{\theta} u_*^3}{\kappa g(\overline{w'\theta'})}, \tag{2.5}$$

where $\bar{\theta}$ is the mean absolute virtual sonic temperature, $\overline{w'\theta'}$ is the covariance of w and θ, and g is the gravitational constant. A large absolute value of L is indicative of neutral conditions; a positive value indicates stable conditions and a negative value indicates unstable conditions. *Ri* is defined as:

$$Ri = \frac{g(\partial\bar{\theta}/\partial z)}{\bar{\theta}(\partial\bar{u}/\partial z)^2}. \tag{2.6}$$

Small absolute values of *Ri* indicate neutral conditions while positive values approaching 0.2 indicate stable conditions. Large negative values indicate unstable conditions (Ayra, 2001). To calculate *Ri*, logarithmic finite differences were utilized (Ayra, 2001).

Continuous vertical profiles of $\bar{u}$ were defined using least square fits to $\bar{u}$ discrete vertical profiles. Two common models are the logarithmic and power law profiles. These are defined as:

$$\bar{u}(z) = \frac{u_*}{\kappa}\left[ln\left(\frac{z}{z_o}\right) - \psi\left(\frac{z}{L}\right)\right], \tag{2.7}$$

$$u(z) = \bar{u}_{ref}\left(\frac{z}{z_{ref}}\right)^p. \tag{2.8}$$

In Eqs. 2.7 and 2.8, κ is the von Karman constant (taken as 0.4), z_o is the roughness height, ψ is the stability function given as: $\psi = -4.7(z/L)$ for stable conditions, $\bar{u}_{ref}$ is the mean horizontal velocity at the reference height, z_{ref}, and p is the empirically based

power constant. The log law has a theoretical basis (Ayra, 2001), and is widely utilized (Stull, 1988). The power law has no theoretical basis, but contains only one empirically based constant, versus three for the log law.

2.3.2.3 Horizontal Flux

PM_{10} concentration and wind data can be used in multiple ways to calculate the horizontal flux, F_x. F_x, is defined as:

$$F_x(x) = \int_{z=0}^{z=\infty} \int_{t=0}^{t=t_{max}} c(x,z,t)u(x,z,t)dtdz. \quad (2.9)$$

Equation 2.9 is evaluated at the roadside yields the horizontal roadside flux, F_o. The capture fraction, CF is defined by: $CF=1-F_x/F_o$. The transmitted fraction is defined by: $TF= F_x/F_o$. Vertical profiles of PM_{10} concentration and wind speed must be approximated to evaluate Eq. 2.9. Etyemezian et al. (2004) approximates profiles of c and u assuming sensor measurements are reprehensive over prescribed height intervals. This work and Veranth et al. (2003) approximate vertical profiles for $\bar{c}_{int}$, and $\bar{u}$ instead of c and u. As a result, the temporal integration in Eq. 2.9 is replaced by the temporal integration and temporal averaging performed when calculating $\bar{c}_{int}$ and $\bar{u}$, respectively.

For this work, using the methods proposed by Etyemezian et al. (2004) and Veranth et al. (2003) to evaluate Eq. 2.9 resulted in inaccurate estimates for CF. This was a result of the PM_{10} near-road DustTraks, located at x = 6 and 17 m, being too far below the top of the PM_{10} plume. To ameliorate this situation, a third method was

developed. This method utilizes additional physics in place of PM_{10} measurements near the top of the PM_{10} plume.

The new method is based upon the Gaussian-plume model proposed by Van Olden (1978):

$$\bar{c}_{int}(x,z)/Q = (A(x)\exp\ [(-B\,z/\bar{z}\,(x))^s]\,), \tag{2.10}$$

where Q is the source strength (kg m^{-1}), A is a coefficient quantifying the downwind decrease of $\bar{c}_{int}(x,z)$, and s, the shape factor. Van Olden (1978) suggested s = 1.5 and this work uses that value. B is a constant defined as:

$$B = \Gamma(2/s)/\Gamma(1/s), \tag{2.11}$$

where Γ was the gamma function. The vertical center of mass of the PM_{10} plume, $\bar{z}$, is:

$$\bar{z}(x) = \frac{\int_0^\infty z\bar{c}_{int}(x,z)dz}{\int_0^\infty \bar{c}_{int}(x,z)dz}. \tag{2.12}$$

Equation 2.10 suggests that the relationship between $\ln(\bar{c}_{int}(x,z))$ and z^s is linear and as a result is simpler to parameterize than the nonlinear relationship of $\bar{c}_{int}(x,z)$ and z^s. Consequently, the new method calculates the vertical profile of $\bar{c}_{int}(x,z)$ indirectly by parameterizing the relationship of $\ln(\bar{c}_{int}(x,z))$ and z^s and subsequently computing the profile of $\bar{c}_{int}(x,z)$ and z by taking exponentials and roots of the respective variables.

The new method divided the concentration profile into three zones: 1) the zone below the lowest DustTrak, 2) the zone between the lowest and highest DustTrak monitor, and 3) the zone above the highest DustTrak monitor. This is shown in Figure 2.2. For the lowest zone, $\ln(\bar{c}_{int}(x,z))$ was assumed to be constant from the ground to the bottom DustTrak monitor. For the intermediate zone, within the DustTrak monitors, $\ln(\bar{c}_{int}(x,z))$ was assumed to vary linearly as a function of z^s between adjacent DustTrak monitors. Above the highest DustTrak monitor, the Van Olden model is used.

Above the topmost DustTrak monitor, the Van Olden model indicates that $\ln(\bar{c}_{int})$ decreases linearly with increasing z^s. This rate is decrease is calculated by Eq. 2.13.

$$\partial \ln \bar{c}_{int}/\partial z^s = -[B/\bar{z}(x)]^s. \tag{2.13}$$

Equation 2.13 was calculated by taking logarithms and then derivatives of both sides of Eq. 2.10. To use Eq. 2.13, $\bar{z}(x)$ must be calculated. The downwind dependence of $\bar{z}(x)$ is modeled by the ordinary differential equation (ODE) (Venkatram, 2004):

$$d\bar{z}/dx = K(q\bar{z})/(\bar{u}(q\bar{z})q\bar{z}), \tag{2.14}$$

where K is the vertical turbulent diffusion coefficient and q is defined by:

$$q = [s\{\Gamma(2/s)/\Gamma(1/s)\}^s]^{1/(1-s)}. \tag{2.15}$$

In Eq. 2.14, q is a constant that relates the vertical dispersion to distance traveled downwind. The initial condition assumed for Eq. 2.14 was $\bar{z}(0) = 1$ m. Vertical profiles for $K(q\bar{z})$ and $\bar{u}(q\bar{z})$ are required for Eq. 2.14. Venkatram (2004) inserted, $K(qz) = \kappa u_* qz$, for a neutral surface layer and a power law wind profile for $\bar{u}(z)$ yielding:

$$\bar{z} = (1/q)\left[(p+1)\kappa q u_* x z_r^p / \bar{u}_r\right]^{1/(p+1)}. \quad (2.16)$$

This work utilizes the profile for stable atmospheric conditions, $K(qz) = (\kappa u_* qz)/\left(1 + 4.7(q\,z/L)\right)$. When substituted into Eq. 2.14 with the power law profile, Eq. 2.17 results:

$$\frac{\bar{z}^{p+1}}{p+1} + \frac{4.7\,q\bar{z}^{p+2}}{(p+2)L} = \frac{\kappa u_* z_r^p}{u_r q^p} x. \quad (2.17)$$

Equation 2.17 was solved by a simple bisection root finding technique (Chapra and Canale, 2006).

2.3.2.4 Validation of New Method/ Impact of Low Tower Height at x = 6 and 17 m.

It is important to estimate possible errors introduced in the calculation of captured fraction, *CF*, by using the proposed method to replace DustTrak measurements near the top of the cloud at x = 6 and 17 m downwind. To estimate these errors, the Veranth et al. (2003) and Etyemezian et al. (2004) data sets are subject to the same uncertainty. The

PM_{10} concentration data near the top of the dust cloud are removed from the data sets of Veranth et al. (2003) and Etyemezian et al. (2004) as shown in Figure 2.3. The proposed method is then implemented on the remaining data and the resulting CF is compared to the value reported in Veranth et al. (2003) and Etyemezian et al. (2004).

2.4 Results

2.4.1 Roughness and Boundary Layer Meteorology

2.4.1.1 Entire Field Campaign

Figure. 2.4 indicates that the aerodynamic shelter within the vegetation from the mean wind, $\bar{u}$, was minimal. The least square fits for both the logarithmic and power law parameterize the vertical profile of $\bar{u}$ well, less than 5% relative error for any of the four measurements, even within the vegetation.

The mean values for z_o, z/L, Ri, u_* ,p, $\bar{u}_{ref}$, and tke presented in Table 2.1 indicate calm, stable conditions. Ri specifically was slightly above the critical Ri value (Ayra, 2001). Also, the value of p was high when compared to the neutral value of ~1/7 (Ayra, 2001) as a result of high stability (Ayra, 2001). The z_o measured is comparable to that measured in "fairly level grass plains" (Ayra, 2001). Finally, the wind direction was nearly orthogonal to the direction of the road.

Vertical profiles for two turbulent quantities, u_* and tke, are presented in Figure 2.5 and exhibit aerodynamic shelter within the vegetative canopy. Within the canopy, these profiles indicated a monatomic increase in turbulence with height. Above the canopy, the turbulence was invariant with height, an indication of the constant stress surface layer. Similar results were shown in Kaimal and Finnigan (1994).

2.4.1.2 Individual Runs

The distributions for wind direction and speed along with *z/L*, *Ri*, *tke*, and u_* are now presented for the 44 vehicle runs.

Besides being calm on average for the duration of the field study, the mean wind magnitude and direction were consistent, as shown in Figure 2.6. The wind speed varied from ~1 m s^{-1} to a little less than 3.0 m s^{-1}. The direction was bounded by ~250° to ~225°. The majority of the runs had a $\bar{u}_{ref}$ of ~2.5 m s^{-1} out of 250°. This was important because the PM_{10} plumes had a consistent path of travel through the canopy.

Stable conditions were prevalent for all the runs, as shown by the histograms for *z/L*, *Ri*, u_* *tke* presented in Figure 2.7. The histograms are based on data found in Table 2.2and show that there were no runs exhibiting unstable conditions or high turbulence.

2.4.2 Concentration and Flux

2.4.2.1 Concentration

The time series of PM_{10} concentration, shown in Figure 2.8, indicate that concentrations decreased by nearly two orders of magnitude from the roadside measurement, x = 6 m from the vehicle path, and x = 106 m. Also, the duration for a plume to pass at a given downwind location increased from ~15 sec at x = 6 m to ≈120 s at x = 106 m as a consequence of mixing. The ambient concentration observed during periods of no vehicular traffic was ~ 20 μg/m^3 and was an order of magnitude lower than the lowest plume concentrations. The data from all eight DustTraks consistently measured dust plumes, although the data from the top DustTrak on the far downwind location (106, 9.0 m) did not detect two of the forty-four plumes, as noted in Table 2.2.

The time-integrated concentration, c_{int}, decreases with increasing height and downwind distance, as shown in Figure 2.9. The rate of decrease is more rapid in the vertical than in the horizontal. For example, the profile at x = 106 indicates a vertical decrease of c_{int} by a factor of 10 over a vertical distance of 7 m. In the horizontal, the 2 m high measurements at x = 6 m and x = 106 m and z = 2 m indicate a decrease of c_{int} by a factor of 5 over a distance of 100 m. Figure 2.10 indicates that the horizontal decrease of c_{int} was exponential in form and was nearly identical for both the z = 0.5 m and z = 2.0 m heights. These heights were within the roughness layer, below the height ~1.5 H_{can} where H_{can} is the height of the canopy (Ayra, 2001).

Both Figures 2.9 and 2.10 suggest that c_{int} was nearly constant within the roughness layer; this is in contrast with the surface layer, located above the roughness layer, where models (Veranth et al., 2003) predict an exponential decrease in c_{int} with increasing height. This behavior, of separate concentration regimes within the roughness and surface layers, was shown by simulation of spores in canopies by Lagrangian dispersion models (Aylor and Flesh, 2001) and is most likely a result of the distinct characteristics for flow, within and just above the canopy, and the lower atmospheric boundary layer flow above the roughness layer (Pardyjak et al., 2008).

2.4.2.2 Flux

Figure 2.11 illustrates the exponental decay of the horizontal flux of $PM_{10,}$, F_x, normalized by its value measured at x = 6 m, F_o. The error bars are 95% confidence intervals. At x = 17 m, the flux was between 103% and 69% of the roadside value at x = 6 m (with 95% confidence). As a result of the overlapping error bars at x = 6 and 17 m, these two fluxes were statistically indistinguishable. At x = 106 m, the flux had

decreased to between 66% and 40% of the roadside value. The data used to obtain Figure 2.11 are shown in Table 2.3.

The wide distribution of F_x/F_o calcuated at x =17 and 106 m for each of the 44 vehcile trips is shown in Figure 2.12. Also the distributions are skewed compared to the mean values presented in Figure 2.11; the majority of the measured F_{17}/F_o and F_{106}/F_o values are less than the means shown in Figure 2.11.

2.4.2.3 Validation of New Method/ Impact of Low Tower Height at x = 6 and 17 m.

The data in Table 2.4 suggest that utilizing the new method in place of having DustTraks near the top of the PM_{10} plume at locations near the road (x = 6 and 17 m) introduces relative errors in the calculated transmitted fraction, *TF*, that are less than 10%. The relative error in *TF* that results in using the new method with short DustTrak towers is small compared to *TF* values reported in the Veranth et al. (2003) and Etyemezian et al. (2004) studies: 110% and 15%, respectively.

2.5 Conclusions

The field study results lend support to the hypothesis that fugitive dust removal near unpaved roads may be determined by surface roughness and meteorology. These conditions varied significantly between the current, Veranth et al. (2003), and Etyemezian et al. (2004) field studies. Based on the three studies, removal becomes significant with either increasing roughness or atmospheric stability. The measured removal rates increase from negligible to about 85% as surface roughness increases from negligible to urban-scale. The current study estimated 60 and 35% removal of PM_{10} within 100 m at a roughness characterized by a grassy plain and under very calm, stable

conditions. The relative error introduced by using the proposed method for calculating the transmitted fraction, TF, when PM_{10} near the top of the dust cloud is absent was less than 10%. The PM_{10} concentration was found to be nearly uniform within the roughness layer, 1.5 times the vegetative canopy height. This was in contrast to simple concentration profile models (Veranth et al., 2003) implemented in the surface layer, above the roughness layer, but showed some agreement with Lagrangian model simulations of spore transport within a canopy (Aylor and Flesh, 2001). Also the canopy is shown to provide significant shelter from ambient turbulence in contrast to the mean wind for which the canopy provided little shelter.

2.6 Acknowledgements

This work was generously supported by the Southwest Center for Environmental Research and Policy (SCERP) under project number A-04-03 and the strategic Environmental Research and Development Program (SERDP) project number RC-1730. Melissa Armijo of the New Mexico state office of public lands was essential for obtaining land use permissions. Prathap Ramamurthy operated the 3-D sonic anemometers, participated in the van trips and assisted in the initial analysis. John Andersen and Kelly Allred of New Mexico State University characterized the local vegetation.

Table 2.1. Meteorological characterization based on entire 1.75-hour field campaign. Conditions indicate stable conditions with an aerodynamic roughness, z_o, of 0.08 m intermediate of that for Etyemezian et al. (2004) (z_o =0.005 m) and Veranth et al. (2003) (z_o=0.1 m) sites. Sonic data taken at x=59 m.

Meteorological Parameter	Value	Data Source/Method
$\bar{u}_{ref}$ z/L u_* *tke* *angle with road (270°* is orthogonal*)*	2.2 (m s^{-1}) 0.25 0.15 (m s^{-1}) 0.25 (m^2 s^{-2}) 242°	3D sonic anemometer at coordinate (59.0, 5.0 m)/Eddy-covariance
z_o p	0.08 m 0.40	$\bar{u}$ measured at 4 3D sonic anemometers at x =59 m/Least-squares curve fit
Ri	0.23	3D sonic anemometers at coordinates (59.0, 5.0 m) and (59.0 3.12 m)/Finite Difference of mean virtual absolute temperature

Table 2.2. The mean turbulence quantities and horizontal fluxes for the 44 van trips.

Run	*Ri*	*tke* ($m^2 s^{-2}$)	u_* ($m\ s^{-1}$)	*z/L*	F_6	F_{17}	F_{106}
					(mg m^{-1} of road)		
1	0.36	0.65	0.21	0.02	468	226	213
2	0.27	0.33	0.15	0.05	914	978	464
3	0.25	0.27	0.17	0.06	1051	148	948
4	0.17	0.25	0.13	0.16	717	1036	739
5	0.15	0.23	0.15	0.09	550	878	569
6	0.17	0.23	0.14	0.10	1454	716	763
7	0.19	0.26	0.15	0.16	519	530	451
8	0.22	0.24	0.14	0.12	761	843	438
9	0.16	0.18	0.08	0.15	1135	1284	393
10	0.17	0.14	0.16	0.19	1057	714	777
11	0.18	0.14	0.14	0.24	379	412	535
12	0.20	0.11	0.15	0.27	1056	688	677
13	0.19	0.15	0.19	0.17	957	590	507
14	0.19	0.17	0.19	0.22	1322	574	397
15	0.19	0.20	0.12	0.41	342	725	414
16	0.20	0.19	0.16	0.23	877	555	346
17	0.18	0.15	0.15	0.25	1343	687	572
18	0.16	0.13	0.17	0.21	190	385	160
19	0.16	0.12	0.14	0.28	940	608	298
20	0.16	0.11	0.06	1.16	1338	790	494
21	0.17	0.11	0.11	0.28	555	498	359
22	0.19	0.10	0.16	0.22	550	339	278
23	0.21	0.10	0.08	0.31	1430	1348	605
24	0.20	0.10	0.06	1.53	892	617	562
25	0.18	0.09	0.14	0.34	421	364	126
26	0.18	0.09	0.13	0.35	466	473	678
27	0.17	0.09	0.15	0.31	674	502	554
28	0.20	0.08	0.12	0.44	600	1282	624
29	0.21	0.06	0.11	0.58	1492	601	648
30	0.24	0.05	0.10	0.73	176	94	244
31	0.25	0.04	0.09	0.75	705	510	658
32	0.23	0.04	0.08	0.95	41	83	104
33	0.24	0.04	0.08	1.05	1239	1099	590
34	0.28	0.03	0.07	1.27	1254	1929	499
35	0.34	0.02	0.07	1.21	895	559	488
36	0.40	0.02	0.06	1.33	1225	1594	600
37	0.37	0.03	0.06	1.90	1299	1038	410
38	0.33	0.03	0.06	1.94	2253	1621	350
39	0.31	0.03	0.06	1.95	908	801	395
40	0.30	0.03	0.06	1.96	734	518	362
41	0.28	0.04	0.05	0.96	1015	553	628
42	0.54	0.14	0.05	5.27	672	394	834
43	0.77	0.08	0.03	1.97	1666	1615	118
44	0.37	0.08	0.06	0.80	703	845	335

Table 2.3. Time integrated concentrations, c_{int}, at downwind locations for the 44 van trips.

	c_{int} (mg m^{-3} s) measured at $\begin{pmatrix} \text{x (m)} \\ \text{z (m)} \end{pmatrix}$							
Run	**6.0 0.5**	**6.0 2.0**	**17.0 0.5**	**17.0 2.0**	**59.0 5.0**	**106.0 0.5**	**106.0 2.0**	**106.0 9.0**
1	16	25	6.6	9.0	3.7	2.3	2.0	1.5
2	30	44	28	38	9.4	3.6	5.0	2.8
3	46	39	6.3	4.2	10	8.4	8.2	5.2
4	29	27	39	32	9.3	9.1	9.2	2.8
5	16	23	29	27	6.8	7.8	6.7	2.1
6	56	62	35	21	12	11	10	2.9
7	21	20	15	18	11	4.2	5.2	2.1
8	28	31	33	26	9.4	6.9	6.4	1.3
9	34	59	52	49	8.3	7.6	7.0	1.0
10	81	34	37	21	7.7	13	14	2.1
11	20	17	21	14	8.5	8.7	10	1.7
12	56	49	32	26	16	12	12	2.7
13	24	50	25	20	3.6	9.9	11	1.2
14	63	53	26	17	7.4	6.3	6.3	1.3
15	19	13	30	26	2.9	6.4	7.6	1.1
16	42	32	23	17	4.4	4.1	4.7	1.2
17	34	60	32	19	11	14	12	0.68
18	4.7	8.5	16	11	2.5	2.6	2.2	0.49
19	49	36	26	20	3.6	6.0	6.3	0.49
20	47	73	40	32	13	10	11	1.0
21	24	25	22	18	8.1	7.2	6.8	0.95
22	32	21	15	11	5.0	8.3	7.3	0.27
23	60	74	81	49	19	12	12	1.7
24	78	38	40	28	81	12	14	1.3
25	28	18	17	14	2.4	2.1	28	0.32
26	20	24	26	17	5.4	14	16	1.5
27	39	31	27	18	6.2	16	14	0.97
28	31	32	76	51	14	14	18	1.3
29	110	80	36	28	6	21	24	0.70
30	13	10	7.0	4.6	2.2	14	8.0	0.32
31	58	44	39	27	14	25	33	0.43
32	3.6	2.7	7.1	4.6	3.5	9.0	5.7	0.0
33	100	83	95	61	24	15	25	1.1
34	87	99	170	120	19	33	38	0.0
35	81	65	51	34	9.5	20	20	1.0
36	91	97	130	100	13	32	35	0.2
37	120	90	87	67	22	16	18	0.63
38	160	180	140	110	20	19	23	0.53
39	95	58	69	50	7.3	17	16	0.61
40	60	53	47	31	13	18	18	0.20
41	100	67	16	45	12	42	38	0.067
42	65	51	56	22	14	46	39	0.93
43	180	89	120	100	24	13	2.4	0.27
44	52	41	51	46	10	11	15	0.16

Table 2.4. Estimation of error introduced by calculating the transmitted fraction, *TF*, using the method currently proposed to replace missing data near the top of the PM_{10} dust cloud. To estimate the error, PM_{10} data near the top of the dust cloud are removed from the Veranth et al. (2003) and Etyemezian et al. (2004) datasets, as shown in Figure 2.3, and the new method is applied to the truncated data sets. The resulting *TF* is compared to *TF* published in Veranth et al. (2003) and Etyemezian et al. (2004). The relative error is less than 10%.

Datasets	**Published *TF***	**New Method for calculating *TF* when PM_{10} data near top of the Dust cloud is absent**	**Relative Error**
Veranth et al. (2003)	0.15	0.22	7%
Etyemezian et al. (2004)	[1.1 0.9]	1.2	9%

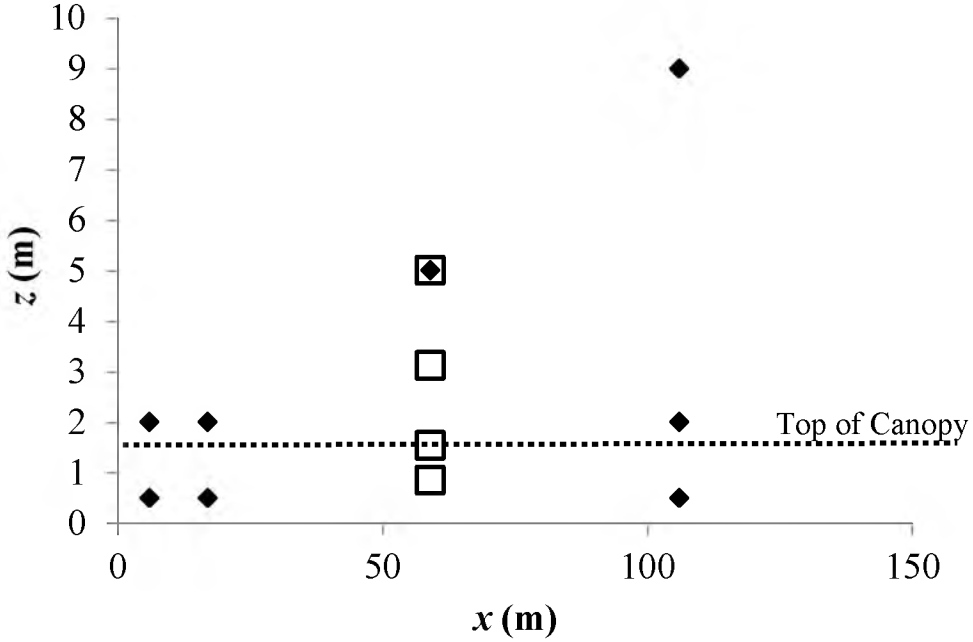

Figure 2.1. Locations of DustTrak monitors ◆ and sonic anemometers ☐ utilized to measure the captured and transmitted fractions, denoted *CF* and *TF*, respectively, of roadside PM_{10} fugitive dust. Coordinate locations for the DustTraks were (x,z): (6,0.5 m) (6,2 m) (17, 0.5 m) (17, 2 m) (59, 5 m) (106, 0.5 m) (106,2 m) (106,9 m). Coordinate locations for the sonics were (59, 0.85 m) (59, 1.54 m) (59, 3.12 m) (59,5 m). (0, 0 m) was located at the path of travel for the vehicle.

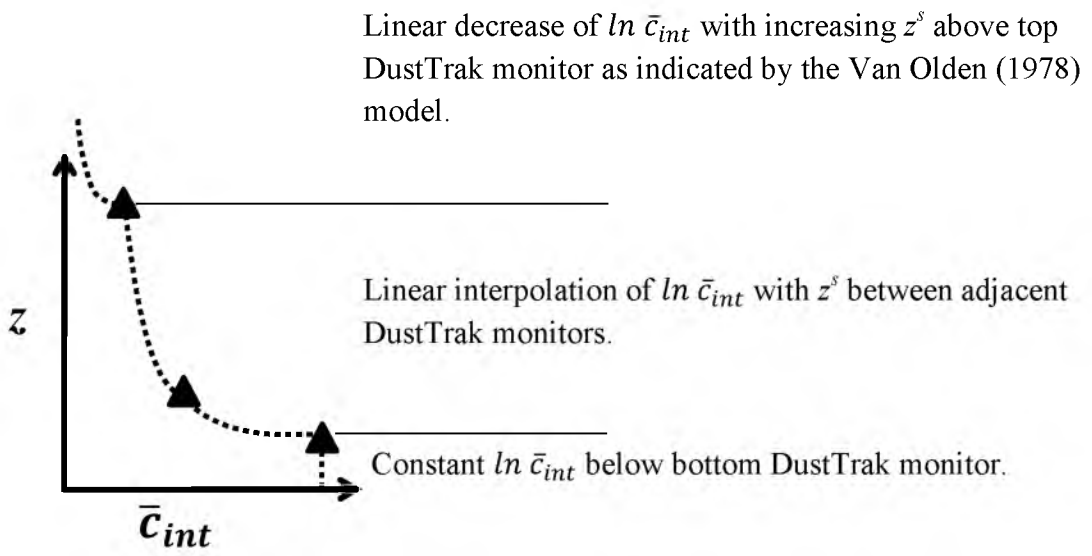

Figure 2.2. Illustration of the methodology used to estimate the vertical profiles of time-integrated concentration, $\bar{c}_{int}$, from discrete DustTrak data ▲. The profiles are used to calculate capture fraction, *CF*, in Eq. 2.9. Because Eq. 2.10 indicates that $ln\ \bar{c}_{int}$ varies linearly with z^s, the vertical profile of $\bar{c}_{int}$ is parameterized in terms of $ln\ \bar{c}_{int}$ and z^s as indicated by the three zones shown. The vertical profile of $\bar{c}_{int}$ is obtained by taking exponentials of $ln\ \bar{c}_{int}$ and roots of z^s at all heights.

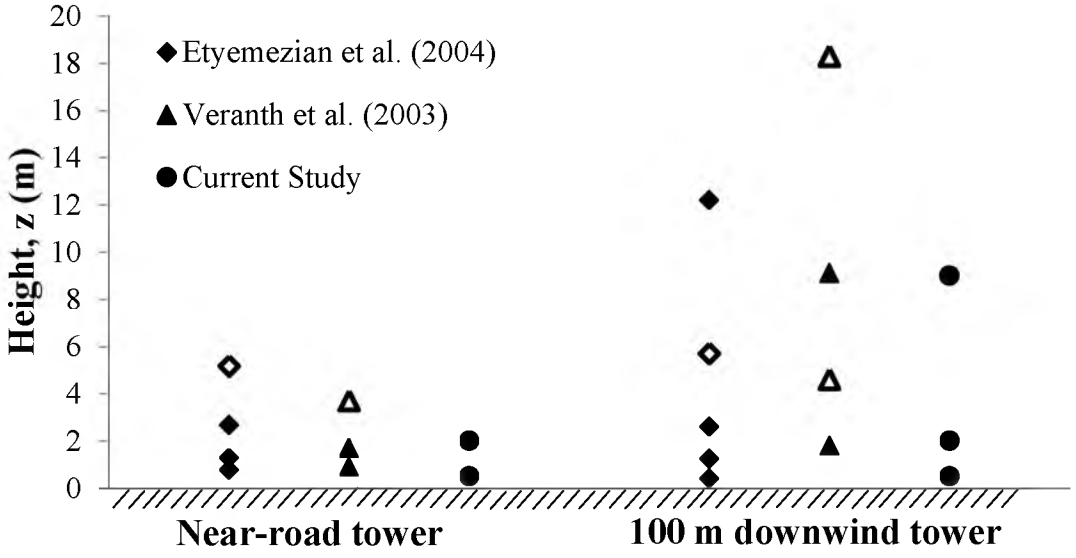

Figure 2.3 Heights of DustTrak PM_{10} sensors from the Etyemezian et al. (2004) and Veranth et al. (2003) studies used to estimate the error introduced by using the proposed method to substitute for DustTrak monitor data near the top of the dust cloud when calculating the transmitted fraction, *TF*. Solid symbols indicate the PM_{10} data retained in the error analysis; hollow symbols indicate data that are removed to perform the error analysis. The current studies DustTrak heights are shown for comparison.

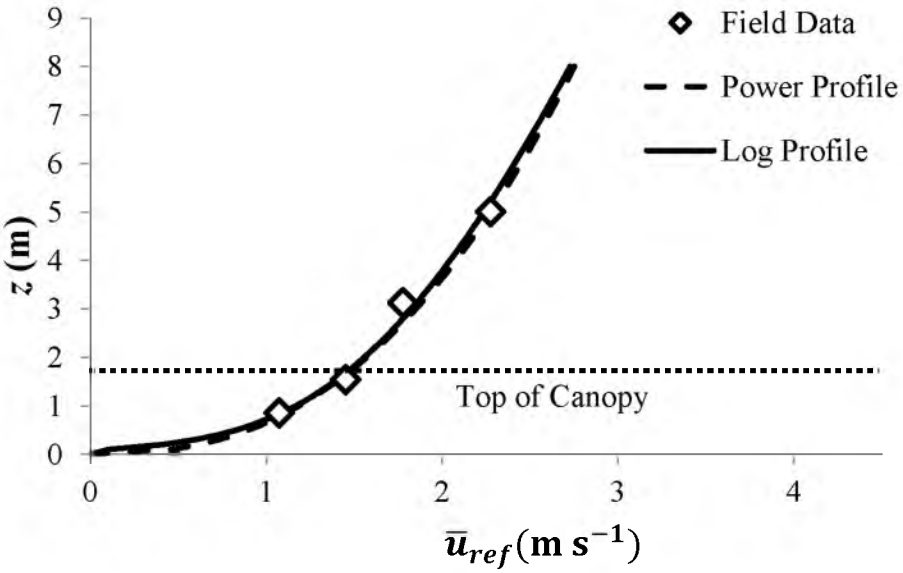

Figure 2.4. Logarithmic (solid line) and power law (dashed line) fits to 1.75 hour mean data taken within and above the ~1.75 m high vegetative canopy. The power law profile is used to calculate the captured fraction, *CF*, while the log profile is more commonly used by boundary-layer meteorologists. Measurements were taken 59 m downwind of road. Fitting values for this profile are found in Table 2.1 with the exception that the log profile utilizes the least squares value $u_* = 0.17$ m s^{-1}, instead of the eddy covariance value $u_* = 0.15$ m s^{-1} .

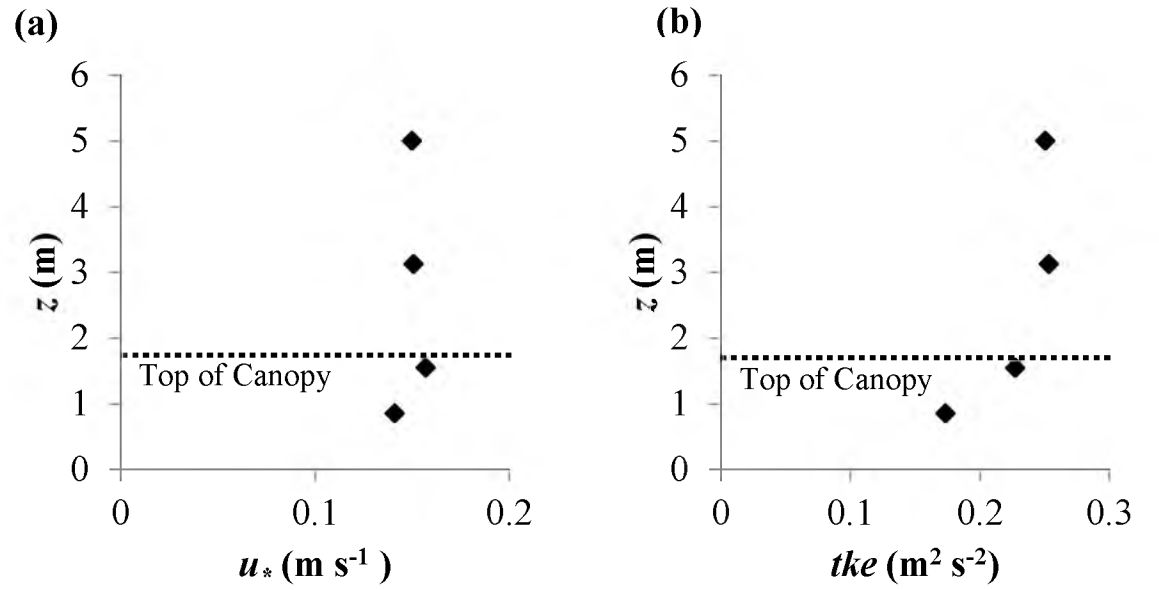

Figure 2.5. Vertical profiles of the turbulent quantities (a), u_*, the turbulent velocity scale, and (b) *tke*, turbulent kinetic energy, measured by the sonics at x= 59.0 m downwind. Plot (a) displays negligible shelter for u_* within the canopy. Plot (b) displays the transition from turbulent shelter within the canopy to a constant value of the lower atmospheric boundary layer as illustrated in Kaimal and Finnigan (1994). Together the plots indicate the canopy was sufficiently dense to affect some mean turbulent quantities.

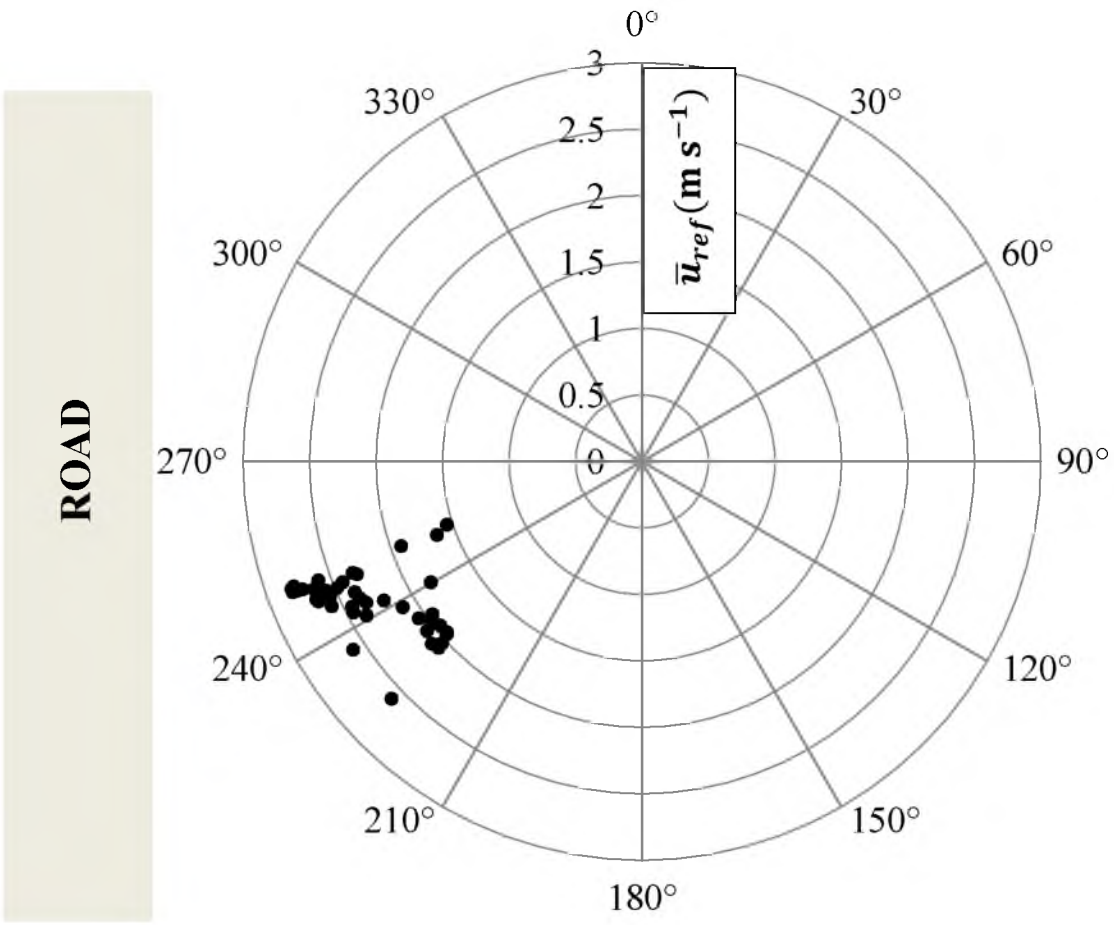

Figure 2.6. The reference wind speed and wind source direction for each of the 44 vehicle trips as measured at z= 5 m and x =59 m. Wind consistently transported dust plumes downwind to sensors at an angle ~30˚orthogonal to road, insuring a nearly constant time and distance of travel to the downwind DustTrak sensors.

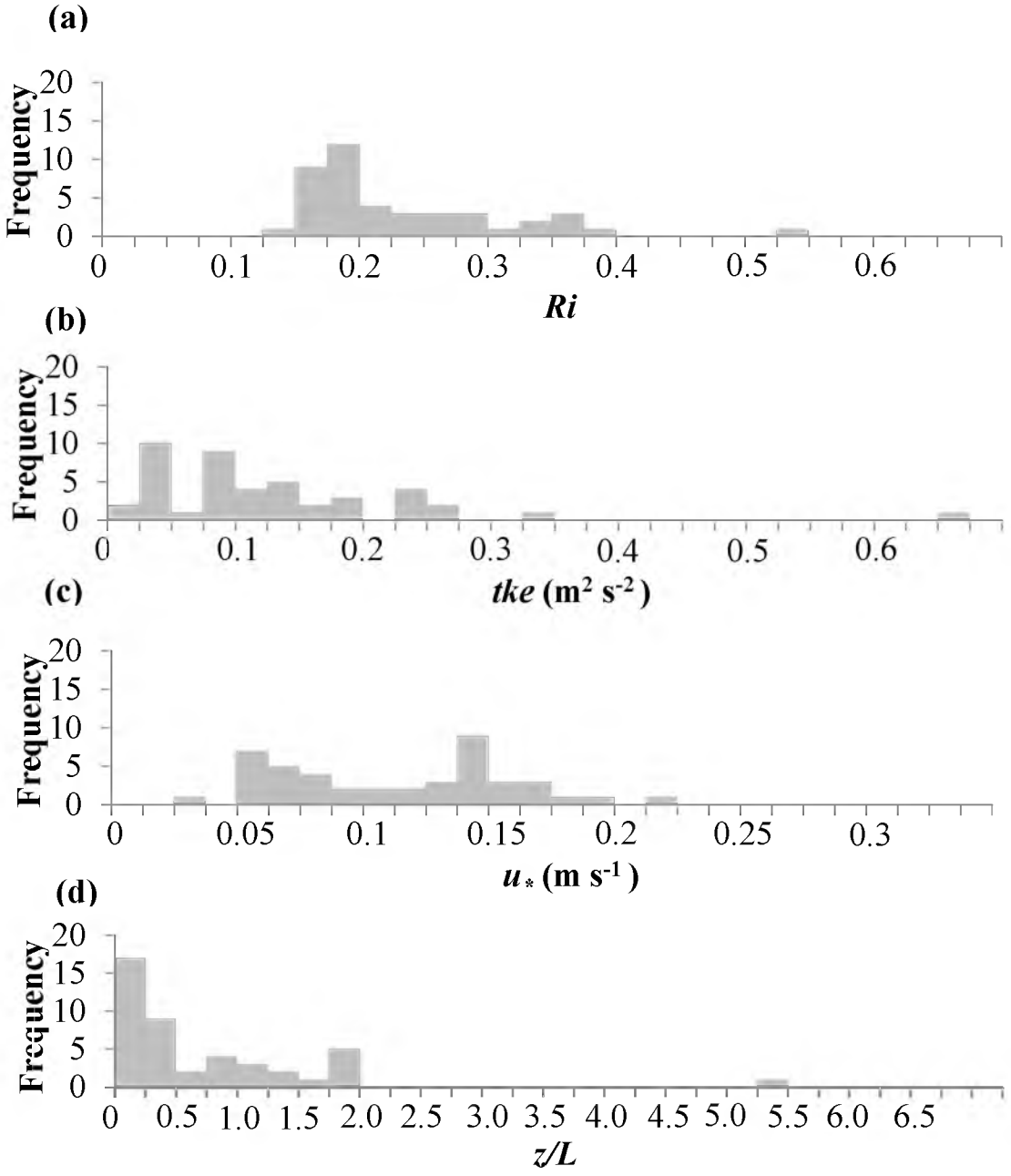

Figure 2.7. The histograms of the mean turbulent quantities a) *Ri* b) *tke* c) u_* d) *z/L tke* for the 44 vehicle runs as measured at z = 5 m and x= 59 m. The distributions indicated stable, calm conditions prevailed for the entirety of the 1.75 hour field campaign. The data are located in Table 2.2.

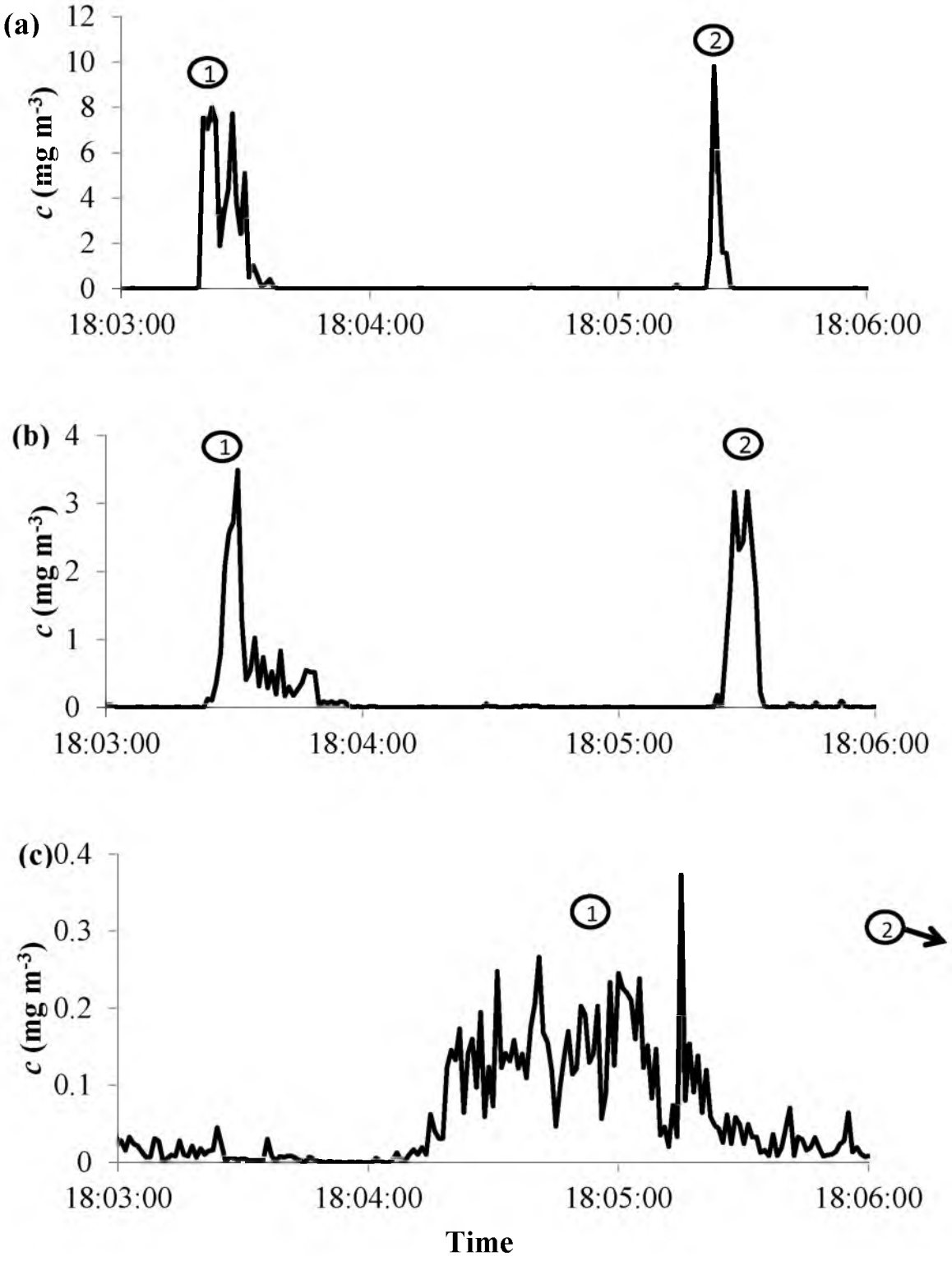

Figure 2.8. Time series of PM_{10} concentration, at a) (6.0, 2.0 m), b) (17.0, 2.0 m), and c) (106.0 2.0 m). Plume 1 is identified in all three panels. Note differing scales in concentration and increased time for the plume to pass because of dispersion when comparing to panels a) and c).

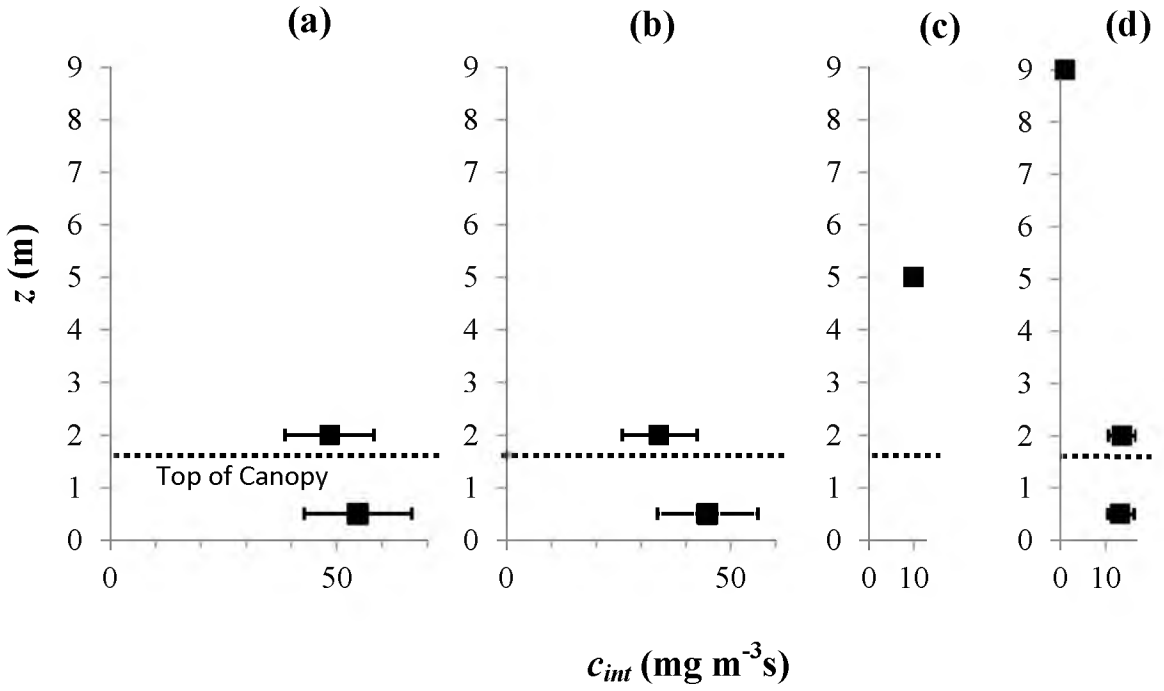

Figure 2.9. Panels displaying the vertical profiles of time-integrated concentration, c_{int}, at the four downwind locations of DustTraks. (a) x = 6 m (b) x = 17 m (c) x = 59 m and (d) x = 106 m. The plot indicates a horizontal decrease in c_{int} over scales of 100 m and a vertical decrease over scales of 10 m. Also c_{int} appears to be approximently constant within the roughness layer (~1.5 H_{can} where H_{can} is the height of the canopy) (Ayra, 2001). The data used to produce the plot are displayed in Table 2.3.

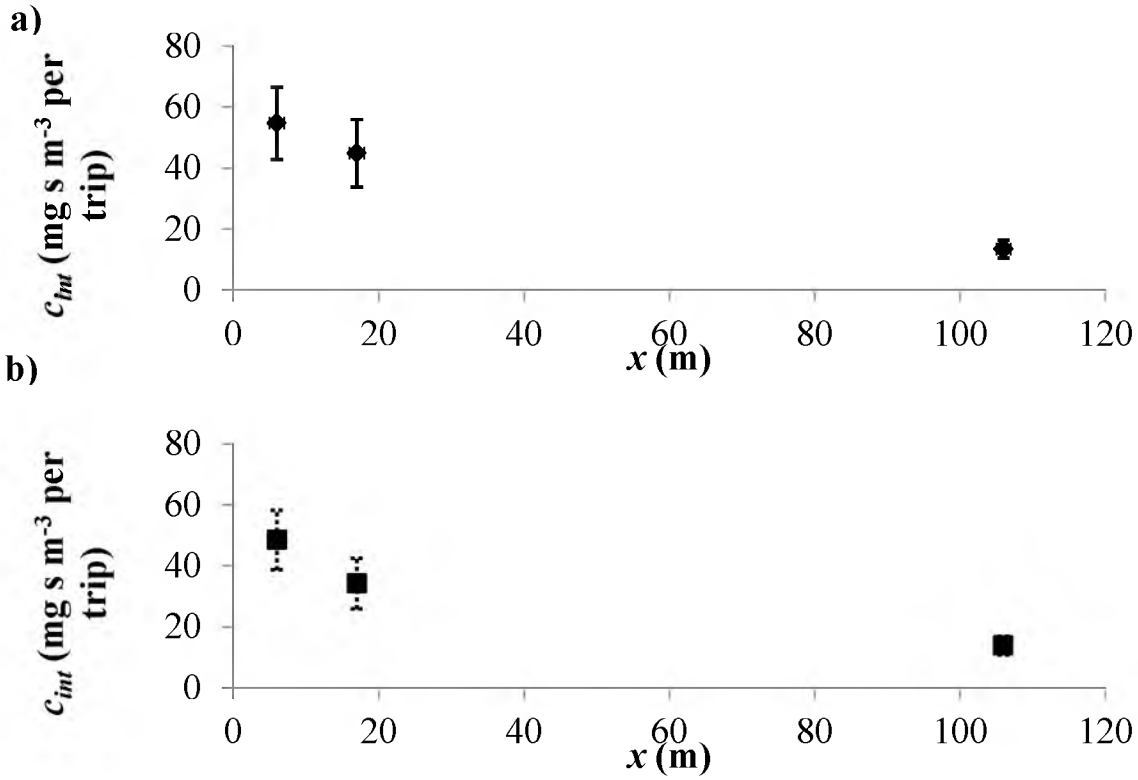

Figure 2.10. Downwind attenuation of time-integrated concentration, c_{int} a) at z = 0.5 m(◆) and b) z = 2.0 m (■) with 95% confidence error bars. The decrease of c_{int} with increasing downwind distance was exponental and was nearly identical for both heights, which were within the roughness layer ~1.5H_{can}.

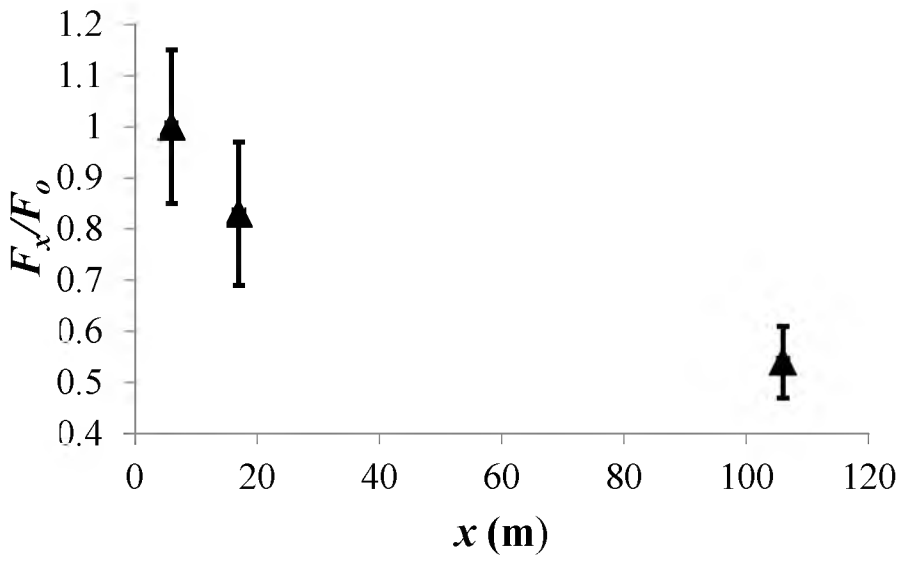

Figure 2.11. The downwind attenuation of horizontal flux, F_x normalized by its value at x = 6 m, F_o. The transmitted fraction, *TF*, is equal to F_x/F_o; captured fraction, *CF*, is equal to 1- F_x/F_o. The decrease in the transmitted fraction is exponental with increasing downwind distance and was statistically significant for the site under the calm meterological conditions. The data used to produce Figure 2.10 are located in Table 2.3.

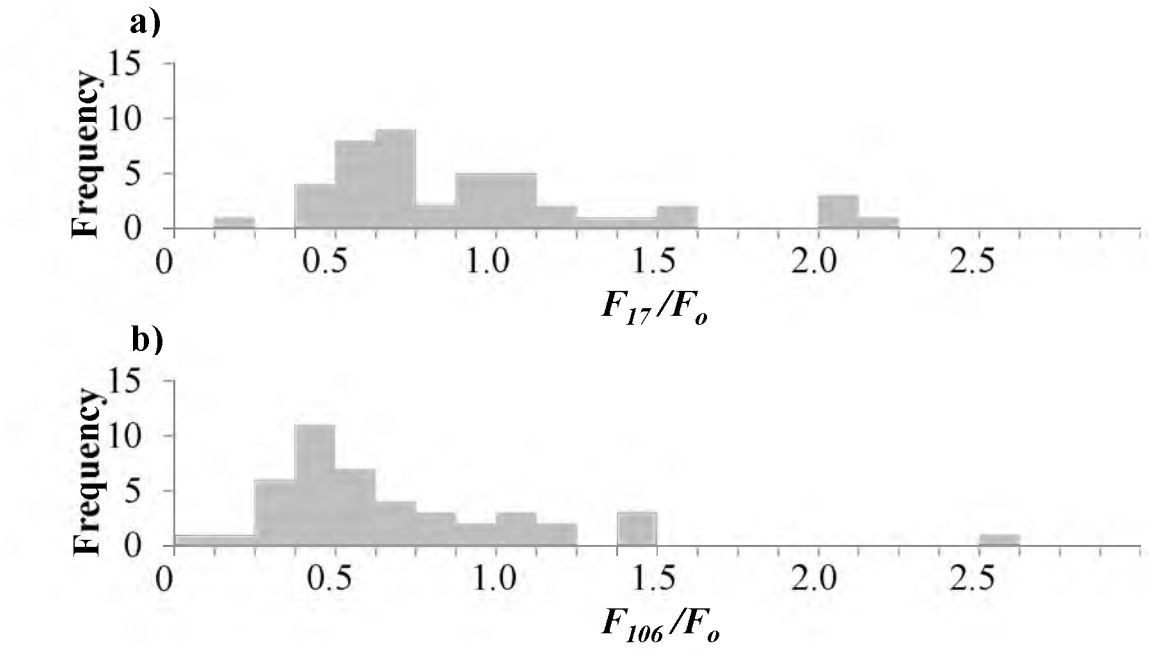

Figure 2.12. The distributions of F_{17}/F_o and F_{106}/F_o calculated for the 44 van trips a) F_{17}/F_o and b) F_{106}/F_o. The transmitted fraction, TF, is equal to F_x/F_o at x. There was a wide distribution of measured values for TF at x=17 and 106 m. This caused a relatively large 95% confidence interval in the reported measurements. F_o is calculated 6 m downwind of the path traveled by the van. The data used to produce this figure are located in Table 2.3.

2.7 References

Arya, S.P., 2001: *Introduction to micrometeorology*, Orlando: Academic Press.

Aylor, D. E. and T. K. Flesh, 2001: Estimating spore release rates using a Lagrangian stochastic simulation model. *Journal of Applied Meteorology,* **40**, 1196-1208.

Aubinet, M., T. Vesala, and D. Papale (Eds.), 2012: *Eddy Covariance*. New York: Springer.

Chapra, S.C. and R. P. Canale, 2006: *Numerical methods for engineers*. New York: McGraw Hill.

Countess, R., 2001: Methodology for estimating fugitive windblown and mechanically resuspended road dust emissions applicable for regional scale air quality modeling. Western governors Association by Countess Environmental: Westlake Village, CA.

EPA, 2006: AP-42, Compilation of Air Pollutant Emission Factors, Vol. 1. Stationary, Point, and Area Sources, Chapter 13.2.2 Unpaved Roads. US Environmental Protection Agency, Washington, DC. Available at the URL: http://www.epa.gov/ttn/chief/ap42/ch13/final/c13s0202.pdf

Etyemezian, V., S. Ahonen, D. Nikolic, J. Gillies, H. Kuhns, D. Gillette, and J. Veranth, 2004: Deposition and removal of fugitive dust in the arid southwestern United States: measurements and model results. *Journal of the Air and Waste Management Association* **54**, 1099-1111.

Kaimal, J.C., and J. J. Finnigan, 1994: *Atmospheric boundary layer flows: their structure and Measurement*, Oxford University Press, US.

Pace, T.G., 2005: Methodology to estimate the transportable fraction (*TF*) of fugtive dust emissions for urban scale air quality analyses. USEPA.

Pardyjak, E.R., S. O. Speckart, F. Yin, and J. M. Veranth, 2008: Near-source deposition of vehicle generated fugitive dust on vegetation and buildings: model development and theory. *Atmospheric Environment*, **42**, 6442-6452.

Speckart, S.O., E. R. Pardyjak, and J. M. Veranth, 2013: Impact of roughness and meteorology upon near-source transport of vehicle-generated fugitive dust Part 2: Relevant roughness and meteorological parameters. Submitted to Atmospheric Environment.

Stull, R. B., 1988: *An introduction to boundary layer meteorology*, Kluwer Academic Publishers, Dordrecht, The Netherlands

Veranth, J.M., G. Seshadri, and E. Pardyjak, 2003: Vehicle-Generated Fugitive Dust Transport: Analytic Models and Field Study. *Atmospheric Environment*, **37**, 2295-2303.

Van Ulden, A.P., 1978: Simple estimates for vertical diffusion from sources near the ground. Atmospheric Environment, **12**, 2125-2129.

Venkatram, A., 2004: On estimating emissions through horizontal fluxes. Atmospheric Environment **38**, 1337-1344.

Watson, J.G. and J. C. Chow, 2000: Reconciling urban fugitive dust emissions inventory and ambient source concentration estimates: summary of current knowledge and needed research, Desert Research Institute, Reno, NV, www.epa.gov/ttn/chief/efdocs/fugitivedust.pdf.

Wilzack, J.M., S. P. Oncley, and S. A. Stage, 2001: Sonic anemometer tilt corrections algorithms. *Boundary-Layer Meteorology*, **99**, 127-150.

CHAPTER 3

NEAR-SOURCE DEPOSITION OF VEHICLE-GENERATED FUGITIVE DUST ON VEGETATION AND BUILDINGS: MODEL DEVELOPMENT AND THEORY

The content of this chapter was previously published as an article with the following citation: E. R. Pardyjak, S.O. Speckart, F. Yin, J.M. Veranth, Near source deposition of vehicle generated fugitive dust on vegetation and buildings: Model development and theory, Atmospheric Environment, 42 (2008), pp. 6442-6452.
 The definition of H^* used in this chapter was modified from the definition utilized in the peer-reviewed article for consistency in the dissertation.

3.1 Abstract

This paper describes the development of a simple quasi-2D Eulerian atmospheric dispersion model that accounts for dry deposition of fugitive dust onto vegetation and buildings. The focus of this work is on the effects of atmospheric surface layer parameterizations on deposition in the "impact zone" near unpaved roads where horizontal advection of a dust cloud through roughness is important. A wind model for computing average and turbulent wind fields is presented for flow within and above a

roughness canopy. The canopy model has been developed to capture the most essential transport and deposition physics while minimizing the number of difficult-to-obtain input parameters. The deposition model is based on a bulk sink term in the transport equation that lumps the various dry deposition physical processes. Wind field, turbulence, and deposition results are presented for a range of atmospheric stabilities and roughness. The canopy model produces results in which deposition within a canopy is enhanced under certain initial, atmospheric, and roughness conditions, while under other conditions, much less deposition occurs. The primary limitation of the model is the ability to accurately determine (typically using experimental data) the vegetative deposition parameter (clearance frequency). To understand the clearance frequency better, a dimensionless parameter called the deposition effectiveness is identified that can be used to estimate deposition in the canopy. In general, the model captures the essential physics of near-source dust transport and provides a tool that can efficiently simulate site-specific conditions in practical situations.

3.2 Introduction

Vehicle-generated fugitive dust is the uncontrolled emission of particulate matter associated with vehicles driving over unpaved roads. These emissions are particularly important in populated arid regions with many kilometers of unpaved roads such as the cities along the U.S./Mexico border. The amount of fugitive dust that is transported long distances from these sources can have a great impact on health (Davidson et al., 2005) and visibility (Watson and Chow, 1994). A number of abatement strategies exist including the application of liquids onto unpaved roads (Harley et al., 1989) but many options are uneconomical or ineffective in arid climates with extensive rural roads. It has

been proposed that another strategy for reducing these emissions is to utilize natural vegetation and windbreaks (Pace, 2005). In addition, studies indicate (Watson and Chow, 2000) that current EPA emission factors overpredict long-range transport. One hypothesis for this overestimation is that the emission factor model does not account for particle removal by vegetation or other roughness elements near the source. In order to understand the net emissions from unpaved roads and devise potential abatement strategies, it is necessary to quantify the amount of dust that is deposited near the source before the dust cloud is well mixed.

Many studies have focused on measuring and modeling the dry deposition of particles onto vegetation and other surface roughness (for reviews see e.g., Nicholson, 1988; Sehmel, 1980; Seinfeld and Pandis, 1998). Dry deposition of particles in the atmospheric boundary layer is governed by the turbulent flow characteristics, the physical and chemical properties of the material being deposited, and the nature of the surface (Seinfeld and Pandis, 1998). Deposition of particles onto surfaces occurs primarily by the following mechanisms: impaction, Brownian diffusion, interception, gravitational settling (or sedimentation) and phoretic (diffusiophoresis, thermophoresis, electrophoresis) precipitation (Nicholson, 1988). Impaction and gravitational settling occur when particles cross streamlines as a result of particle inertia. In Brownian diffusion, particles cross streamlines as a result of molecular bombardment of air molecules on particles. Interception occurs when the radius of the particle is large compared to the particles distance to the surface of the intercepting element (e.g., leaf). Much of the existing literature related to particle deposition onto roughness elements (e.g., Caffrey et al., 1998; Chamberlain, 1975; Hicks, 2006; Raupach et al., 2001; Slinn, 1982) considers transport

far downwind of the source where concentrations are relatively uniform with height and the horizontal surface is considered a sink. This type of problem is typically modeled using a deposition velocity formulation that considers different physical processes as a resistance network analogy (Seinfeld and Pandis, 1998).

Deposition near the source, or more specifically in the "impact zone," however, is less well understood. Figure 3.1 illustrates the limiting cases for dust transport (adapted from Etyemezian et al., 2004) near an unpaved road. The limiting cases include the impact, transition, and far downwind zones. In the impact zone, the height of the dust cloud is of the same order of magnitude as the height of the vegetation, terrain irregularities, fences, buildings, or other roughness elements. The concentration of dust is highest near the ground. In the transition zone, the cloud is much taller and vertical concentration gradients are lower compared to the impact zone. In the far downwind zone, the dust is fairly uniformly distributed throughout the height of the atmospheric surface layer, except very near the ground. This study focuses on dust removal very close to the road where the dust cloud is in the impact zone.

Etyemezian et al. (2004) studied the behavior of a dust cloud downwind of a dirt road at Ft. Bliss, near El Paso, Texas U.S.A. during late spring 2002. The test site consisted of small dunes with widely spaced desert shrub vegetation (aerodynamic roughness of ~0.001-0.01 m) and neutral to unstable atmospheric conditions. The field data were compared to a line source Gaussian plume model in a near-road dust simulation. The measurements indicated that the loss of PM_{10} (particulate matter with an aerodynamic diameter of 10 μm or less) within 100 m downwind of the source was within measurement uncertainty (less than ~10%). The EPA Industrial Source Code

version 3 (ISC3), a Gaussian-based model, indicated the loss of PM_{10} to be less than 5%. Etyemezian et al. (2004) concluded that the EPA ISC3 model is a simplistic but reasonable first approximation for this problem.

Veranth et al. (2003) studied a similar dust dispersion problem downstream of a dirt road in Utah's west desert at The U.S. Army Dugway Proving Grounds (DPG). They investigated the loss of PM_{10} through a mock array of buildings downwind of an unpaved road under stable atmospheric conditions. The downstream surface roughness was created using shipping containers (2.5 m high, 2.4 m deep, and 12.2 m long) in a rectangular 10×12 array. The data revealed a removal of 85% for PM_{10} within the first 100 m downwind. Etyemezian et al. (2004) also used the Gaussian-based model to analyze this experiment assuming very stable conditions and a much larger roughness height (0.71 m) than for the Ft. Bliss study. The Gaussian model predicted only 30% removal for the DPG experiment. We hypothesize that the discrepancy between the Ft. Bliss and DPG data is a result of the Gaussian model's inability (due to the model's basic assumptions being violated) to capture the complex physics associated with flow through buildings capped by a stable inversion. The discrepancy between the two problems has motivated the authors of the present paper to develop a simple model that more accurately captures the physics associated with dust transport through roughness elements subject to different atmospheric stabilities.

In order to develop a practical model for deposition, the wind and turbulence field through the roughness elements must be carefully modeled. In recent years, a great deal of progress has been made regarding understanding turbulent flow through and above obstacles in the atmospheric surface layer. In particular, flows associated with vegetation

(Finnigan, 2000; Raupach and Thom, 1981) and buildings (Belcher, 2005; Britter and Hanna, 2003) have received much attention. While the details of the fundamental processes that govern the flow within vegetative and building canopies are quite different, some of the bulk properties can be modeled similarly. For example, the results of Macdonald (2000) for mean flow and turbulence parameterizations for groups of buildings, which is based on the vegetative canopy model, yield a good comparison to experimental results. One of the goals of the present work was to build on this previous canopy research to develop a simple model for the mean velocity and turbulence that can be easily applied to fugitive road dust problems in the impact zone. This has been done using a simple two-dimensional Eulerian atmospheric diffusion equation model described below. An attempt is made to minimize the number of difficult-to-obtain input parameters while retaining important physical processes. For example, if the geometry of the problem is known (i.e., height of the canopy, type of canopy, road width, distance from road to the roughness, and typical vehicle height) and the deposition coefficient (described in detail in Section 3.2) can be estimated, the model can be implemented if the upstream wind speed is known at a reference height along with an estimate for atmospheric stability. Other wind (Harman and Finnigan, 2007; Macdonald, 2000; Massman, 1997; Poggi et al., 2004) and deposition models (Aylor and Flesch, 2001; Raupach et al., 2001; Slinn, 1982) require detailed knowledge of the roughness elements. Below, we present the development of the model and the general performance of the model.

3.3 Methods

3.3.1 Atmospheric Diffusion Model

Eulerian transport models, which balance flow in and out of stationary grid cells, and Lagrangian models, which track the movement of individual particles, are more general than Gaussian dispersion models because they are able to more easily incorporate complex physical processes (Ramaswami et al., 2005; Seinfeld and Pandis, 1998). Because of the complexity and computational time associated with Lagrangian dispersion models, this study utilized numerical solutions to a quasi-two-dimensional Eulerian atmospheric diffusion equation (ADE). For this work, an ADE has been derived from a mass balance on a control volume (CV) in which small particles are allowed to transport in and out of the CV by mean advection and turbulent motions of the atmosphere. Molecular diffusion is assumed negligible compared to turbulent diffusion and turbulent diffusion is modeled using *K-Theory*; additionally, source (dust generated by vehicular motion) and sink (deposition) terms may be defined in each cell following Seinfeld and Pandis (1998). ADE models are now relatively common in air quality work. A Gaussian model is a special case of the solution of an ADE obtained for flows with homogeneous turbulence along with steady uniform winds (Seinfeld and Pandis, 1998). However, wind speed and turbulence in the rough wall atmospheric surface layer have complex gradients that do not always satisfy the simplifying assumptions of the Gaussian model.

The 2D ADE used in this study is modified to consider dust deposition on rough walled surfaces (e.g., vegetation or buildings) or the ground (flat surface), as shown below in Eq. 3.1:

$$\underbrace{\frac{\partial c}{\partial t}}_{I} = \underbrace{-\frac{\partial c\bar{u}}{\partial x}}_{II} + \underbrace{\frac{\partial}{\partial z}\left(K_{zz}\frac{\partial c}{\partial z}\right)}_{III} + \underbrace{\frac{\partial}{\partial x}\left(K_{xx}\frac{\partial c}{\partial x}\right)}_{IV} - \underbrace{\frac{\partial cV_s}{\partial z}}_{V} - \underbrace{V_d A_v c}_{VI}. \qquad (3.1)$$

In Eq. 3.1, c is the concentration of dust, $\bar{u}$ is the time-averaged local streamwise velocity, K_{zz} and K_{xx} are respectively the vertical and horizontal turbulent mixing coefficients, V_s is the gravitational settling velocity, V_d is the horizontal deposition velocity onto the roughness elements, and A_v is the effective deposition area per volume of space and includes the ground surface. Equation 3.1 is an ensemble-averaged equation; hence, c and $\bar{u}$ are ensemble-averaged quantities. Equation 3.1 is an unsteady equation, it simulates an emission, a vehicle trip, at the time t=0 s and the resulting advection downwind. The mass suspended over the initial mass, M_s/M_o, is a measure of the fraction of the initial plume that is still suspended at a given time and is found by integrating c over the spatial domain. The physical interpretation of the terms is as follows: term *I* is the local accumulation of dust; term *II* is the advection of dust by the mean flow; term *III* represents the turbulent diffusion in the vertical direction; term *IV* is the horizontal turbulent diffusion; term *V* is the gravitational setting; and term *VI* represents the total practical deposition sink to the vegetation. Term *VI* does not explicitly differentiate all of the different mechanisms associated with deposition onto roughness elements; rather, it combines the processes together into one lumped term. As noted above, this is a "quasi" 2D model because the velocity field is specified by a canopy profile model that is described in the following sections, not by a set of prognostic equations. The canopy model described herein does not explicitly resolve the geometry of the roughness elements (e.g., leaves or buildings), but rather accounts for net roughness effects

indirectly through parameterizations of $\bar{u}$, K_{zz} , and V_d. Preliminary results indicated that for typical wind speeds, the horizontal turbulent diffusion was much less than the horizontal advection. Hence, in our implementation, term *IV* is neglected in Eq. 3.1. For very low or zero wind speed problems, term IV should be included and estimates for K_{xx} may be obtained from classical turbulent diffusion references such as Turner (1990).

3.3.2 Deposition Model

Specifying the effective deposition area per unit volume A_V can be quite difficult for complex vegetative or anthropogenic surfaces, and the numeric value for V_d depends on the assumptions made regarding the surface area. However, the $V_d A_V$ product can be directly obtained from measurements of mass deposited per time and aerosol concentration. This combined term is treated as a single modeled sink parameter. Because the leaf area index is assumed constant with height in the canopy, the product $V_d A_V$ is assumed constant with height in the canopy (except at the bottom cell where it includes the ground surface). Because of the simplicity of this model, the term must be parameterized with experimental data. Here it has been adjusted to match the experimental data of Veranth et al. (2007). In addition, since no vegetative deposition occurs above the canopy, $V_d A_V = 0$ above the canopy.

The gravitational settling velocity V_s is specified for Stoke's flow using the simple model outlined in many texts, namely,

$$V_s = -\frac{1}{18}\frac{D_p^2 \rho_p g}{\mu} \tag{3.2}$$

Here, g is the gravitational acceleration constant (9.81 m-s^{-2}), ρ_p ,the density of the particle (taken as 2500 kg m^{-3} (Nickovic et al., 2001)) and μ, the dynamic viscosity of air (specified as 1.8×10^{-5} kg m s^{-1}). The model is valid for particle diameters in the range of $1\mu m \le D_p \le 20\mu m$. This formula assumes equilibrium between gravitational and viscous forces. Although the particles are also subjected to inertial forces, the viscous forces dominate at the size scales of the particles. For the simulations described in this work, a particle diameter of $7\mu m$ was used as the mass mean diameter of typical soil dust PM_{10}. Gravitational forces are modeled using the same approach as Nathan et al. (2002) and Katul et al. (2005).

3.3.3 Mean Wind Flow Model

For this work, a model that utilizes simple boundary layer parameterizations to include the effects of rough-wall canopy drag is implemented. The canopy drag model is essentially a simplification of the Macdonald (2000) urban canopy model that was based on the work of Cionco (1965). For the canopy model, the user is only required to input the height of the vegetation H_{can}, an upstream mean reference velocity $\bar{u}_{ref}$ at the reference height z_{ref}, the upstream aerodynamic roughness length z_o, the Monin-Obukhov length scale L, and a roughness specific attenuation coefficient a (described below). The upstream boundary layer profile is assumed to be logarithmic and is calculated as:

$$\frac{\bar{u}(z)}{\bar{u}_{ref}} = \frac{\ln\left(\frac{z}{z_o}\right) - \psi\left(\frac{z}{L}\right)}{\ln\left(\frac{z_{ref}}{z_o}\right) - \psi\left(\frac{z}{L}\right)}. \tag{3.3}$$

The measure of atmospheric stability used here is the Monin-Obukhov length scale $L = u_*^3 / [\kappa Q_o (g / T_o)]$, where T_o and Q_o are the absolute surface temperature and kinematic heat flux, respectively, u_* is the friction velocity, and $\kappa = 0.41$ is the von Karman constant. The stability parameters in Eq. 3.3 are given by Arya (2001):

$$\psi(z/L) = -5\left(\frac{z}{L}\right) \qquad z/L \geq 0 \qquad \text{Neutral and Stable}$$

$$\psi(z/L) = \ln\left[\left(\frac{1+x^2}{2}\right)\left(\frac{1+x}{2}\right)^2\right] - 2\tan^{-1} x + \frac{\pi}{2} \qquad z/L < 0 \qquad \text{Unstable}$$

where, $x = (1 - 15(z/L))^{1/4}$. Using the input specified for the upstream boundary layer parameters, an estimate for the upstream friction velocity is made by rewriting the previous equation in the form

$$\bar{u}(z) = \frac{u_*}{\kappa}\left[\ln\left(\frac{z}{z_o}\right) - \psi\left(\frac{z}{L}\right)\right], \tag{3.4}$$

and solving for u_*. As a first approximation, it is assumed that the upstream u_* and z_o values apply in the displaced log layer above the canopy. The velocity in the displaced log layer is given by the following equation:

$$\bar{u}(z) = \frac{u_*}{\kappa}\left[\ln\left(\frac{z-d}{z_o}\right) - \psi\left(\frac{z-d}{L}\right)\right]. \tag{3.5}$$

To complete the solution, the velocity at the canopy height within the vegetation $\bar{u}_{Hcan} = \bar{u}(z = H_{can})$ and the displacement height, d, must be calculated. For simplicity, we assume that the flow within the canopy is independent of atmospheric stability and follow Cionco (1965), assuming that an exponential solution applies within the canopy and that the displaced log profile applies above the canopy. The exponential solution is given by:

$$\bar{u}(z) = u_{Hcan} \exp\left[a\left(\frac{z}{H_{can}} - 1 \right) \right]. \tag{3.6}$$

Here, a is the attenuation coefficient associated with specific types of roughness (Cionco, 1978). Larger values of a indicate an increased momentum sink associated with the roughness. The attenuation coefficient is dependent on a wide range of factors including: the flexibility, the shape, surface area, and spacing of the roughness elements (Cionco, 1965). Typical values of a for different types of vegetation are provided in Table 3.1. Some generalizations for the calculation of the attenuation coefficient exist such as Macdonald (2000) for idealized building arrays and Cionco (1965) for vegetation. Generally, however, a values must be obtained by measuring velocity profiles within the canopy and fitting an exponential solution to them.

Other parameterizations for the wind profile within canopies include Massman et al. (1997) and Poggi et al. (2007). Inputs for these profiles include: a foliage drag coefficient, a foliage leaf area density function, and a foliage shelter factor for momentum. These parameterizations reduce to Eq. 3.6 when the three aforementioned

variables are assumed constant over the canopy height. This assumption is made in this current work. Following Massman et al. (1997) and using the Poggi (2007) relationship, $u_*/u_{Hcan} = 0.3$ and assuming negligible sheltering, it is possible to relate a to the "canopy drag length scale," i.e., $L_d = 0.18a$. L_d is defined as the product of the integrated foliage drag coefficient and the leaf area index. Note that this approximation would only be valid when using the current model to simulate flow through vegetation, not buildings.

Up to this point, the method is very similar to the technique proposed by Macdonald (2000). Here, we diverge from Macdonald's method by forcing the velocities and the slopes of the velocity profiles to be matched at the canopy height H_{can}. This simplifies Macdonald's method by eliminated a matching layer and fixes the values of d and $\bar{u}_{Hcan}$. The displacement height d and $\bar{u}_{Hcan}$ are then obtained by solving the following two equations:

$$\frac{H_{can}}{H_{can}-d}\phi\left(\frac{H_{can}-d}{L}\right) = a\frac{\bar{u}_{Hcan}\kappa}{u_*} \tag{3.7}$$

$$\bar{u}_{Hcan} = \frac{u_*}{\kappa}\ln\left(\frac{H_{can}-d}{z_o}\right) - \psi\left(\frac{H_{can}-d}{L}\right). \tag{3.8}$$

The universal stability functions are given by Arya (2001) as:

$$\phi\left(\frac{z-d}{L}\right) = 1+5\left(\frac{z-d}{L}\right) \quad \text{for} \quad z/L \geq 0 \quad \text{Neutral and Stable}$$

$$\phi\left(\frac{z-d}{L}\right) = \left(1-15\frac{z-d}{L}\right)^{-1/4} \quad \text{for} \quad z/L < 0 \quad \text{Unstable}$$

Since Eq. 3.7 and 3.8 are not explicit in d, a numerical method is required to obtain a solution. For the solutions given here, a simple iterative bisection method was used (Chapra and Canale, 2006). Figure 3.2 shows an example of three different velocity profiles with identical input parameters except for upstream stability.

3.3.4 Turbulence Model

The vertical turbulent flux of particle concentration within the vegetation is modeled using a simple gradient method, namely

$$-\overline{w'c'} = K_{zz}\frac{\partial c}{\partial z}$$

as shown in Eq. 3.1. In the present model, it is assumed that the concentration diffusion coefficient K_{zz} is the same as the momentum diffusion coefficient. Hence, upstream of the canopy a simple log law boundary layer model is used where K_{zz} is specified based on Monin-Obukhov similarity as

$$K_{zz} = \frac{\kappa u_* z}{\phi(z/L)}. \tag{3.9}$$

Within the canopy, a mixing length model that is independent of atmospheric stability is assumed and specified in the form:

$$-\overline{u'w'} = l^2\left(\frac{\partial \bar{u}}{\partial z}\right)^2 = K_{zz}\frac{\partial u}{\partial z}. \tag{3.10}$$

In Eq. 3.10, the velocity gradient is calculated directly using finite differences from the mean flow field. Above the canopy, the mixing length scale is modeled as the sum of the canopy length scale (l_{cu}) and the surface layer length scale (l_{sl}) (i.e., $l = l_{cu} + l_{sl}$), where the mixing length l_{sl} is given by

$$l_{sl} = \frac{k(z-d)}{\phi\left(\frac{z-d}{L}\right)}. \tag{3.11}$$

Within the canopy, the mixing length is broken up into an upper l_{cu} ($z/H_{can} > 0.3$) and lower l_{cl} ($z/H_{can} \le 0.3$) canopy mixing length following Cionco (1965). For $0.3H_{can} < z \le H_{can}$, the mixing length is assumed constant and modeled following Macdonald (2000) by substituting Eq. 3.6 into Eq. 3.10 and solving for the mixing length at $z = H_{can}$. This model assumes that the shear stress at the canopy height is the same as the shear stress in the surface layer. This yields the following approximation for the mixing length in the upper part of the canopy:

$$l_{cu} = \frac{H_{can}u_*}{a\bar{u}_{Hcan}}. \tag{3.12}$$

For $z/H_{can} \leq 0.3$, the mixing length is assumed to increase linearly from zero at the ground to the value predicted by Eq. 3.12 at $z/H_{can} = 0.3$. It should be noted that although the conditions in the canopy are assumed independent of stability, a dependence of stability is introduced by using the value of d obtained by matching the exponential and logarithmic curves as described in Section 3.3 above.

3.3.5 Numerical Implementation

The velocity parameterizations described above assume horizontal homogeneity. In the actual simulations, there was a finite fetch F between the road and the start of the roughness elements (see Figure 3.1b). A rough wall turbulent boundary layer (Eq. 3.3, with $z_o/H_{can} = 0.02$) was assumed upwind of the vegetative canopy; the flow was immediately assumed to follow the canopy profiles parameterizations within the vegetation. To eliminate this discontinuity, the initial flow field was forced to be mass consistent via a classical variational analysis procedure (Sherman, 1978). The resulting mass consistent wind field and turbulence models described above were input into a numerical simulation of Eq. 3.1 using Matlab subject to the following boundary conditions: $dc/dx = 0$ at the inlet and outlet, $dc/dz = 0$ at the top of the domain, and $c = 0$ at the ground. The dust cloud was initialized with a uniform concentration of c_o = 75 mg-m^{-3} over a rectangular region centered on the road with a height H_{dc} and width W_{dc}. The height was varied throughout the simulations but the cloud width was fixed at 3 m corresponding to the width of a typical travel lane. The spatial domain was rectangular with a streamwise length of 630m and a height of 50m. The fetch F from the center of the road to the upwind edge of the domain was 30m for the simulations.

The spatial domain was discretized using finite volumes (Versteeg and Malalasekera, 1995). The advective terms were modeled by a first-order upwind finite difference to insure numerical stability. The diffusive terms were modeled using second-order central differences because the diffusive terms were not subject to numerical instabilities. The body terms are exact and the temporal dependence of Eq. 3.1 is modeled using an Alternating Direction Implicit (ADI) technique (Anderson, 1995). Variable time steps are used during a typical 125s simulation. Smaller time steps of the order of 0.01s are used in the first 10s. Larger time steps of the order of 0.25 to 1s are used for the rest of the simulation. To minimize computational effort, a nonuniform mesh is utilized by solving Eq. 3.1 on a logarithmic mesh (Anderson, 1995). The grid is stretched both in the vertical and horizontal directions with stretching factors of 0.07 and 0.004, respectively, which yielded the minimum grid sizes in vertical and horizontal directions of 5.6 cm and 50.8 cm, respectively. A typical simulation runs on a Celeron PC laptop in about two and one half minutes. This involves about 30,000 nodes (300 in the streamwise direction and 100 in the vertical) and 500 time steps. The large number of time steps is necessary to ensure mass conservation of the dust particles. This is done by running each time step twice, once without vegetative deposition and another with vegetative deposition (Boybeyi, 2000; Schieffe and Morris, 1993).

3.4 Results

3.4.1 Turbulence Model

Figure 3.3 illustrates the performance of the mixing length model (Eq. 3.12) against a number of experimental data sets. The data set was compiled from a wide range of wind tunnel and field experiments described in Table 3.1. An average value for the in-

canopy mixing length was calculated directly from the available data sets using Eq. 3.10 and then compared to Eq. 3.12. With the exception of the Seginer et al. (1976) wind tunnel study of flow through surface mounted cylinders, the data appear to be quite linear over the range $0.076 < u_* / (au_{Hcan}) < 0.36$. Linear regressions of the data yields a best fit of $l_{cu} / H_{can} = 0.7(u_* / au_{Hcan}) + 0.07$ with $R^2 = 0.89$. Hence, the model tends to underpredict the mixing length in the canopy.

Figure 3.4 shows the modeled momentum fluxes in the canopy compared to measured fluxes separated into (a) low, (b) medium, and (c) high attenuation coefficients. The model matches the data quite well in the majority of the canopies; however, it underpredicts turbulence in the upper ~25 % of dense (a > 2.5) canopies by as much as ~20%.

3.4.2 Road Dust Simulation

A number of factors determine the fraction of the initial dust cloud deposited onto roughness elements. In this work, we focus on the effects of roughness length, atmospheric stability, and deposition effectiveness of the canopy. In order to maintain this focus, a test canopy with dimensions similar to a real unpaved road was implemented as described in Section 3.5. In addition, the dimensionless initial dust cloud height was $H^* = H_{can} / H_{dc} = 1/2$ and a dimensionless fetch $F^* = F / H_{can} = 2$ was utilized. This example case is representative of relatively small bushes adjacent to an unpaved road (typical of an arid environment), but would not be representative of a dirt road near the edge of a tall forest where $H^* >> 1$ and $F^* << 1$. Figure 3.5a shows the effect of three different attenuation coefficients on the mass fraction of suspended particles (M_s/M_o) as a

function of dimensionless advection time for neutral atmospheric stability. Here, M_o is the initial mass in the dust cloud and M_s in the mass remaining in the air at some later time. In this simulation, the deposition term $V_d A_V$ was held constant such that the effect of the modeled wind profile and turbulence within the canopy were isolated. As expected, more dense canopies result in higher attenuation coefficients, reduced wind speed within the canopy, and enhanced deposition. Similarly, Figure 3.5b shows the effect of atmospheric stability on a canopy with a moderate attenuation coefficient (a = 2.25). For the case shown (with 2 m s^{-1} wind speed upstream and 2 m tall canopy) 30 m downstream of the road, there is a 67% reduction in M_s/M_o for the stable atmospheric stability case compared to the unstable case.

3.5 Discussion

Understanding the effectiveness of particle deposition onto various types of roughness is of great importance. A bulk measure of this effectiveness that utilizes the methodology outlined in this paper can be obtained by considering the ratio of the turbulent diffusion time scale to a deposition time scale. Here, the deposition time scale refers to the horizontal deposition associated primarily with impaction of the dust cloud onto roughness elements (i.e., "filtering") and may be defined as $\tau_d = (V_d A_v)^{-1}$. The inverse of this deposition time scale is also referred to by (Veranth et al., 2007) as the clearance frequency because it represents the fraction of particles in a control volume that are removed per unit time by deposition to vegetation and other surfaces. Another time scale associated with the time required for a particle to move out of the canopy (over a

height H_{can}) through turbulent diffusion can be defined as $\tau_t = H_{can}^2 / K_{zz}(H_{can})$. The ratio of these two time scales is

$$T^* = \frac{V_d A_v H_{can}^2}{K_{zz}(H_{can})} = \frac{\tau_t}{\tau_d} \tag{3.13}$$

In Eq. 3.13, $K_{zz}(H_{can})$ is the turbulent diffusivity at the top of the canopy. T^* provides a bulk metric to determine the expected deposition rate effectiveness of a canopy associated with the horizontal advection of dust. T^* is dependent on the specific geometry of the canopy, particle deposition physics, and atmospheric turbulence. Considering the limits of T^* is particularly useful. As $\tau_t / \tau_d \to \infty$, we expect that the suspended mass fraction $M_s / M_o \to 0$ because most of the particles should be removed from the air stream before they diffuse out of the canopy. Similarly, as $\tau_t / \tau_d \to 0$, M_s/M_o should approach the well-mixed case where horizontal deposition is of little importance (e.g., far downwind in Figure 1a) since the particulate cloud disperses rapidly compared to the time required to deposit particulate matter onto roughness elements. Figure 3.6 shows M_s/M_o as a function of the deposition rate effectiveness on a semilog plot. The plot is composed of three distinct regimes: (1) $T^* < 1$, turbulence rapidly mixes particles and M_s/M_o decreases slowly with increasing T^*, (2) $1 < T^* < 10$, M_s/M_o decreases rapidly as the importance of deposition increases, and (3) $T^* > 10$, M_s/M_o begins to decrease more slowly in response to very low particle concentrations in the canopy.

Figure 3.7 shows the effect of the ratio of the initial dust cloud height to the vegetative canopy height, H^* on mass fraction suspended at equivalent nondimensional

times after the start of the simulations. As expected, for short dust clouds $H^* >> 1$, much of the dust is removed as it is advected horizontally through the roughness elements. The mass fraction suspended rapidly decreases with increasing H^* until $H^* \sim 1$ as the importance of the horizontal impaction on the roughness elements increases. For $H^* < 0.25$, horizontal removal is insignificant and the problem approaches the classical well-mixed vertical deposition onto a surface case.

Figure. 3.8 summarizes the model's utility to help describe the effect of roughness and atmospheric stability on deposition in vegetative or building canopies. For highly unstable atmospheric conditions, significant changes in roughness result in very small changes in deposition. For stable atmospheric conditions, relatively small increases in roughness result in significantly enhanced deposition. For example, consider a canopy with an attenuation coefficient of 3.5 shown in Figure 3.8. The decrease in M_s/M_o from H_{can}/L = -0.2 to H_{can}/L = 0 is less than ~8%, while the decrease from H_{can}/L = 0 to H_{can}/L =-0.2 is ~35%. In addition, Figure 3.8 helps explain the discrepancy between the convective low vegetation Ft. Bliss results and the high roughness stable conditions for the Dugway Proving Ground experiment described in the introduction. The figure indicates that as atmospheric stability and surface roughness increase (increasing H_{can}/L and increasing a) M_s/M_o decreases. Hence, the very low roughness and convective conditions for Ft. Bliss favor transport while the high roughness and stable conditions of Dugway favor deposition.

One of the advantages of using the Eulerian transport model given in Eq. 3.1 is that it allows one to analyze and understand the contribution of each of the terms to the total transport. Figure 3.9 shows the contributions of the various terms from Eq. 3.1 20

meters downwind of the leading edge of the canopy with most of the plume still contained within the vegetation. Figure 3.9a shows the contribution of the plume 20 seconds after the start of the simulation. As expected, the deposition term (term *V*) is always a sink within the canopy (i.e., negative values) and zero above. The other three terms on the right-hand side of Eq. 3.1(term *II*, III, and *IV*) may be positive or negative depending on vertical location and time. As shown in Figure. 3.9a, the mean streamwise advection is the dominant transport term. The sign of the advection term is positive near the ground ($0 < z/H_{can} < 0.14$) and negative for $z/H_{can} > 0.14$. Since the velocities are nearly constant in the streamwise direction, the advection term is dominated by the streamwise gradient of the concentration. Hence, where term *II* is positive, the concentration is increasing with streamwise distance and where term *II* is negative, the concentration must be decreasing. Due to the directional behavior of advection, this is equivalent to stating that at higher elevations the dust plume is advected downwind at a greater rate than at the bottom of the canopy where velocities are very low. That is, the higher locations are observing the departure of the bulk of the dust plume, while lower heights are still observing the cloud's arrival.

The vertical turbulent diffusion (term *III*) is dependent on the gradient of the product of the local vertical concentration gradient and K_{zz}. Since K_{zz} increases monotonically, term *III* follows the curvature of the concentration profile. Hence, term *III* is positive below the lowest inflection point in the concentration profile ($z/H_{can} < 0.1$), negative from $0.1 < z/H_{can} < 0.22$ and positive again $z/H_{can} > 0.22$. This is intuitively expected, as the concentration will decrease near the peak and increase at the tails due to diffusion. Since the settling velocity V_s is constant for a given simulation (one particle

size and type), the gravity settling (term *IV*) is only a function of the concentration gradient. Hence, for small particles, term *IV* takes on small positive values below the peak and negative values above the peak.

3.6 Conclusions

In this paper, we describe the development of a quasi-2D Eulerian atmospheric diffusion model applied to the transport and deposition of fugitive dust near an unpaved road. Specifically, this work addresses a gap in the literature associated with transport and deposition in the "impact zone" where horizontal deposition may be of importance. The primary attribute of the present modeling technique is that a user can investigate the effects of various deposition scenarios associated with different roughness and atmospheric stabilities, while only needing to supply a small number of difficult to obtain input parameters. Since the model also runs rapidly, a large number of cases can be run parametrically to investigate the importance of various input variables, allowing decision makers more information regarding planning scenarios.

The model also provides insight toward reconciling the differences between field experiments in the literature where large differences were observed in deposition rates for different stabilities and canopy roughness. The primary limitation of the model is the ability to accurately determine the vegetative deposition parameter, or so-called clearance frequency. To understand the clearance frequency better, a dimensionless parameter called the deposition effectiveness is identified. It can be used to estimate deposition in the canopy. In general, the model captures the essential physics of near-source dust transport and provides a tool that that can efficiently simulate site-specific conditions in practical situations.

3.7 Acknowledgements

This work was sponsored by the Strategic Environmental Research and Development Program project CP1190 and by Southwest Center for Environmental Research and Policy project A-02-7 and A-04-03. We also wish to thank Mr. Thomas Booth for his hard work and contributions to the mean wind model.

Table 3.1. Table of the various experimental data used in Figures 3.3 and 3.4. WT indicates wind tunnel measurements and Field indicates measurements that were acquired at full scale in the field. Note that the Moga forest data (originally acquired by Brunet, but unpublished) were adapted directly from Kaimal and Finnigan (1994).

Canopy Type	**Experiment**	**Reference**	**Attenuation Coefficient *a***	**Symbol**
Urban	WT	(Kastner-Klein and Rotach, 2004)	1.26	•
Triangular cylinders	WT	(Novak et al., 2000)	1.3	▲
Square cylinders	WT	(Novak et al., 2000)	2.0	◇
Square cylinders	WT	(Poggi et al., 2004)	1.0	■
Rectangular cylinders	WT	(Raupach et al., 1986)	0.84	×
Circular cylinders	WT	(Novak et al., 2000)	3.0	+
Circular cylinders	WT	(Seginer et al., 1976)	1.7	●
Wheat	WT	(Brunet et al., 1994)	1.6	◆
Corn field	Field	(Shaw et al., 1974)	2.4	▲
Corn field	Field	(Wilson et al., 1982)	4.1	△
Moga forest	Field	(Kaimal and Finnigan, 1994)	1.7	■
Bordeaux forest	Field	(Brunet et al., 1994)	3.2	□
Uriarra forest	Field	(Denmead and Bradley, 1987)	1.7	○

a)

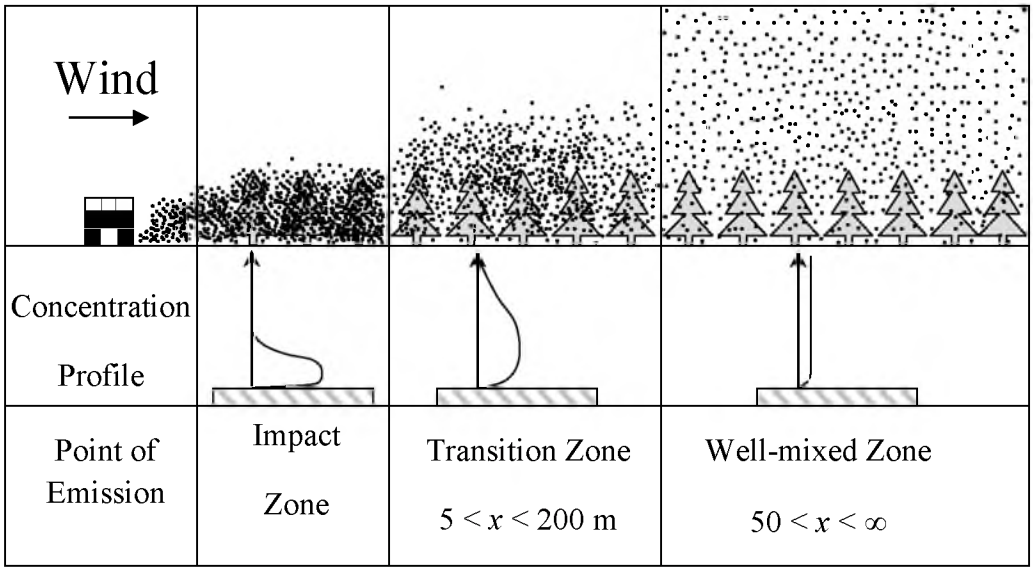

(b)

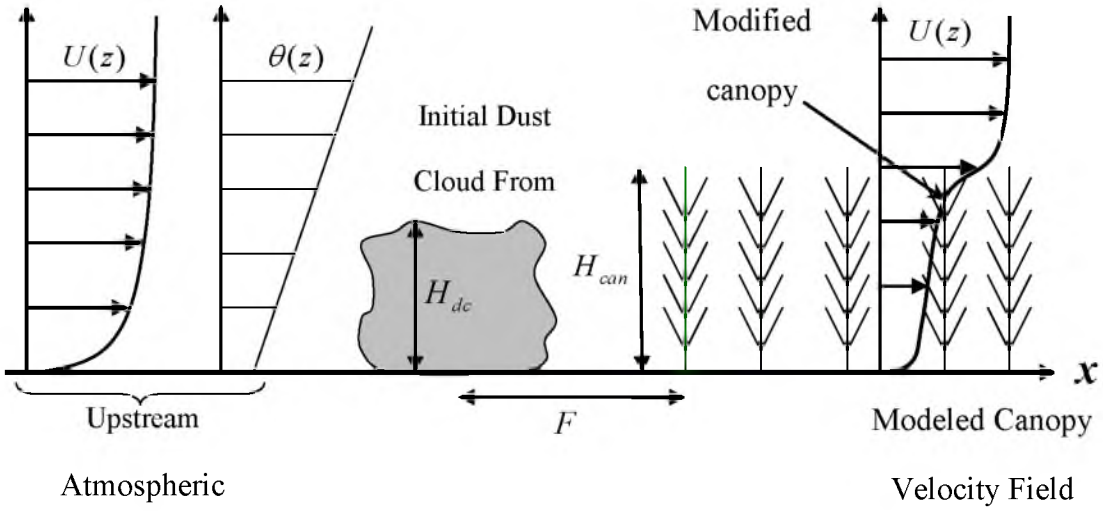

Figure 3.1. Illustration of dust transport downwind of unpaved roads. (a) Limiting cases in dust transport (adapted from Etyemezian et al. 2004). (b) Schematic defining the basic fugitive dust cloud problem in the impact zone.

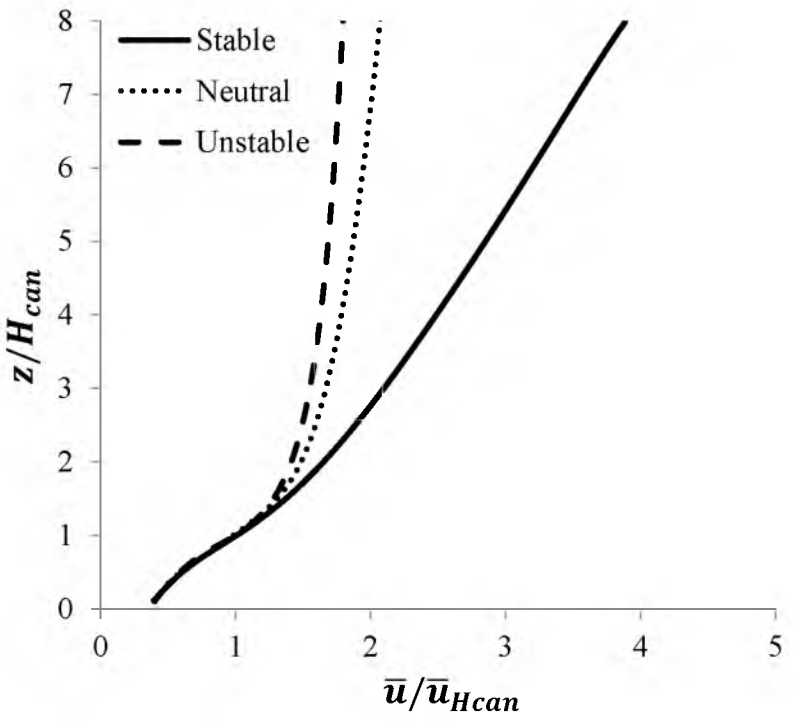

Figure 3.2. Mean wind speed profiles using the canopy velocity model described in Section 3.3.3 H_{can} is the height of the canopy, u is the mean wind speed and u_{Hcan} is the velocity at $z = H_{can}$. For these calculations, the attenuation was taken as $a = 1$ and the dimensionless stability parameters for the stable and unstable cases where $H_{can}/L = 0.2$ and $H_{can}/L = -0.2$, respectively.

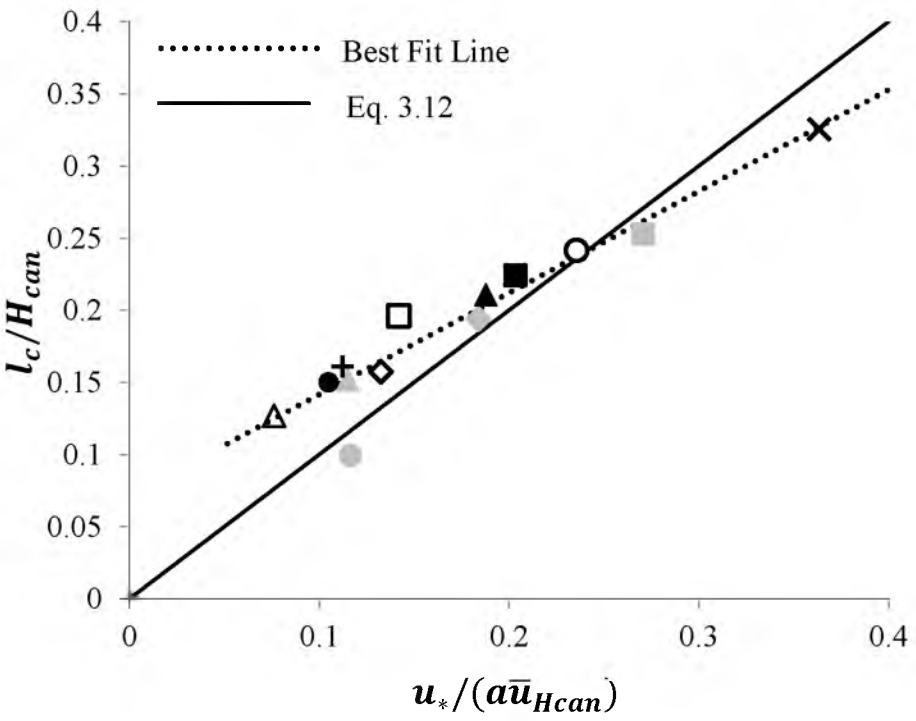

Figure 3.3. Dimensionless canopy mixing length, l_{cu}, model (Eq. 3.12) plotted with data from various roughness sources. The equation of the best fit line is given by $l_{cu}/H_{can} = 0.7\left(u_*/a\bar{u}_{Hcan}\right) + 0.07$ with $R^2 = 0.89$. Definitions of the symbols are given in Table 3.1.

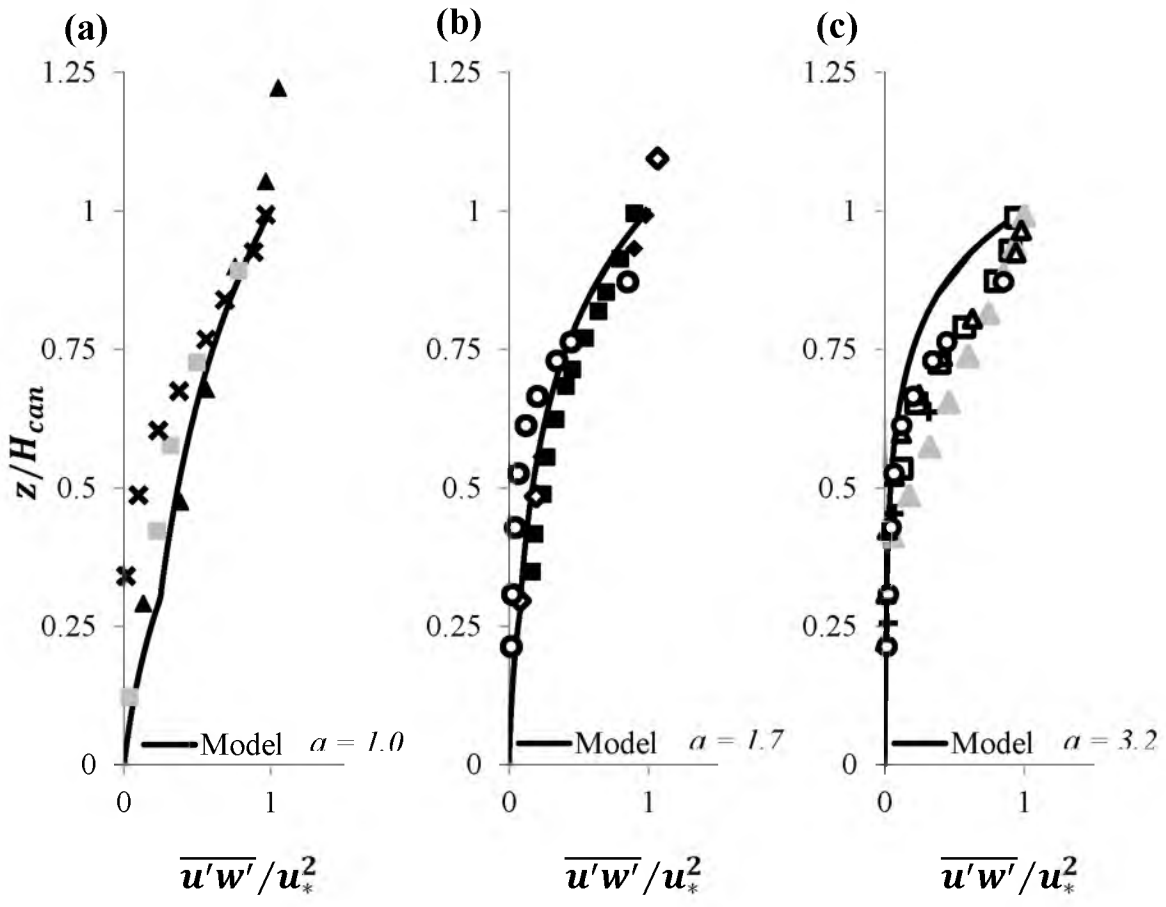

Figure 3.4. Modeled and experimental vertical profiles of the normalized momentum flux for (a) lower $0.84 \le a \le 1.3$, (b) moderate $1.6 \le a \le 2.0$ and (c) higher $2.4 \le a \le 4.1$ attenuation coefficients. Definitions of the symbols are given in Table 3.1.

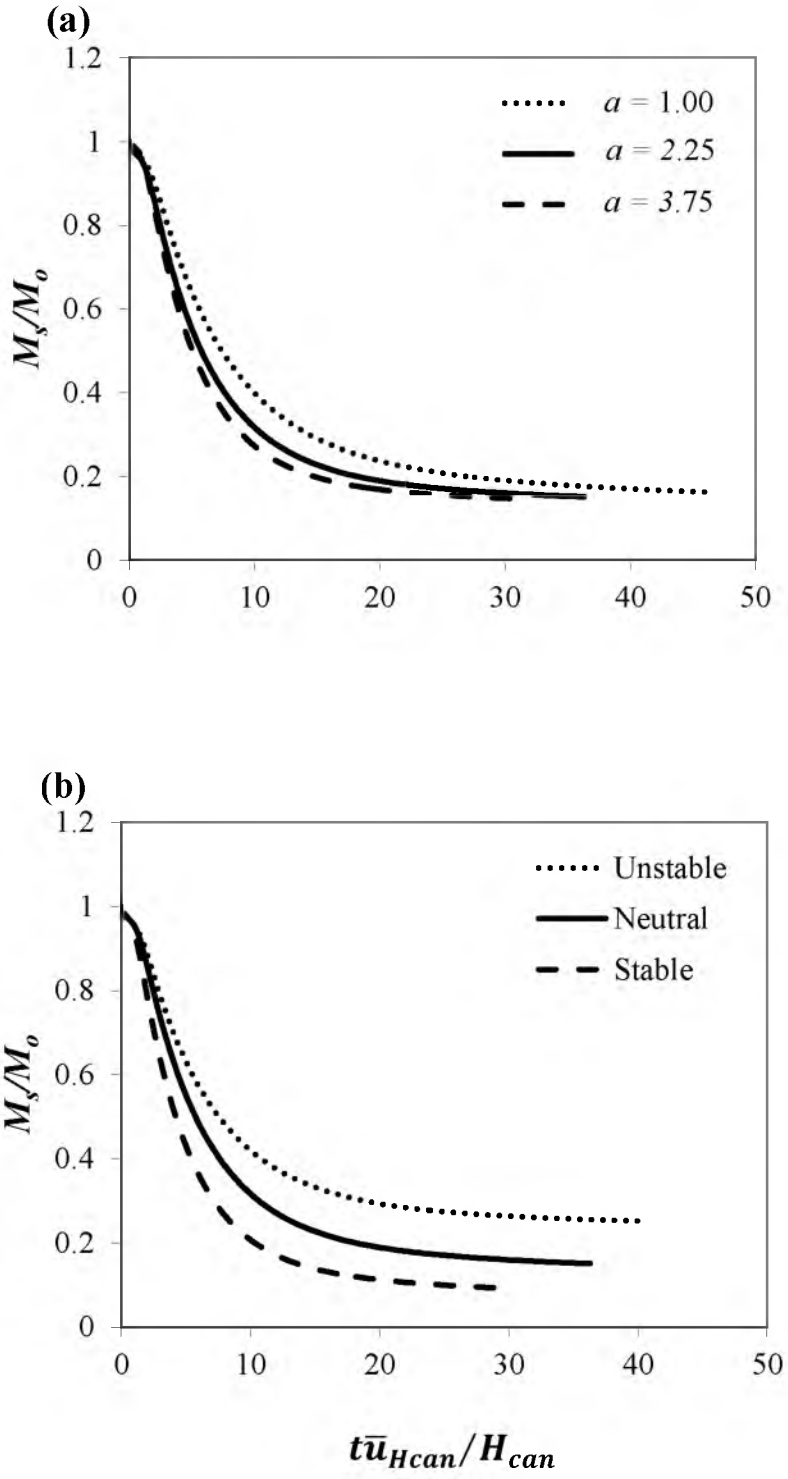

Figure 3.5. Mass fraction of suspended particles, M_s/M_o as a function of nondimension advection time, tu_{Hcan}/H_{can}, for (a) three canopies with different attenuation coefficients (and corresponding T^* = 8.5, 17, 27 for a = 1.0, 2.25 and 3.75) and neutral stability; (b) and for a canopy with a = 2.25 and T^* = 17 with different atmospheric stabilities (stable: H_{can}/L = 0.2, unstable: H_{can}/L = -0.2).

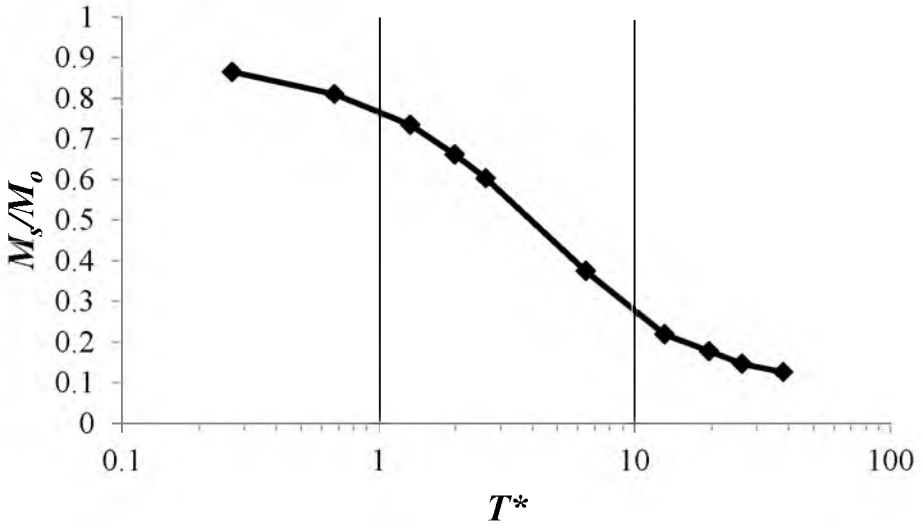

Figure 3.6. Mass fraction of suspended particles, M_s/M_o, as a function of the deposition rate effectiveness, T^*, for ($a = 3.25$, $F^* = 2$, $H^* = 1$, $u_{Hcan}t / H_{can} = 20$). Vertical grid lines indicate three different regimes as noted in text. Note that as T^* approaches zero M_s/M_o should approach the fraction suspended for flow over a flat wall.

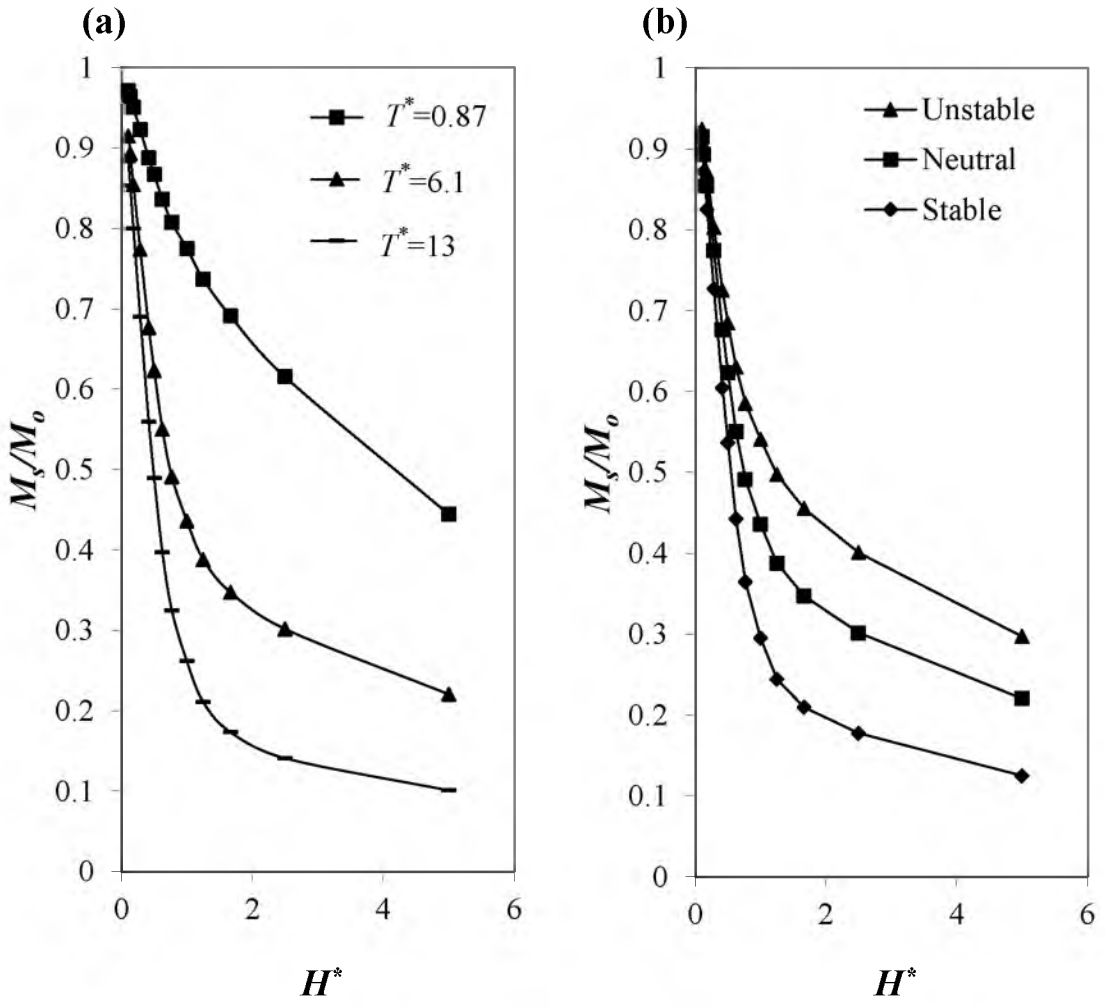

Figure 3.7. Mass fraction of suspended particles, M_s/M_o , as a function of dimensionless dust cloud height, H^*, for (a) varying deposition effectiveness, T^*, (neutral stability, a = 2.25, $F^* = 2$, $tu_{Hcan}/H_{can} = 10$) and (b) varying atmospheric stability (a = 2.25, $F^* = 2$, $tu_{Hcan}/H_{can} = 10$, $T^* = 6.1$).

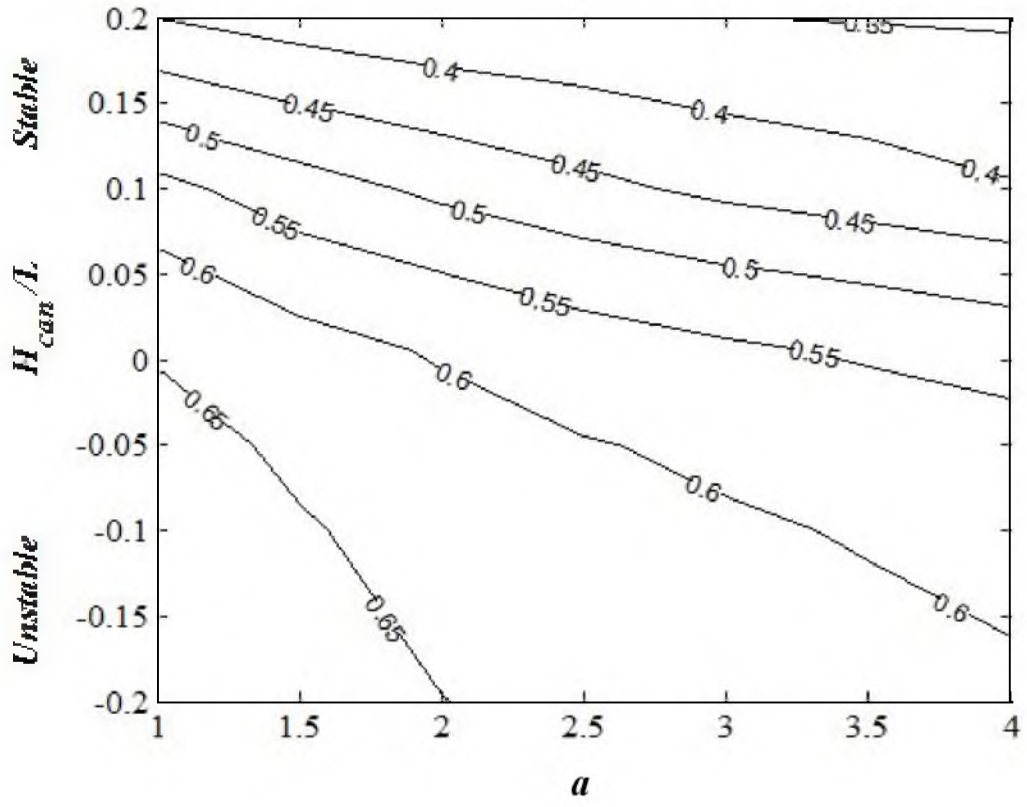

Figure 3.8. Contour plot of M_s/M_o illustrating the effect of atmospheric stability (H_{can}/L) and roughness (a) on mass fraction of suspended particles, M_s/M_o, for a hypothetical vegetative canopy. ($H^* = 1$, $A_v V_d = 0.01$ s^{-1}, $F^* = 2$, $tU_{Hcan}/H_{can} = 20$).

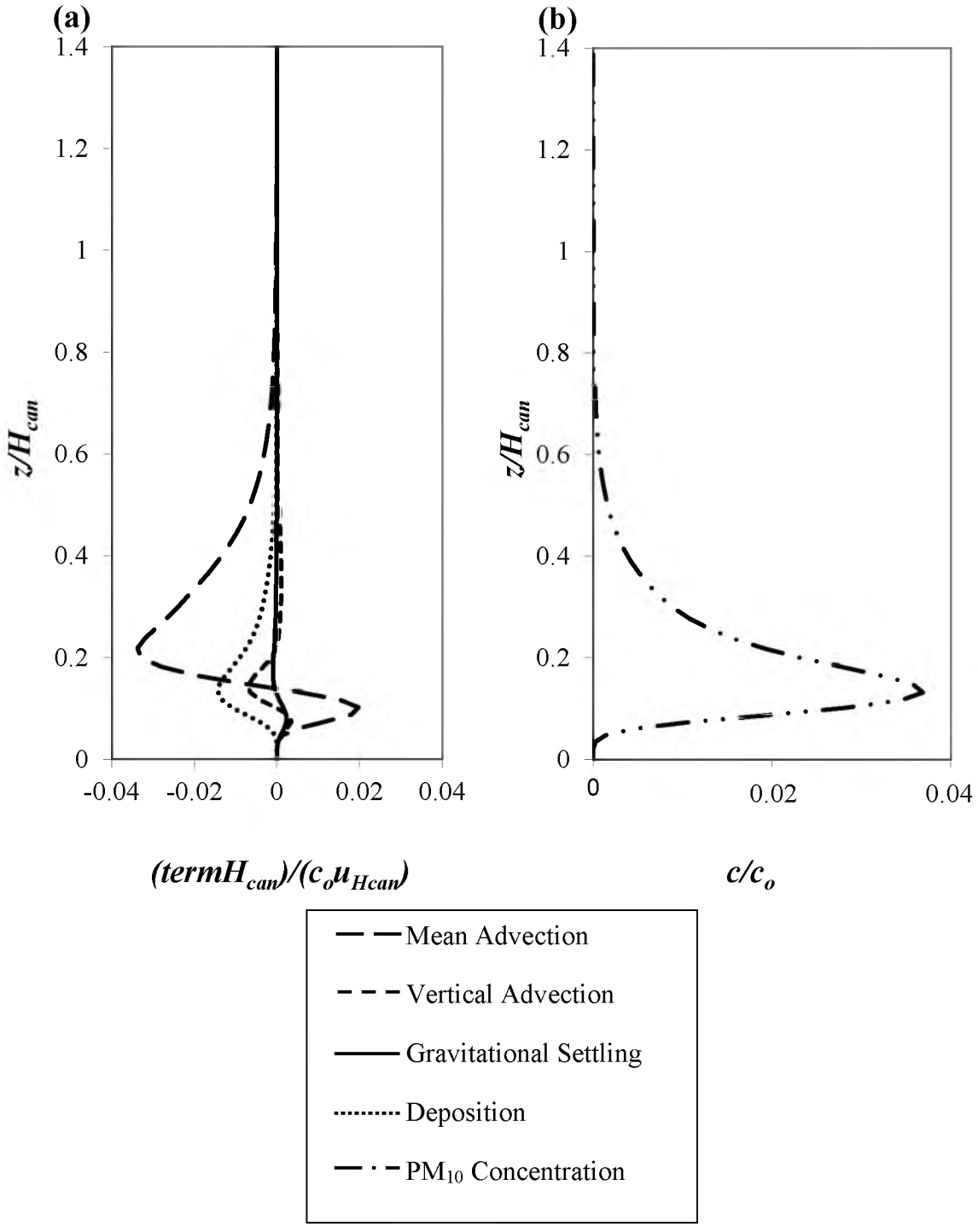

Figure 3.9.Illustration of transport terms of Eq. 3.1 together with PM_{10} concentration profiles. (a) Nondimensional vertical variation of the various terms in the ADE transport equation, Eq. 3.1 ($a = 2.25$, $H^* = 1$, $F^* = 2$, $T^* = 22$, $tu_{Hcan}/H_{can} = 6$).(b) Vertical concentration profile normalized by the initial concentration, c_o, at the identical time t = 20 s and location x = 20 m.

3.7 References

Anderson, J.D., 1995: *Computational fluid dynamics*. McGraw Hill, New York.

Aylor, D.E. and T. K Flesch, 2001: Estimating spore release rates using a Lagrangian stochastic simulation model. *Journal of Applied Meteorology*, **40**, 1196-1208.

Belcher, S.E., 2005: Mixing and transport in urban areas. *Philosophical Transactions of the Royal Society A*, **363**, 2947-2968.

Boybeyi, Z., 2000: *Mesoscale atmospheric dispersion*. WIT Press, Boston.

Britter, R.E. and S. R. Hanna, 2003: Flow and dispersion in urban areas, Annual. Review of Fluid Mechanics, **35**, 469-496.

Brunet, Y., J. J. Finnigan, and M. R. Raupach, 1994: A wind tunnel study of air flow in waving wheat: single-point velocity statistics. *Boundary-Layer Meteorology*, **70**, 95-132.

Caffrey P.F., J. M. Ondov, J. Maria, Zufall, and C. I. Davidson, 1998: Determination of size-dependent dry particle deposition velocities with multiple intrinsic elemental tracers. *Environmental Science Technology*, *32*, 1615–1622.

Chamberlain, A.C., 1975: The movement of particles in plant communities. *Vegetation and the Atmosphere*, **1**, 155-203.

Chapra, S.C. and R. P. Canale, 2006: *Numerical methods for engineers*. McGraw Hill, New York.

Cionco, R.M., 1965: Mathematical model for air flow in vegetative canopy. *Journal of Applied Meteorology*, **4**, 517-522.

Cionco, R.M., 1978: Analysis of canopy index values for various canopy densities. *Boundary-Layer Meteorology*, **15**, 81-93.

Davidson, C.I., R. F. Phalen, and P. A. Solomon, 2005: Airborne particulate matter and human health: A review. *Aerosol Science & Technology*, **39**, 737-749.

Denmead, O.T. and E. F. Bradley, 1987: On scalar transport in plant canopies. Irrigation Science, **8**, 131-149.

Etyemezian, V., S. Ahonen, D. Nikolic, J. Gillies, H. Kuhns, D. Gillette, and J. Veranth, 2004: Deposition and removal of fugitive dust in the arid southwestern United States: measurements and model results. *Journal of the Air and Waste Management Association* **54**, 1099-1111.

Finnigan, J.J., 2000: Turbulence in plant canopies. *Annual. Review of Fluid Mechanics*, **32**, 519-571.

Katul G.G., A. Porporato, R. Nathan, M. Siqueira, M. B. Soons, D. Poggi, H. S. Horn, and S. A. Levin, 2005: Mechanistic analytical models for long-distance seed dispersal by wind. *The American Naturalist*, **166**, 3

Harley, R.A., S. E. Hunts, and G. R. Cass, 1989: Strategies for the control of particulate air quality: least-cost solutions based on receptor-oriented models. Environmental Science & Technology, **23**, 1007-1014.

Harman, I.N. and J. J. Finnigan, 2007: A simple unified theory for flow in the canopy and roughness sublayer. Boundary-Layer Meteorology, **123**, 339-363.

Hicks B.B., 2006: Dry deposition to forests, *On the use of data from clearings. agricultural and forest Meteorology,* **136**, 214-221.

Kaimal, J.C. and J. J. Finnigan, 1994: *Atmospheric boundary layer flows: Their structure and measurement*. Oxford University Press US.

Kastner-Klein, P. and M. W. Rotach, 2004: Mean flow and turbulence characteristics in an urban roughness sublayer. *Boundary-Layer Meteorology*, **111**, 55-84.

Macdonald, R.W., 2000: Modelling the mean velocity profile in the urban canopy layer. *Boundary-Layer Meteorology*, **97**, 25-45.

Massman W.J.,1997: An analytical one-dimensional model of momentum transfer by vegetation of arbitrary structure. *Boundary-Layer Meteorology*, **83**, 407-421.

Nathan R., G. G. Katul, H. S. Horn, S. M. Thomas, R. Oren, R. Avissar, S. W. Pacala, and S. A. Levin, 2002: Mechanisms of long-distance dispersal of seeds by wind. *Nature*, **418**,409-413.

Nicholson, K.W., 1988: The dry deposition of small particles: A review of experimental measurements. *Atmospheric Environment*, **22**, 2653-2666.

Nickovic, S., G. Kallos, A. Papadopoulos, and O. Kakaliagou, 2001: A model for prediction of desert dust cycle in the atmosphere. *Journal of Geophysical Research*, **106**, 18113-18130.

Novak, M.D., J. S. Warland, A. L Orchansky, R. Ketler, and S. Green, 2000: Wind tunnel and field measurements of turbulent flow in forests. Part I: uniformly thinned stands. *Boundary-Layer Meteorology*, **95**, 457-495.

Pace, T.G., 2005: Methodology to estimate the transportable fraction (TF) of fugitive dust emissions for regional and urban scale air quality analyses, USEPA.

Poggi, D., and G. G. Katul, 2007: Turbulent flows on forested hilly terrain: the recirculation region. *Quarterly Journal of the Royal Meteorological Society*, **133**, 1027-1039

Poggi, D., A. Porporato, L. Ridolfi, J. D. Albertson, and G. G. Katul, 2004: The effect of vegetation density on canopy sub-layer turbulence. *Boundary-Layer Meteorology*, **111**, 565-587.

Ramaswami, A., J. B. Milford, and M. J. Small, 2005: *Integrated environmental modeling: pollutant transport, fate and risk in the environment*. Wiley.

Raupach, M.R., and B. J. Legg, 1986: Experiments on scalar dispersion within a model plant canopy. Part I: The turbulence structure. *Boundary-Layer Meteorology*, **35**, 21-52.

Raupach, M.R. and A. S. Thom, 1981: Turbulence in and above plant canopies. *Annual Review of Fluid Mechanics*, **13**, 97-129.

Raupach, M.R., N. Woods, G. Dorr, J.F. Leys, and H.A., Cleugh, 2001: The entrapment of particles by windbreaks. *Atmospheric Environment*. **35**,3373–3383.

Schieffe, R.D. and R. E. Morris, 1993: A review of the development and application of the urban airshed model. *Atmospheric Environment*, 27, 23-29.

Seginer, I., P. J Mulhearn, E. F. Bradley, and J. J. Finnigan, 1976: Turbulent flow in a model plant canopy. *Boundary-Layer Meteorology*, **10**, 423-453.

Sehmel, G.A., 1980: Particle and gas dry deposition- A review. *Atmospheric Environment*, **14**, 983-1011.

Seinfeld, J.H. and S. N. Pandis, 1998: *Atmospheric chemistry and physics - from air pollution to climate change.* Wiley, Hoboken.

Shaw, R.H., R. H. Silversides, and G. W. Thurtell, 1974: Some observations of turbulence and turbulent transport within and above plant canopies. *Boundary-Layer Meteorology*, **5**, 429-449.

Sherman, C.A., 1978: A mass-consistent model for wind fields over complex terrain. *Journal of Applied. Meteorology*, **17**,: 312-319.

Slinn, W.G.N., 1982: Predictions for particle depostion to vegetative canopies. *Atmospheric Environment*, **16**, 1785-1794.

Turner, D. B., 1970: Workbook of atmospheric dispersion estimates. Washington, U.S. Government Printing Office.

Veranth, J.M., G. Seshadri, and E. Pardyjak, 2003: Vehicle-Generated Fugitive Dust Transport: Analytic Models and Field Study. *Atmospheric Environment*, **37**, 2295-2303.

Veranth, J.M., S. O. Speckart, F. Yin, V. Etyemezian, and E. R. Pardyjak, 2007: Near-source deposition of vehicle-generated fugitive dust on vegetative surfaces and buildings, part II: Field deposition measurements and model validation submitted to *Atmospheric. Environment*.

Versteeg, H.K. and W. Malalasekera, 1995: *An introduction to computational fluid dynamics–the finite volume approach*. Longman Scientific & Technical.

Watson, J.G. and J. C. Chow, 1994: Clear sky visibility as a challenge for society. *Annual Review Energy Environment*, **19**, 241-266.

Watson, J.G. and J. C. Chow 2000: Reconciling urban fugitive dust emissions inventory and ambient source contribution estimates: Summary of current knowledge and needed research. DRI Document.

Wilson, J.D., D. P. Ward, G.W. Thurtell, and G. E. Kidd, 1982: Statistics of atmospheric turbulence within and above a corn canopy. *Boundary-Layer Meteorology*, **24**, 495-519.

CHAPTER 4

REMOVAL OF PM_{10} IN THE NEAR-SOURCE ZONE DOWNWIND OF UNPAVED ROADS PART 2: QUANTIFYING NEAR-SOURCE CAPTURE

The content of this chapter is ready for submission to the peer-reviewed journal Atmospheric Environment.

4.1 Abstract

A simple, quantitative formula analogous to the Pace (2005) model for near-source capture of vehicle-generated PM_{10} from unpaved roads is developed for routine net-emission calculations used in regional air quality monitoring. The formula has two variables: H^* the ratio of the canopy height to the height of the initial roadside plume, which is related to the probability of a particle entering the canopy; and T_m^*, which is a surrogate for the probability of deposition for a particle within the canopy. The formula contains coefficients that have been determined by a least squares best fit to Lagrangian dispersion simulations varying H^* and T_m^*. It is found that the fraction transmitted is related to H^* and T_m^* by: $(1 - \exp(-2.8H^*))\exp(-2.0T_m^{*0.64}) + \exp(-2.8H^*)$. In order to parameterize the Raupach et al. (2001) deposition model for use in the Lagrangian dispersion simulations, the results from three previous field studies are utilized to determine an appropriate value for vegetative element size in the deposition model.

4.2 Introduction

Vehicle traffic on unpaved roads is a source for the US EPA regulated pollutant PM_{10}. These emissions are currently estimated using the EPA AP-42 model (EPA, 2006). It has been proposed that the interaction of a PM_{10} plume with downwind roughness elements acts to remove a portion of the suspended mass (Watson and Chow, 2000). The removed fraction is referred to as the captured fraction, (*CF*), while the fraction of the plume that remains airborne and is transported into the regional air shed is referred to as the transmitted fraction, (*TF*). Pace (2005) introduced a simple conceptual model relating *TF* to the height and density of the downwind roughness elements (see Figure 1.1). As downwind roughness height and density increase, a smaller fraction of the roadside emission of PM_{10} is transported downwind. Pace (2005) suggested a number of *TF* estimates for vegetation of given heights. These *TF*s are shown in Table 1.1 and are referred to as near-source capture (NSC).

Pace (2005) "welcomes further refinement" to his conceptual model and this work is a response to the invitation. A simple mathematical formula is developed that is analogous to the Pace (2005) conceptual model and accounts for varying vegetation height (which indicates the probability of a particle entering the canopy), as well as vegetative density along and atmospheric stability (which indicate the probability of particle deposition within the canopy). The formula has coefficients that are determined by a least squares regression to 56 QUIC-PLUME (Singh et al., 2011) Lagrangian dispersion simulation results for *TF* under varying vegetative height and density conditions.

Three field studies conducted in the western and southwestern United States have measured *TF*; their results are used in this study to parameterize the deposition model

(Judd et al., 2001) utilized in the Lagrangian dispersion simulations. The sites of the three field studies have well-characterized canopies (height measurements for roughness with an infinite fetch) and characterized meteorological conditions (measurements of vertical profile of mean winds). The density of the canopies can be calculated by utilizing the measurement of canopy height and the meteorological measurements as outlined in this work. The locations of the experiments are: Dugway, UT (Veranth et al., 2003), Ft. Bliss, TX (Etyemezian et al., 2004) and Las Cruces, NM (Speckart et al., 2013). The field studies span measured *TF*s from 1.0 to 0.15 and aerodynamic roughness, z_o (Ayra, 2001) from 0.005 to 0.71 m.

4.3 Methods

4.3.1 Canopy Model

A simple canopy model is utilized to relate local roughness conditions to PM_{10} near source capture (NSC). The aggregate of roughness elements, which are assumed continue to indefinitely downwind of the road, comprise a canopy. The roughness elements consist of vegetation, anthropogenic features, and small, < 0.5 m, terrain features. In the canopy model, the roughness elements present are unresolved; only the aggregate effects roughness elements are modeled. The canopy is horizontally homogeneous. The canopy height, H_{can}, is taken to be the height of the tallest elements within the canopy, and roughness density is assumed constant with height within the canopy. The effect of the streamlining is assumed negligible, the orientation of elements is assumed to be isotropic, and a single size is assumed to characterize the distribution of element sizes.

The density of roughness elements is measured by quantifying roughness element surface area per unit volume of canopy and is assumed to be distributed uniformly over the volume of the canopy. For vegetative elements, the vegetative density, α, (the vegetative surface area per unit volume of vegetative canopy) is calculated by estimating the leaf area index, LAI (the vegetative surface area per unit ground area covered by the canopy). Because roughness density is assumed to be distributed uniformly, $\alpha = LAI/H_{can}$. To obtain LAI, and subsequently α, this work utilizes meteorological data to calculate the aerodynamic roughness height, z_o, (Arya, 2001) which is related to LAI according to Eq. 4.1 (Choudhury and Monteith, 1988):

$$LAI = (z_o/(0.28H_{can}))^2/0.2. \quad (4.1)$$

In Eq. 4.1, the roughness due to larger scale surface irregularities, such as sand dunes, is assumed to have negligible effect upon z_o compared to the vegetation. LAI can also be determined by estimating z_o from a table of land surface types located in Ayra (2001). Additional methods for obtaining LAI include performing measurements in the field using devices such as the LAI-2200 (Licor, Inc. Lincoln, NE). These devices relate short-wave radiation scatter to infer LAI. Finally, LAI can be estimated from satellite data using the MODIS database: (http://daac.ornl.gov/cgibin/MODIS/GLBVIZ_1 Glb/modis_subset_order_global_col5.pl last accessed March 2013). Although α and LAI are defined for vegetative surface areas, this study computes α and LAI, including surfaces that are not vegetative (such as anthropogenic surfaces present in urban canopies).

Veranth et al. (2003) employed shipping containers to simulate an urban canopy. For urban canopies, a useful parameter to measure roughness element density is the frontal area density, A_f. A_f is the ratio of the total frontal area of all the roughness elements to the total footprint for the array of roughness elements.

The mean wind and vertical turbulent mixing, both responsible for PM_{10} transport within a canopy, are modified by the presence of roughness elements; the magnitude of modification becoming greater with increasing roughness element density. For sparse canopies, canopies where the removal of momentum by vegetation is negligible, surface layer (the bottom layer of the atmosphere which is adjacent to the ground) parameterizations for mean wind and turbulent mixing are applied (Ayra, 2001). If removal of momentum by vegetation is significant, as indicated by a significant reduction in momentum within the canopy, mean wind and vertical turbulent mixing models specific to intermediate and dense canopies are utilized . These models for intermediate and dense canopies are presented in Pardyjak et al. (2008). This work uses wind data from the three field studies, Veranth et al. (2003), Etyemezian et al. (2004), and Speckart et al. (2013), to determine the appropriate choice of models (Ayra, 2001 or Pardyjak et al., 2008) for mean wind and vertical turbulent transport.

For the current work, the vertical turbulent transport out of the canopy is of critical importance and is estimated using Eq. 4.2:

$$K_{zz}(H_{can}) = \frac{\kappa u_*(H_{can} - d)}{\phi((H - d)/L}, \tag{4.2}$$

where K_{zz} is the turbulent mixing coefficient evaluated at H_{can}, κ is the von Karman constant =0.4, L is the Monin-Obukhov length scale defined as $L = u_*^3 / [\kappa Q_o (g / T_o)]$. T_o and Q_o are the absolute surface temperature and kinematic heat fluxes, respectively, u_* is the turbulent velocity scale, and $\phi(H\text{-}d)/L$ is the universal stability function given by Arya (2001) as:

$$\phi\left(\frac{H_{can}-d}{L}\right) = 1 + 5\left(\frac{H_{can}-d}{L}\right) \qquad H_{can}/L \geq 0 \quad \text{Neutral and Stable} \quad (4.3)$$

$$\phi\left(\frac{H_{can}-d}{L}\right) = \left(1 - 15\frac{H_{can}-d}{L}\right)^{-1/4}, \qquad H_{can}/L < 0 \quad \text{Unstable} \quad (4.4)$$

where d is the displacement height, which is negligible for sparse canopies and for intermediate and dense canopies can be determined from field measurements of $\bar{u}$ (the time averaged streamwise velocity) or modeled (Pardyjak et al., 2008).

Mean wind models within both sparse and dense canopies are important in this work. For sparse canopies, logarithmic profiles, such as $\bar{u} = u_*/\kappa\,(\ln(z/z_o) + \psi(z/L))$, where $\psi(z/L)$ is a stability function, are utilized (Ayra, 2001). For dense canopies, profiles such as $\bar{u} = \bar{u}_{Hcan}\exp(a(z/H_{can} - 1))$ where a is the attenuation coefficient and $\bar{u}_{Hcan}$ is the mean wind speed at a height of H_{can}, are used within the canopy ($z < H_{can}$). a is related to both A_f, using $a = 9.6A_f$ (Macdonald, 2000), and LAI (Pardyjak et al., 2008). Above the canopy ($z > H_{can}$) a modified version of the logarithmic profile is used that incorporates d: $\bar{u} = u_*/\kappa\,(\ln((z-d)/z_o) + \varphi((z-d)/L))$.

4.3.2 Functional Form of *TF* and *CF*

Pardyjak et al. (2008) found that two canopy parameters, H^* and T^*, were fundamental to relating PM_{10} removal to the roughness parameters introduced in Section 4.3.1:

$$H^* = \frac{H_{can}}{H_{dc}} \tag{4.5}$$

and

$$T^* = \frac{\alpha V_d H_{can}^2}{K_{zz}(H_{can})} = \frac{\tau_t}{\tau_d}. \tag{4.6}$$

In Eq. 4.6, H_{can} is the height of the canopy and H_{dc} is the initial height of the dust cloud at the roadside, assumed to be 2 m in this work. In Eq. 4.6, $K_{zz}(H_{can})$ is the vertical turbulent diffusivity at the top of the canopy and is a function of atmospheric stability; α is the vegetative surface area per unit canopy volume, τ_t and τ_d are the time scales of vertical turbulent diffusion and of particle deposition, respectively. V_d is the deposition velocity, and is very difficult to parameterize for field conditions (Petroff et al., 2008). As a result of V_d being very difficult to parameterize, T^* is very difficult to parameterize.

To overcome the difficulty in parameterizing V_d, this work proposes an approximation for V_d. It is asserted that V_d is proportional to the turbulent velocity scale, u_*, based on examining multiple studies (including wind tunnel and fields studies) presented in Petroff et al.(2008).

A measureable parameter, T_m^* that is directly proportional to T^* results from asserting that V_d is proportional to u_*. An expression for T_m^* results from substituting $u_*$for V_d in Eq. 4.6:

$$T_m^* = \frac{\alpha u_* H_{can}^2}{K_{zz}(H_{can})} = \frac{\tau_t}{\tau_d}. \tag{4.7}$$

It is important to recognize the consequences of T^* and T_m^* being directly proportional to each other. The values for T^* and T_m^* are seldom, if ever, equal; however, both variables are assumed to respond to identically changes in canopy structure or vertical turbulent mixing. For example, doubling canopy density, α, doubles both T^* and T_m^*.

For the simple canopy model presented in Section 4.3.1, the following equation is proposed for calculating the transmitted, *TF*, and captured, *CF*, fractions of PM_{10}:

$$(1 - CF) = TF = IF * (1 - \mathrm{CRE}) + (1 - IF), \tag{4.8}$$

where *IF* is the fraction of the initial dust cloud that interacts with the canopy (the interactive fraction). *CRE* is the canopy removal efficiency which is the fraction of *IF* that is removed by the canopy. The first term on the right-hand side (RHS), *IF*(1-CRE)*, is the fraction of the initial plume that interacts with the canopy and is subject to removal. The second term on the RHS, *(1-IF)* indicates the fraction of the initial plume that is not influenced by the canopy. As the canopy height is increased, a larger and larger fraction of the roadside plume interacts with the canopy, i.e., the first term on the RHS increases. As the canopy becomes denser, *CRE* increases closer to its maximum value of 1.

IF is a function of only H^* and *CRE* is a function of only T^*. It is proposed to parameterize *CRE* as:

$$(1\text{- }CRE) = \exp(-sT_m^{*n}), \tag{4.9}$$

where s and n are a positive constants. The form of Eq. 4.9 is based upon ADE simulations presented in Pardyjak et al. (2008) shown in Figure 4.1. It is found that substituting Eq. 4.9 into Eq. 4.8, while keeping H_{can} constant (i.e., keeping *IF* constant in Eq. 4.8), results in a plot of the form shown in Figure 4.1.

It is proposed to parameterize *IF* as:

$$IF(H^*) = 1 - \exp(-bH^*), \tag{4.10}$$

where, b is a positive constant. The form of Eq. 4.10 was obtained by considering Figure 4.2. It is found that substituting Eq. 4.10 into Eq. 4.8, while keeping T_m^* constant (i.e., keeping *CRE* constant in Eq. 4.8), results in a plot of the form shown in Figure 4.2. Equation 4.10 assumes that there is negligible distance between the leading edge of vegetative canopy and the roadside; hence, atmospheric stability has negligible influence on *IF*.

Substituting Eqs. 4.9 and 4.10 into Eq. 4.8 yields a quantitative expression relating *TF* and *CF* to H^* and T_m^*.

$$(1 - CF) = TF = (1 - \exp(-bH^*))\exp(-sT_m^{*n}) + \exp(-bH^*). \tag{4.11}$$

It remains to determine the parameters *b, s,* and *n*. Numerical simulations will be used for this purpose, owing to the small number of well-characterized field studies.

4.3.3 Simulations

The final step in parameterizing the Pace (2005) model is to determine the constants *s*, *b*, and *n*. Because at present there are only three field studies with a canopy characterized sufficiently well to parameterize H^* and T_m^* , 56 Lagrangian dispersion simulations varying H^* and T_m^* parameters, while maintaining all other roughness and meteorological parameters constant, are utilized. Equation 4.11 is fit in a least squares sense to the simulation data to determine *b*, *s*, and *n*.

Pollutant transport models consist of Eulerian models such as the atmospheric diffusion equations (ADE) utilized in Pardyjak et al. (2008) and Lagrangian dispersion models (Singh et al., 2011) that incorporate a relatively high degree of physics. ADE models utilize assumptions that are violated near the unpaved road: that the length scale of turbulence is significantly smaller than the length scale associated with concentration gradients (Seinfield and Pandis, 1998). As a result, ADE models tend to be overdispersive, as shown by Etyemezian et al. (2003). Because of this weakness in the ADE, it is only used as a reference from Pardyjak et al. (2008) for describing the form of Eq. 4.9 and Eq. 4.10.

To determine the parameters *s, b,* and *n,* the QUIC-PLUME Lagrangian dispersion model (Singh et al., 2011) is utilized to perform 56 simulations that vary only H^* and T_m^* parameters. Lagrangian dispersion models have been implemented for spore transport (Aylor and Flesh, 2001) and large particle transport within canopies (Bouvet et al., 2006). QUIC-PLUME is a fast response building aware dispersion model developed

to quickly estimate the impacts of accidental terrorist releases of toxic substances, and is capable of modeling particle and gas transport, has been implemented on graphical processing units (GPU), and consists of three components. The first QUIC –URB is a building aware wind model that generates output similar to 3D ensemble averaged wind fields. The QUIC –URB wind field together with simple parameterizations for the 3D turbulence field serve as the inputs to the second component QUIC-PLUME, which implements the 3D Langevin equations. Lastly, QUIC-GUI is a graphical user interface with data visualization tools.

4.3.3.1 PM_{10} Deposition Model

To perform the 56 simulations that vary only H^* and T_m^* parameters, a deposition model is needed for V_d. Three field studies (Etyemezian et al., 2004; Speckart et al., 2013; Veranth et al., 2003) are used to parameterize the Raupach et al. (2001) model for V_d. In this model, a particle of a given size, d_p, traveling at a velocity of U interacts with a vegetative element described by a single length scale, d_e. Vegetative orientation is neglected. The Stokes number, St, for the particle element pair is calculated as:

$$St = \frac{2\rho_p d_p^2 U}{18\rho_a \nu_a d_e} \tag{4.12}$$

where ρ_p is the density of the particle (assumed 1000 kg/m^3), ρ_a is the density of air, and ν_a is the kinematic viscosity of air. The latter two are evaluated at the temperature and pressured measured during the Las Cruces and Dugway field studies. Values of 295 K and 860 mbar were assumed for the Ft. Bliss site (all three field sites had an elevation of

about 1250 m within approximately 80 m). Once St is calculated, V_d can be calculated by

$$V_d = U(St/(St + p))^q, \tag{4.13}$$

where p and q are constants. Raupach et al. (2001) utilized 0.8 and 2 for p and q. In a Lagrangian reference frame, the concentration decreases as:

$$dc/dt = -V_d \alpha C. \tag{4.14}$$

Equation 4.16 can be integrated along the particle path assuming V_d, α, and U to be constant, yielding:

$$\sigma = C_1/C_o = \exp((-V_d \alpha S_b/U), \tag{4.15}$$

where S_b is the distance traveled by the particle within the vegetative canopy during the time of integration and C_1 and C_o are the concentrations at the beginning and end of the period of integration, respectively. In the final step, Eq. 4.15 is utilized to calculate particle removal.

The vegetative element size, d_e, must be determined to calculate St (Eq. 4.12) to utilize the Raupach et al. (2001) model. To estimate d_e, each of the roughness and meteorological conditions for all three field studies were simulated, the values and models used are located in Table 4.1, and d_e was varied until the QUIC-PLUME

simulated *TF* agreed with the *TF* measured for each of the field studies. It is assumed that the same value of d_e will be obtained from the simulation of the three field studies.

Simulating the Veranth et al. (2003) (Dugway) field study is unique because it featured two canopies: 1) a 10 x 12 array of shipping containers with interspersed vegetation occupying an area 180 x 176 m and 2) ambient vegetation surrounding the shipping container array. The urban canopy was directly downwind of the roadside emission and is considered as the pertinent canopy at Dugway. The ambient vegetation is referred to as the surroundings in Table 4.1. The urban array canopy was sufficiently dense to use the models presented by Pardyjak et al. (2008) for vertical turbulent transport and streamwise momentum within canopies.

4.3.3.2 Simulation Details

The computational details of the 56 simulations that varied only the H^* and T_m^* parameters, as well as the simulations of the three field studies performed to determine a universal vegetative element size, d_e, to use in the deposition model, are now presented. The plume was assumed to be composed of 5μm particles. The simulation domain was 50 m in height, 1160 m in the direction of the road and extended 30 m upwind of the road and 120 m downwind. The domain contained 100, 29, and 160 nodes in the respective directions. Winds were assumed orthogonal to the road. The road was modeled by an area source 1160 m in length and 2 m in width and height. The emission consisted of a steady release of 1,160,000 particles over 250 s. The transmitted fraction, *TF*, was calculated by counting particles as they crossed the roadside and 100 m downwind within the inner 20 m along the road from 220 s to the end of the simulation.

4.4 Results

4.4.1 Simulations

A contour plot of transmitted fraction, *TF*, as a function of H^* and T_m^* is shown in Figure 4.3. The figure is generated from the results of the 56 QUIC-PLUME simulations (those that vary only H^* and T_m^* while maintaining all other site and meteorological conditions) and contains the results from the three field studies. The Dugway and Ft. Bliss experiments are both extremes in canopy density and height. The Dugway canopy is a dense and tall canopy (high T^* and H^*), resulting in a high removal rate $TF \sim 0.13$; while the Ft. Bliss canopy is very sparse and very short (low T_m^* and H^*), resulting in a negligible removal rate $TF \sim 1.0$. The Las Cruces site is an example of a taller sparse canopy (low $T_m^*$and high H^*) that results in a moderate removal rate $TF \sim 0.6$. Increases in canopy height (H^*) and canopy density T_m^* exponentially decrease the transmitted fraction, *TF*. For relatively sparse canopies, shown on the lower portion of the figure, a relatively small increase in density greatly reduces *TF* and for tall and dense canopies, on the upper right-hand corner, *TF* is insensitive to changes in either canopy height or density. This suggests that there is a "law of decreasing returns" in the mitigation of fugitive dust. Once a critical height and density are reached, the addition of more vegetation would not enhance the canopy's removal ability.

The unknown coefficients in Eq. 4.11, *b, s,* and *n* were determined by a least-squares fit to the 56 QUIC-PLUME simulations. The resulting coefficients in Eq. 4.13 are $b = 2.0$, $s = 2.0$, and $n = 0.64$. Hence, Eq. 4.11 becomes:

$$(1 - CF) = TF = (1 - \exp(-2.8H^*))\exp(-2.0T_m^{*0.64}) + \exp(-2.8H^*). \quad (4.16)$$

This equation is compared to the experimental data in Figure 4.4 (The equation is solved for $\exp(-2.0T_m^{*0.64})$ which is equal to 1-Canopy Removal Efficiency). Canopies at the far left, such as Ft. Bliss, are sparse and inefficient at removing particles. Dense canopies such as Dugway are efficient at removing particles and intermediate canopies such as Las Cruces have intermediate particle removal efficiencies. At T_m^*~3, the removal efficiency reaches a limit and increases in canopy density fail to increase removal efficiency.

A value of $d_e \approx 50$ μm was estimated for the vegetative element size using the QUIC-PLUME simulations. Specifically, simulations were run in which all of field site conditions matched, while d_e was varied parametrically until the simulations matched the transmitted fraction, TF, of the field studies. This very small value is likely is a result of the smallest vegetative elements being the most effective in removing particles (Petroff, 2008; Slinn, 1982) together with small eddies associated with turbulence within the canopy. Belot and Gauthier (1975) found that for PM_{10} particles, deposition occurs predominantly (>90%) on leaves and needles rather than twigs while Moran et al. (2013) found that relatively small eddies in turbulence enhance deposition.

4.5 Conclusions

A quantitative model analogous to the model of Pace (2005) for the downwind removal of vehicle generated PM_{10} near (~ 100 m) unpaved roads is developed. The new model is simple formula that accounts for downwind roughness height and roughens density which are quantified by the parameters H^* and T_m^*, respectively. The parameters are based on a simple canopy model (Pardyjak et al., 2008) with inputs of H_{can} (the canopy height), H_{dc} (the initial, roadside height of the dust cloud) and LAI (the leaf area index). Boundary-layer meteorological inputs are: u_* (friction velocity) and L (the

Monin-Obukhov length scale). A simplification assuming that the deposition velocity, V_d, scales with u_* is utilized to calculate T_m^*. Other definitions for H^* and T_m^* are possible, but it is important to incorporate both the roughness height and density and some dependence of V_d upon turbulence within the roughness elements.

To determine the unknown coefficients of the simple formula, the Lagrangian dispersion model QUIC-PLUME is utilized with varying H^* and T_m^* while maintaining all other parameters. To model deposition, the model of Raupach et al. (2001) is utilized with a single vegetative element size that is determined by comparison of the transmitted fraction, *TF,* for QUIC-PLUME simulations of the field studies to the, *TF*, reported by the field studies. The simple formula with the coefficients determined by a least square fits to 56 QUIC-PLUME simulations that vary H^* and T_m^* indicate that *TF* decreases exponentially with increasing H^* and T_m^* .

4.6 Acknowledgements

This work was generously supported by the Southwest Consortium for Environmental Research and Policy (SCERP) under project number A-04-03 and the strategic Environmental Research and Development Program (SERDP) project number RC-1730.

Table 4.1. The site parameters and calculated captured fraction, *CF*, and transmitted fraction, *TF* of the PM_{10} plume as it travels from the roadside to 100 m downwind.

Field Study	**Etyemezian et al. (2004)** **Ft. Bliss, TX**	**Speckart et al. (2013)** **Las Cruces, NM**	**Veranth et al. (2003)** **Dugway, UT**
u_*(m s^{-1})	0.35	0.15	0.30
L(m)	-1000	20	1500
H_{can}/ $H_{can\ surroundings}$	0.5 m/0.5 m	1.8 m/1.8 m	2.5 m/1.0 m
z_o/ $z_{o\ surroundings}$	0.005 m/0.005 m	0.08 m/ 0.08 m	0.7 m/0.1 m
$LAI/LAI_{surroundings}$	0.006/0.006	0.1/0.1	1.0/0.6
a	NA	NA	0.96
d (m)	0	0	0.52
H^*	0.25	1	1.25
T_m^*	0.02	0.33	3.2
CF (%)	0	50	15
TF (%)	100	50	15

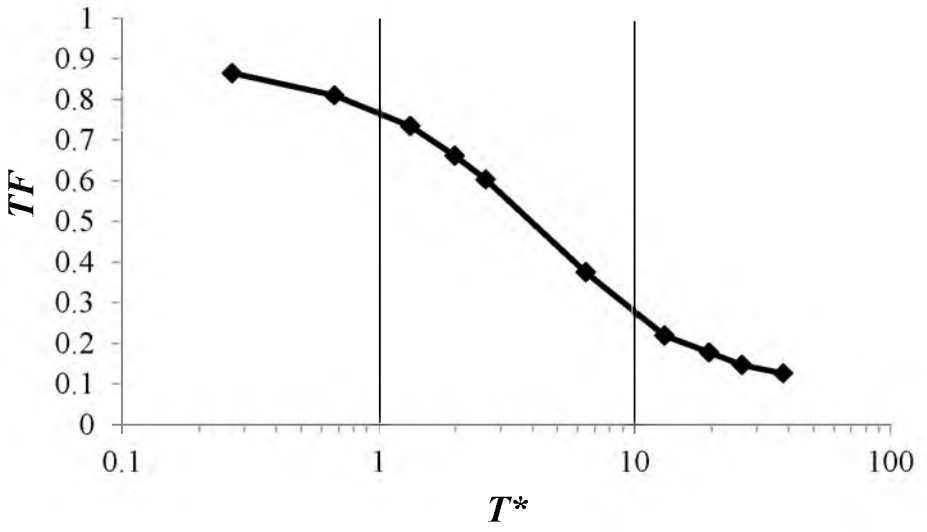

Figure 4.1. For a canopy of given height, the transmitted fraction, *TF*, decreases with increasing T^* (or its surrogate T_m^*). Adapted from Pardyjak et al. (2008) Figure 6.

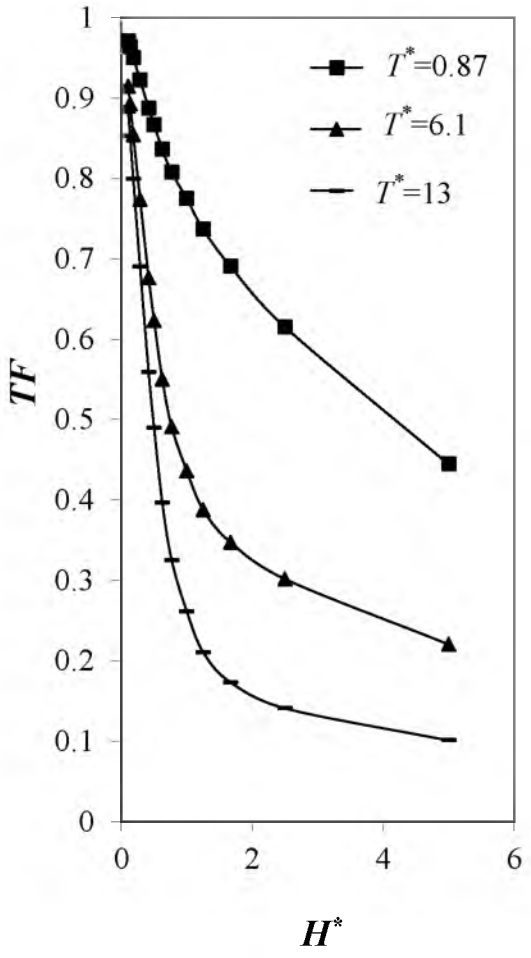

Figure 4.2. The dependence of the transmitted fraction, *TF*, upon the ratio of canopy height to initial plume height, H^*; shown by the family of curves for different T^*. Data are from the atmospheric diffusion equation (ADE) model of Pardyjak et al. (2008). T^* increases as the canopies ability to remove particles.

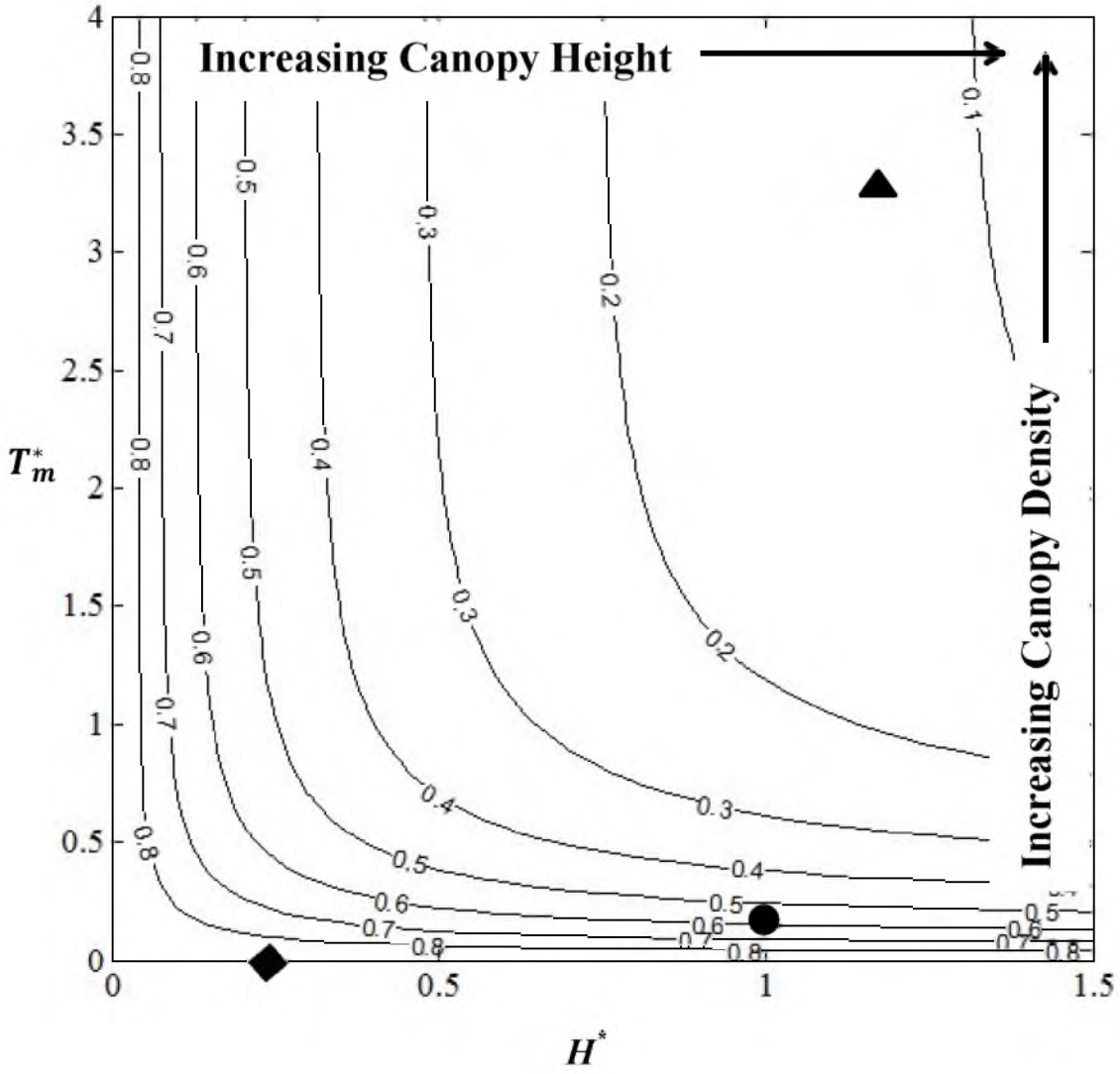

Figure 4.3. Contours of constant transmitted fraction, *TF*, as a function of H^* and T_m^* together with the field data from the Veranth et a. (2003) (▲) (Dugway, UT) ,Speckart et al. (2013) (●) (Las Cruces, NM), and Etyemezian et al. (2004) (Ft. Bliss, TX), (◆), field studies. Contours are generated from the results of 56 QUIC-PLUME simulations varying only H^* and T_m^*. .

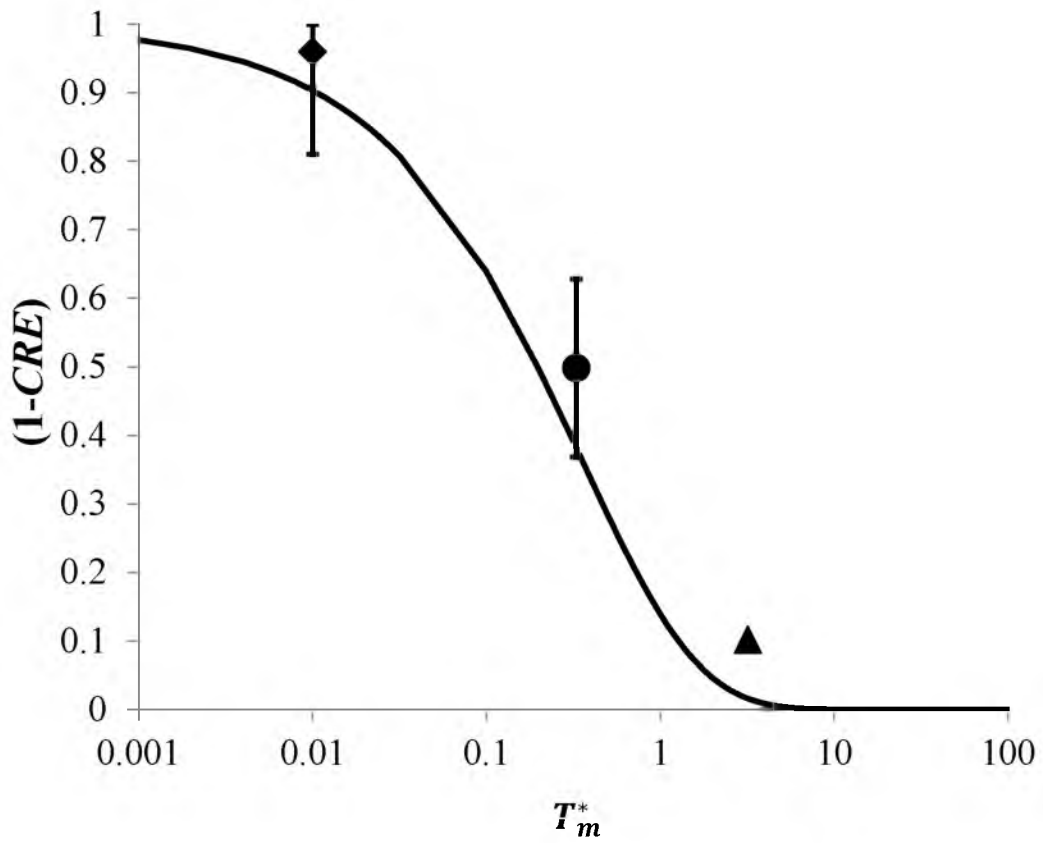

Figure 4.4. The canopy removal efficiency calculated by Eq. 4.16, shown by the solid line, compared to the three field studies, Veranth et al. (2003) (▲) (Dugway , UT), Speckart et al. (2013) (●) (Las Cruces, NM), and Etyemezian et al. (2004) (◆) (Ft. Bliss, TX).

4.7 References

Arya, S.P., 2001: *Introduction to micrometeorology*, Orlando: Academic Press.

Aylor, D.E. and T. K. Flesch, 2001: Estimating spore release rates using a Lagrangian stochastic simulation model. *Journal of Applied Meteorolg*, **40**, 1196–1208.

Belot, Y. and D. Gauthier, 1975: *Transport of micronic particles from atmosphere to foliar surfaces*. Located in: De Vries, D.A. and N. H. Afgan, (Eds.), *Heat and Mass Transfer in the Biosphere*. Scripta Book, Washington, DC.

Bouvet, T., B. Loubel, J. Wilson, and A. Tuzel, 2007: Filtering of windborne particles by a natural windbreak. *Boundary-Layer Meteorology*, **123**, 481-509

Choudhury, B. J. and J. L. Monteith, 1988: A four-layer model for the heat budget of homogeneous land surfaces. *The Quarterly Journal of the Royal Meteorological* Society, **114**, 373–398.

EPA, 2006: AP-42, Compilation of Air Pollutant Emission Factors, Vol. 1. Stationary, Point, and Area Sources, Chapter 13.2.2 Unpaved Roads. US Environmental Protection Agency, Washington, DC. http://www.epa.gov/ttn/chief/ap42/ch13/final/c13s0202.pdf

Etyemezian, V., S. Ahonen, D. Nikolic, J. Gillies, H. Kuhns, D. Gillette, and J. Veranth, 2004: Deposition and removal of fugitive dust in the arid southwestern United States: measurements and model results. *Journal of the Air and Waste Management Association* **54**, 1099-1111.

Etyemezian, V., J. Gillies, H. Kuhns, D. Nikolic, J. Watson, J. Veranth, R. Labban, G. Seshadri, and D. Gillett, Field Testing and Evaluation of Dust Deposition and Removal Mechanisms: Final Report; Report Prepared for WESTAR Council, Lake Oswego, OR, by DRI: Las Vegas, NV, 2003.

Macdonald, R.W., 2000: Modelling the mean velocity profile in the urban canopy layer. *Boundary-Layer Meteorology* **97**, 25–45.

Moran, S.M., E. R. Pardyjak, and J. M. Veranth, 2013: The role of turbulence in enhancing particle deposition. Article in press in the Journal *Physics of Fluids*.

Pace, T.G., 2005: Methodology to Estimate the Transportable Fraction (*TF*) of Fugitive Dust Emissions for urban Scale Air Quality Analyses. USEPA.

Pardyjak, E.R., S. O. Speckart, F.Yin, and J. M. Veranth, 2008: Near-source deposition of vehicle generated fugitive dust on vegetation and buildings: model development and theory. *Atmospheric Environment*, **42** 6442-6452.

Petroff, A., A. Mailliat, M. Amielh, and F. Anselmet, 2008: Aerosol dry deposition on vegetative canopies. Part I: review of present knowledge. *Atmospheric Environment* **42**, 3625-3653.

Raupach, M.R., N. Woods, G. Dorr, J.F. Leys, and H.A., Cleugh, 2001: The entrapment of particles by windbreaks. *Atmospheric Environment*. **35**,3373–3383.

Seinfeld, J.H. and S. N. Pandis, 1998: *Atmospheric Chemistry and Physics: From Air Pollution to Climate Change*. Wiley, New York

Singh, B., E. R. Pardyjak, A. Norgren, P. Willemsen, 2011: Accelerating urban fast response Lagrangian dispersion simulations using inexpensive graphics processor parallelism. *Environmental Modeling and Software*, **26**,739-750

Slinn, W.G.N., 1982: Predictions for particle deposition to vegetative canopies. *Atmospheric Environment*, **16**, 1785–1794.

Speckart, S., J. M. Veranth, and E. R. Pardyjak, 2013: Removal of PM_{10} in the near source zone downwind of unpaved roads: part 1 Las Cruces, NM field study. *Journal of Atmospheric Environment*, submitted for publication

Veranth, J.M., G. Seshadri, and E. Pardyjak, 2003: Vehicle-Generated Fugitive Dust Transport: Analytic Models and Field Study. *Atmospheric Environment*, **37**, 2295-2303.

Watson, J.G., and J. C. Chow, 2000: Reconciling urban fugitive dust emissions inventory and ambient source concentration estimates: summary of current knowledge and needed research, Desert Research Institute, Reno, NV, www.epa.gov/ttn/chief/efdocs/fugitivedust.pdf.

Zhu, D., H. D. Kuhns, J. A. Gillies, V. Etyemezian, A. W. Gertler, and S. Brown, 2011: Inferring deposition velocities from changes in aerosol size distributions downwind of a roadway. *Atmospheric Environment* **45**, 957-966.

CHAPTER 5

FAST-RESPONSE SIMULATION OF WINDBREAK FLOW

The content of this chapter is ready for submission to the Journal of Wind Engineering and Industrial Aerodynamics.

5.1 Abstract

Accurate and computationally inexpensive numerical models for determining the mean and turbulent velocity fields surrounding windbreaks are developed for fast and routine calculations to estimate the impact of windbreaks in land management applications such as fugitive dust removal. The mean velocity model utilizes the previously developed QUIC Dispersion Modeling System platform and methodology, which relies on empirical parameterizations together with the principle of mass-conservation to achieve results that are comparable to traditional computational fluid dynamics models, but with far less computational cost. The turbulent velocity field is an implementation of the similarity solution presented by Judd et al. (1996). Both the mean velocity and turbulence models are applicable up and downwind of windbreaks having varying thicknesses. Simulations of both wind tunnel and field study experiments show excellent agreement with the data for windbreaks of varying optical porosity (0 to 0.7) and upstream roughness (1/30 to 1/600 of windbreak height). Results are presented for windbreaks composed of a single row, under neutral atmospheric stratification, and

subject to orthogonal winds.

5.2 Introduction

Windbreaks are long rows of roughness elements that consist of vegetation or other roughness elements that create an aerodynamic shelter from wind. They are distinguished from roughness canopies, which have thicknesses sufficiently deep that they can be regarded as nearly infinite in depth for analysis purposes. Windbreaks are used in many applications including: the mitigation of fugitive dust transport and wind erosion (e.g., Musick and Gillette, 1990; Raupach et al., 2001), improving highway visibility under winter storm conditions (Iversen, 1981; Tabler, 1991), reducing pesticide spray drift (Davis et al., 1994) and the enhancement of crop yields (Cleugh, 1998).

Owing to the importance of windbreaks in land management, criteria defining "best practices" have been presented. Finch (1988) presented such criteria for enhancing crop yields. These criteria indicate parameters such as the ideal location, porosity, and height of a windbreak as a function of inputs such as crop type and terrain. To improve such criteria, both numerical and experimental studies have been undertaken to estimate the performance of windbreaks consisting of a single row.

The literature abounds with studies of windbreaks and consists of data from field studies, wind tunnel experiments, analytical analysis, and numerical modeling. Field studies of windbreaks include: Bradley and Mulhearn (1983), Nord (1991), and Wilson (2004). Wind tunnel studies include: Plate (1971), Judd et al. (1996), Perrera (1981), and Guan et al. (2003). Numerical modeling studies include using various forms of the Reynolds Averaged Navier-Stokes (RANS) equations (Bourdin and Wilson, 2008; Santiago, 2007; Wang et al., 2001; Wilson, 1985). In addition, high-fidelity Large-Eddy

Simulations (LES) are presented by Patton et al. (1998). Analytical analysis include: Counihan et al. (1974) and Wilson (1990). A few of the cited studies present empirically based expressions for the mean wind and turbulence. These studies include: Perrera (1981), Bradley and Mulhearn (1983), Counihan et al. (1974), and Guan (2003).

The extensive windbreak literature concludes that windbreak height, H, optical porosity, β, upstream aerodynamic roughness, z_o, displacement height, d, upwind approach angle relative to the windbreak, and atmospheric stratification influence the mean and turbulent wind fields. The area of shelter decreases with increasing upstream roughness, decreasing porosity, increasing stratification, and increasing oblique angles (Judd et al., 1996; Wilson, 2003).

Recently, fast response alternatives to LES or CFD simulations have been developed (Singh et al., 2008) for quick turn-around calculations. Such fast calculations are easily utilized by users with limited computational resources for routine, repetitive calculations. An example of such a fast response tool is the Los Alamos National Laboratory's Quick Urban & Industrial Complex (QUIC) Dispersion Modeling System (Brown et al., 2013). QUIC is a building resolving tool originally designed to solve for flow and dispersion fields in cities.

The objective of the current work is twofold: 1) To use the methodology and platform of QUIC to develop a fast-response mean wind field windbreak model that is less computationally expensive than computational fluid dynamics (CFD) simulations, to be used for routine windbreak design calculations, and 2) to develop an empirical relation for the turbulent velocity statistics that is valid downwind of a windbreak. The model should correlate well with field and wind tunnel studies over a wide range of windbreak

height, porosity, and upstream roughness conditions. The motivation for both objectives is to develop windbreak simulation package that can be utilized by users with limited computational resources for routine windbreak design calculations (Finch, 1998). Simulation results for single-row windbreaks with orthogonal winds under neutral stratification are presented.

5.3 Methods

5.3.1 QUIC

This work builds on the previously developed QUIC framework to simulate the mean wind fields of windbreaks (Singh et al., 2008; Singh et al., 2011). QUIC was developed at Los Alamos National Laboratory along with collaborators at the University of Utah to model 3-D urban wind fields and their accompanying dispersion of pollutants. QUIC is a diagnostic wind model based upon the work of Röckle (1990), which relies upon empirical parameterizations and mass conservation (instead of closure assumptions typically employed in RANS models; Pope, 2000) to achieve faster simulation times of complex flow physics. In QUIC, an initial, mean velocity field, denoted by u_o, v_o, w_o, is defined based on empirical relationships. This initial velocity field is non-mass-conservative, meaning that sources or sinks of mass must exist to sustain it. Different empirical relationships are applied to different subdomains of u_o, v_o, w_o. For example, the u_o, v_o, w_o within the wake of a building and within a vegetative canopy are described by different parameterizations. To calculate a flow for a domain encompassing both features, the effects of the two flow regimes on each other must be calculated. This calculation is performed by the application of a variational technique which yields the mass-conservative mean velocity field with the minimal variance from u_o, v_o, w_o. The

final, mass-conservative mean velocity field is denoted by u, v, w. Figure 5.1 summarizes the process. QUIC has been found to accurately simulate mean wind fields around isolated buildings, building arrays, and street canyons (Singh et al., 2008).

The variational procedure is shown in Figure 5.1 and is the essence of the methodology implemented in QUIC. This methodology is described in detail in Singh et al. (2008), but summarized here, beginning with Eq. 5.1:

$$E(u,v,w,\lambda) = \iiint \begin{bmatrix} \alpha_1^2(u-u_o)^2 + \alpha_1^2(v-v_o)^2 + \alpha_2(w-w_o)^2 + \\ \lambda\left(\frac{\partial u}{\partial x} + \frac{\partial v}{\partial y} + \frac{\partial w}{\partial z}\right) \end{bmatrix} dxdydz, \quad (5.1)$$

where E(u,v,w,λ) is the variation between the u,v,w and u_o, v_o, w_o, which is minimized, α_i are Gaussian precision moduli, generally taken to be one (Singh et al., 2008), and λ is a Lagrange multiplier. The Euler-Lagrange equations are a solution to Eq. 5.1 that minimizes the variation. They are:

$$u = u_o + \frac{1}{2\alpha_1^2}\frac{\partial \lambda}{\partial x} \quad (5.2a)$$

$$v = v_o + \frac{1}{2\alpha_1^2}\frac{\partial \lambda}{\partial y} \quad (5.2b)$$

$$w = w_o + \frac{1}{2\alpha_2^2}\frac{\partial \lambda}{\partial z}. \quad (5.2c)$$

When Eq. 5.2 is substituted into the continuity equation, $\partial u_i/\partial x_i = 0$, the following Poisson equation results:

$$\frac{\partial^2\lambda}{\partial x^2}+\frac{\partial^2\lambda}{\partial y^2}+\left(\frac{\alpha_2}{\alpha_1}\right)^2\frac{\partial^2\lambda}{\partial z^2}=-2\alpha_1^2\left(\frac{\partial u_o}{\partial x}+\frac{\partial v_o}{\partial y}+\frac{\partial w_o}{\partial z}\right). \quad (5.3)$$

The solution field of Eq. 5.3, λ, is substituted into Eq. 5.2, relating the initial velocity field to the final mass-conservative field. The boundary conditions for solving Eq. 5.3 are as follows: $\lambda = 0$ for a fluid boundary and $\partial\lambda/\partial n = 0$, where n is a surface normal for solid boundaries. Equation 5.3 is solved by a successive over relaxation (SOR) solver (Press et al., 2007) on a staggered finite-volume grid where velocities are defined at cell faces and the Lagrange multipliers are defined at cell volume centers.

5.3.2 Windbreak Flow Characteristics

The utilization of QUIC to model windbreak flows requires a knowledge of the characteristics of windbreak flows to parameterize the initial, empirically based, wind field, u_o, v_o, w_o. These characteristics are now presented so the parameterizations used in QUIC to define u_o, v_o, w_o will have meaning when they are subsequently presented.

In describing windbreak flows, the velocity components corresponding to the x, y, and z directions are referred to as the streamwise (x), u, spanwise (y), v, and the vertical (z), w. The windbreak is assumed to be a sufficient length in the spanwise direction that flow statistics are invariant. The pertinent dimension in the vertical direction is windbreak height, H, and in the streamwise direction it is x/H, with the windbreak base being the origin. The optical porosity, β, is assumed constant with height in the windbreak. For such conditions, there are six distinct regimes, which are illustrated in Figure 5.2. Far upwind (A) is the undisturbed velocity profile of the surface layer (e.g.,

Arya, 2001) referred to as the approach profile. As the flow nears the windbreak, the momentum removed by the windbreak causes a decrease in the streamwise velocity at heights less than *H*. As a consequence of this and mass conservation, an upward vertical velocity is induced. As the flow passes through the windbreak, the bleed flow (B) results on the downwind side and the flow over the top of the windbreak accelerates. This is referred to as the displaced profile (C). Vertical motions displayed in the streamlines of Figure 5.2 are overexaggerated for illustrative purposes. As the flow progresses downwind of the windbreak, the bleed flow evolves into the quiet zone (D). In this zone, the mean momentum and mean turbulent quantities are small compared to the approach profile. The quiet zone extends from an upwind distance of *H* to 3-7 *H* downwind of the windbreak. The accelerated displaced profile and the quiet zone interact through the mixing zone (E), which is characterized by high shear between the displaced profile and the quiet zone. Judd et al. (1996) note that the center of the mixing zone, defined by an inflection point in the vertical mean velocity profile, approximately follows a streamline as the flow progresses downwind. In this work, the streamline that originates upstream of at an elevation of *H* is assumed to be the center of the mixing zone and is indicated by the bold dashed line in Figure 5.2. Finally, note that as a consequence of upward advection, the bleed and quiet zones spread slightly higher than *H* just downwind of the fence.

As the flow progresses downwind, the shear decays and the mixing zone entrains additional fluid. Eventually, the mixing zone intercepts the ground. Further downwind, the mixing zone reestablishes equilibrium and the upwind profile is reestablished. This is noted as the re-equilibrium zone (F) in Figure 5.2.

5.3.3 Implementation of a Windbreak into QUIC

Because QUIC utilizes empirical expressions for an initial wind field, $u_o\, v_o\, w_o$, frequent reference will be made in this section to parameterizations from previous researchers that are utilized to define $u_o\, v_o\, w_o$. As noted in Section 5.3.1, the first step in QUIC is the parameterization of the initial, empirically based, non-mass-conservative field. The flow domain is divided into subdomains according to flow geometry of windbreaks and appropriate parameterizations are applied to each subdomain. The entire domain is subject to the variational procedure that insures the transitions between subdomains are modeled in a mass conservative manner, resulting in the velocity field, u, v, w which is continuous, conserves mass, and minimizes the variation between u, v, w and u_o, v_o, w_o.

To introduce a windbreak into QUIC, the flow field is divided into three subdomains, as shown in Figure 5.3. v_o, w_o are parameterized to be 0 at all points within all three subdomains, while u_o is parameterized differently for each of the three subdomains shown in Figure 5.3. For mathematical tractability, u_o is calculated indirectly by first parameterizing a quantity referred to as aerodynamic porosity, α_o, (Guan et al., 2003) and then calculating u_o, *viz.*,

$$\alpha_o(x, z, \beta, H) = u_o(x, z, \beta, H)/u_a(z). \tag{5.4}$$

Here, $u_a(z)$ is the upstream approach velocity profile and u_o (x,z,β,H) is the local (windbreak modified) velocity. α_o is the description of local enhancement or attenuation of streamwise momentum resulting from the windbreak and is equal to 1 in areas not affected by the windbreak (i.e., high above, far upwind, or downwind of the windbreak).

For subdomain 1, on the upwind side of the windbreak, the parameterization α_o = 1 is used, resulting in $u_o(x,z,\beta,H) = u_a(z)$. This parameterization assumes that for the initial, non-mass conservative velocity field, the windbreak has negligible effect on the upwind side of the windbreak. However, when mass-conservation is applied via the variational procedure to the u_o, v_o, w_o field, the windbreak's modification to the upwind flow is modeled via conservation of mass.

Subdomain 2 contains both the bleed flow and the displaced profile zones. In the bleed flow zone, $\alpha_o = \alpha_{obf} < 1$, where α_{obf}, is $\alpha_o(x,z,\beta,H)$ for the bleed flow region. In the displaced profile zone, $\alpha_o \approx 1$. To model the transition of α_o from the bleed flow zone to the displaced profile zone, the function $\alpha_o = R\tanh + S$ is utilized. R and S are solved subject to the constraints that as $z \to \infty$, $\alpha_o \to 1$ (in the displacement region) and as $z \to -\infty$, $\alpha_o \to \alpha_{obf}$ (in the bleed flow region), resulting in Eq. 5.5:

$$\alpha_o(x,z,\beta,H) = (1-\alpha_{obf})/2 * \tanh\big(1.5/\delta * (z - z_{wmo})\big) + \big(1+\alpha_{obf}\big)/2. \qquad (5.5)$$

To utilize Eq. 5.5 for subdomain 2, three quantities must be parameterized: 1) α_{obf}, 2) δ, the half width of the mixing layer, and 3) z_{wmo}, the origin of the mixing layer. Previously published parameterizations for 1) and 2) will be utilized, while 3) will be defined by QUIC.

Guan et al. (2003) parameterized α_{obf} according to windbreak type in terms of optical porosity depending on the windbreaks thickness and structure, as given in Eq. 5.6:

$$\alpha_{obf} = \beta \qquad \text{thin wind break} \qquad (5.6a)$$

$$\alpha_{obf} = \beta^{0.4} \qquad \text{windbreak with finite internal structure.} \qquad (5.6b)$$

Eq. 5.6*a* applies to the artificial windbreak model and Eq. 5.6*b* to vegetative windbreaks. The half width of the windbreak mixing layer, δ, is zero at the windbreak and increases downwind, according to Eq. 5.7 (Judd et al., 1996):

$$\partial\delta/\partial x = ((0.14\ \Delta u_{ho}/u_{ave}\ )^2 + (2\sigma_w/u_{ho})^2)^{1/2}, \qquad (5.7)$$

where σ_w is the standard deviation of the turbulent vertical velocity fluctuations in the approach profile. $\Delta u_{ho} = u_{ho}(1 - \alpha_{obf})$, where u_{ho} is the approach profile speed at H and $u_{ave} = (1 + \alpha_{obf})/2$. The first term on the right-hand side (RHS) of Eq. 5.7 accounts for the spreading of a traditional mixing layer. The second term on the RHS accounts for the turbulence of the surface layer "buffeting" the thinner traditional mixed layer. This is frequently the dominant mechanism for spread rate (Judd et al., 1996).

In Eq. 5.5, z_{wmo} is the location of an inflection point in the vertical profile of mean velocity. Data indicate that z_{wmo} approximately follows a streamline (Judd et al., 1996) which starts at the top of the windbreak, as illustrated in Figure 5.4. Streamlines near windbreaks exhibit vertical curvature that is absent in our initial wind field because w_o is forced to zero. Consequently, to model the streamline containing z_{wmo}, the variational procedure is performed twice instead of the standard once. The complete methodological sequence is shown in Figure 5.5. In the (u_o,v_o,w_o) wind field, $z_{wmo} = H$. After the first variational procedure, a mass conservative wind field (u',v',w') with streamline curvature results. Subsequent to the calculation of the u',v',w' field, z_{wmo} is moved to the

streamline that originates at height H in the approach profile. The movement of z_{wmo} to the new streamline results in the (u'',v'',w'') wind field which is not mass-conservative. Subsequently, the second variational procedure is applied and the final mass-conservative wind field (u,v,w) results.

In subdomain 3, more than 7.5H downstream of the windbreak, the flow has largely re-equilibrated and can be parameterized by the similarity solution of Perera (1981). The defining equation for the aerodynamic porosity and the pertinent similarity variables in this region are defined in Eq. 5.8.

$$\alpha_o(x,z) = -\frac{9.75(1-\beta)\eta u_{ho}}{\bar{x}u_a(z)}\exp(-0.67\eta^{1.5}) + 1 \tag{5.8a}$$

$$\bar{x} = \frac{x}{H-d} \tag{5.8b}$$

$$\eta = \frac{z}{H-d}\left(\frac{1}{K\bar{x}}\right)^{\frac{1}{n+2}} \tag{5.8c}$$

$$K = \frac{2\kappa^2}{ln\left(\frac{H-d}{z_o}\right)} \tag{5.8d}$$

Here, d is the displacement height, n is the exponent in a power fit to the approach velocity profile (Arya, 2001) (assumed to be approximately n=1/7), and κ is the von Karman constant taken as 0.4.

5.3.4 Turbulence Model

To model the turbulence of windbreaks, the current work utilizes and completes the incomplete similarity solution (Pope, 2000) for windbreak turbulence presented by

Judd et al. (1996). The similarity solution utilizes the square of a turbulent velocity, U_s^2, to calculate second-order turbulence statistics. The mixing zone thickness, 2δ, was used to scale the distance from the center of mixing zone, which is a zone that generates turbulence. Judd et al. (1996) did not present a method for determining U_s^2, nor a 1-D mathematical function for the similarity solution. This work presents a method for determining $U_s^2$and a 1-D function for the Judd et al. (1996) similarity solution. A method for calculating all the elements of the Reynolds's stress tensor is also presented from the work of Counihan et al. (1974).

The incomplete similarity solution presented by Judd et al. (1996) partially describes the attenuation of turbulence in the quiet zone (zone D in Figure 5.2), the enhancement of turbulence within the mixing zone, (zone E in Figure 5.2), and the return to upstream turbulence conditions above the mixing zone, (zone C in Figure 5.2). Turbulence scales with the square of a turbulent velocity, U_s^2, which Judd defines to be the magnitude of the maximum Reynolds stress (the maximum $\overline{u'w'}$ within a vertical profile). Vertical distance was measured relative to the center of the mixing zone, assumed to be at height H and was normalized by 2δ. The following functional forms resulted:

$$\frac{\overline{u'w'}}{U_s^2} = f_{uw}(\xi) \qquad \frac{\overline{u'^2}}{U_s^2} = f_{uu}(\xi) \qquad \frac{\overline{w'^2}}{U_s^2} = f_{ww}(\xi) \tag{5.9}$$

where

$$\xi = (z - H)/2\delta. \tag{5.10}$$

Data from Judd et al. (1996) are shown in Figure 5.6 in terms of the similarity solution. Note the excellent collapse of the data from many downwind distances onto a single curve as well as the attenuation of turbulence for ξ < -0.5 (the quiet zone), an increase of turbulence, -0.5 < ξ < 0.5 (the mixing zone) and a decrease to ambient conditions, ξ > 0.5 (the displaced profile).

To complete the Judd et al. (1996) similarity solution, we propose a parameterization for the function f_{uw} in Eq. 5.9:

$$f(\xi)_{uw} = A\tanh(\xi + c(A,B)) + B\cosh^{-2}(\xi + c(A,B)) + C. \quad (5.11)$$

The parameterization of Eq. 5.11 is chosen because of its excellent mathematical description of the turbulence similarity profiles shown in Figure 5.6 and because it includes *tanh,* which was used in the windbreak mean velocity field, and the first derivative of *tanh*, $\cosh^{-2}$. $c(A,B)$, is defined to be the location of the maximum of $A\tanh(\xi)+B\cosh^{-2}(\xi)+C$ and is included in the arguments of *tanh* and $\cosh^{-2}$ in Eq. 5.11 to ensure that the maximum of Eq. 5.11 occurs at ξ =0. The value of $c(A,B)$ is: $c(A,B) = \text{atanh}(A/(2B))$, a result which is found by equating the vertical derivative of Eq. 5.11 to zero and solving for $c(A,B)$. The parameters A, B, and C are obtained by subjecting Eq. 5.11 to the following constraints, one applied for each of the zones transected by the function f_{uw} :

$$A\tanh(\infty) + B\cosh^{-2}(\infty) + C = \overline{u'w'}_{upstream} \quad (\xi \to \infty) \quad \text{(Displaced Zone)} \quad (5.12a)$$

$$A\tanh(-\infty) + B\cosh^{-2}(-\infty) + C = \overline{u'w'}_{min} \quad (\xi \to -\infty) \quad \text{(Quiet Zone)} \quad (5.12b)$$

$$Atanh(c(A,B)) + Bcosh^{-2}(c(A,B)) + C = U_s^2 \ (\xi = 0), \text{(Mixing Zone Center)} \quad (5.12c)$$

where $\overline{u'w'}_{upstream}$ is the upstream surface layer value of $\overline{u'w'}$, and $\overline{u'w'}_{min}$ is $\overline{u'w'}$ in the bleed flow. It is assumed: $\overline{u'w'}_{min} = \alpha_{bleed\ flow}^2 * \overline{u'w'}_{upstream}$ which is based on applying the definition of $\alpha_{bleed\ flow}$, Eq. 5.4, to second-order turbulent statistics. Also, Eq. 5.12 assumes that $\overline{u'w'}$ is a small non-zero value at the ground instead of its true value, zero. The consequences of this discrepancy are negligible for the resolution of data examined in this work. Using the relations $tanh(c(A,B)) = A/(2B)$, $1\text{-}tanh^2 = cosh^{-2}$ and $c(A,B) > 0$ together with the limits, $cosh^{-2}(\infty) \rightarrow 0$, $cosh^{-2}(-\infty) \rightarrow 0$, $tanh(\infty) \rightarrow 1$, $tanh(-\infty) \rightarrow -1$ yield the values for the constants, which are:

$$A = \left(\overline{u'w'}_{upstream} - \overline{u'w'}_{min}\right)/2 \quad (5.13a)$$

$$B = ((-C + U_s) + ((C - U_s)^2 - A^2)^{0.5})/2 \quad (5.13b)$$

$$C = \left(\overline{u'w'}_{upstream} + \overline{u'w'}_{min}\right)/2. \quad (5.13c)$$

To complete the parameterization of U_s^2 (the square of turbulent velocity scale) a function, $U_s^* = f(x^*)$, is developed. The equation $U_s^* = f(x^*)$ describes the downwind decay of the turbulence enhancement by the windbreak; which, based on the data of Judd et al. (1996) is assumed to decay in three regimes: 1) a regime of slow decay of U_s^2just downwind of the fence, 2) a regime of comparatively rapid decay of U_s^2downwind of the first regime, and 3) the regime farthest downwind, which exhibits a slow final decay of $U_s^2$to the undistributed upstream value, $\overline{u'w'}_{upstream}$. This three regime decay is described by the function: $U_s^* = 0.5*tanh(x^*)+0.5$, shown in Figure 5.7. The variable U_s^* is

defined to be 1 at the location of maximum turbulent enhancement ($U_s = U_{s\,max}$, which occurs at the windbreak) and 0 at the location where the turbulence field has fully recovered ($U_s = \overline{u'w'}^{0.5}_{upstream}$, which occurs far downwind of the windbreak). To satisfy these conditions, U_s^* is defined as:

$$U_s^* = \frac{U_s - \overline{u'w'}^{0.5}_{upstream}}{U_{s\,max} - \overline{u'w'}^{0.5}_{upstream}}, \tag{5.14}$$

where $U_{s\,max}$ is the scale of maximum turbulence enhancement. By considering the data of Perera (1981), Bradley and Mulhearn (1983), and Judd et al. (1996), $U_{s\,max}$ is found to be parameterized by: $U_{s\,max} = D\overline{u'w'}^{0.5}_{upstream}\ln[(1-\alpha_{obf})^2 * \frac{z_o}{H-d)}] + 1 - E$, where D and E are parameters found by least square fits to the data of the aforementioned authors. When the relation for $U_{s\,max}$ is substituted into Eq. 5.14, the following equation results:

$$U_s^* = \frac{\frac{U_s}{\overline{u'w'}^{0.5}_{upstream}} - 1}{Dln[\left(1-\alpha_{obf}\right)^2 * \frac{H-d}{z_o}] - E}. \tag{5.15}$$

The similarity variable x^* is defined to relate the rate of turbulence decay to the location downwind of the windbreak. Based on the data of Perera (1981), Bradley and Mulhearn (1983), and Judd et al. (1996), x^* is defined by:

$$x^* = \left(F\alpha_{obf}^{2.5}\left(\frac{z_o}{H-d}\right)^{.75} + G\right) * \left(x/H - Iln\left(\frac{H-d}{z_o}\right) + J\right), \tag{5.16}$$

where F, G, I, and J are coefficients to be determined by a least squares fit to the experiment data of the aforementioned authors.

The data sets of: Perera (1981), Bradley and Mulhearn (1983), and Judd et al. (1996) are chosen to parameterize the turbulence similarity solution because they had 1) relatively high spatial resolution of turbulence measurements, 2) a large span of windbreak heights normalized by upwind roughness $(H\text{-}d)/z_o = 30$ to $(H\text{-}d)/z_o = 600$, and 3) a large range of optical porosities $\beta = 0$ to $\beta = 0.7$.

The completed similarity solution defines the Reynolds shear stress, $\overline{u'w'}$. The remaining elements of the Reynolds stress tensor, $\overline{u'^2}$ and $\overline{w'^2}$, are parameterized using the following relationships (Counihan et al., 1974):

$$\overline{u'^2} = 5.0\overline{u'w'} \tag{5.17a}$$

$$\overline{w'^2} = 1.5\overline{u'w'}. \tag{5.17b}$$

5.3.5 QUIC Simulation Details

The QUIC simulations were performed on a mesh containing 328 x 5 x 80 nodes and spanning $66H$, $25H$, and $10H$ in the x, y, and z directions, respectively. The windbreak was located $3H$ downwind of the inlet. Uniform spacing was implemented in the x, y directions, while the grid was nonuniform in the vertical direction and was stretched in a parabolic manner with the smallest spacing being $0.1H$. The grid spacing was determined so the flow solution was independent of further refinements to the mesh. The size of the spatial domain was chosen so the mean flow solution would be independent of increases in spatial domain size and so that the mean flow was not altered

by the presence of the windbreak at the inlet or the top of the spatial domain. The independence of the mean flow solution to both the grid spacing and spatial domain size was verified through simulations. The turbulence field was insensitive to spatial domain size and grid spacing because it was a result of an analytical formula rather than a numerical solution. The current mesh required about 3 minutes for convergence on a midlevel laptop operating in serial mode.

For verification purposes, the simulations were compared to the data presented in Perera (1981), Judd et al. (1996), and Bradley and Mulhearn (1983). All field studies examined windbreaks with negligible thickness (i.e., thin windbreaks) and optical porosities varying from β=0.3 to β=0.69. The data incorporated windbreak heights normalized by upstream roughness from $(H\text{-}d)/z_o$ = 30 to 600 and, consequently, provided model verification for many of plausible windbreak configurations.

5.4 Results

5.4.1 Mean Velocity Field

QUIC simulations of the mean wind field resulting from windbreaks show excellent agreement (less than 10% relative difference) with mean wind field data both upwind and downwind of windbreaks of varying porosities, as shown in Figure 5.8, Figure 5.9, and Figure 5.10. Figure 5.8 shows simulation results and data for the *Sld* configuration in the wind tunnel study of Judd et al. (1996) (optical porosity, β = 0.69). Figure 5.9 shows simulation results and data for the windbreak studied in the field experiment of Bradley and Mulhearn (1983) (β = 0.5), and Figure 5.10 shows simulation results and data for the *Shd* configuration of Judd et al. (1996) (β = 0.3). Both experimental studies had a single upstream roughness, $z_o/(H\text{-}d)$. For Bradley and

Mulhearn (1983) $z_o/(H\text{-}d)$ was 0.0017 and for Judd et al. (1996) it was 0.033. Figure 5.8, Figure 5.9, and Figure 5.10 indicate that the QUIC mean wind model agrees well with the experimental data with relative differences that are less than 10% most heights, downwind distances, upwind distances, optical porosities, and upstream roughness. QUIC slightly overpredicts, by about 10%, velocities in the bleed flow zone for the windbreak of Bradley and Mulhearn (1983) and underpredicts velocities far downwind of the low porosity windbreak of Judd et al (1996). It is important to note that the QUIC simulation results in Figures 5.8 through 5.10 are compared to wind tunnel (Judd et al.,1996) and field data (Bradley and Mulhearn, 1983).

5.4.2 Turbulence Field

Figure 5.11 displays a comparison between the experimental data of Perera (1981), Bradley and Mulhearn (1983), and Judd et al. (1996) which measure the downwind decay of the turbulence velocity scale, U_s, together with a model of the decay of U_s, Eq. 5.18,

$$U_s^* = -0.5 * \tanh(x^*) + 0.5. \tag{5.18}$$

U_s^* and x^* were defined in Eqs. 5.15 and 5.16 and contain coefficients parameterized using a least squares fit to the data. Inserting the coefficients into Eqs. 5.15 and 5.16 yields:

$$U_s^* = \frac{\frac{U_s}{\overline{u'w'}^{0.5}_{upstream}} - 1}{0.22ln[\left(1-\alpha_{obf}\right)^2 * \frac{H-d}{z_o}] - 0.13}, \quad (5.19)$$

$$x^* = \left(11.6\alpha_{obf}^{2.5}\left(\frac{z_o}{H-d}\right)^{.75} + 0.074\right) * \left(x/H - 7.9ln\left(\frac{H-d}{z_o}\right) + 21\right), \quad (5.20)$$

The experimental data indicate that for $x^* < -1.5$, U_s^* asymptotically decreases from 1 ($U_s^* = 1$ indicates that $U_s = U_{s\,max}$). For $-1.5 < x^* < 1.5$, U_s^* rapidly decreases. For $x^* > 1.5$, U_s^* asymptotically approaches 0 ($U_s^* = 0$ indicates that $U_s = \overline{u'w'}^{0.5}_{upstream}$). Eqs. 5.19 and 5.20 model the behavior shown by the data. The model and the data indicate that for windbreaks with high $(H\text{-}d)/z_o$, ~600, the recovery of turbulence to undisturbed conditions is slow compared to windbreaks with low values of $(H\text{-}d)/z_o$, ~30.

Figure. 5.12 illustrates the good agreement, less than 5 % relative difference, between the turbulence similarity solution and windbreak data for the *Smd* configuration (β=0.43) of Judd et al. (1996). The QUIC simulation, however, slightly overpredicts turbulence in the quiet zone (by about 5%). It is also important to note that the Reynolds stresses do not equal zero at the ground. This is a consequence of the form Eq. 5.11.

5.5 Conclusions

This work developed a fast response model of the mean velocities resulting from windbreaks within the framework of the previously published QUIC methodology. The incomplete turbulence similarity solution proposed by Judd et al. (1996) was completed by parameterizing the turbulent velocity scale, U_s and developing a mathematical formula to express the similarity solution. Both the mean wind and turbulence fields agree well, within 10%, to experimental data of windbreaks encompassing optical porosities from 0.3

to 0.7 and windbreak heights normalized by upstream surface roughness, $(H\text{-}d)/z_o$, from 30 to 600. The parameterizations for both flow fields were found accurate for all upwind and downwind locations. The turbulent velocity field was found to require a greater distance for full recovery to upstream conditions with increasing $(H\text{-}d)/z_o$. The QUIC mean wind field model requires, at most, two to three minutes executing on simple, inexpensive computers and was found to be as accurate as large eddy simulation (LES) models of windbreak flows (Patton et al., 1998). The fast computational time and accurate results made the QUIC windbreak model useful for fast, repetitive, and routine calculations to assist land managers in designing windbreaks and writing guidelines for general windbreak design.

Table 5.1. Values used to normalize the turbulence data in Figure. 5.11.

Field Study	$(H\text{-}d)/z_o$	β	$\overline{u'w'}^{0.5}_{upstream}$
Judd et al. (1996) *Shd*	30	0.3	0.90 m s^{-1}
Judd et al. (1996) *Smd*	30	0.43	0.90 m s^{-1}
Judd et al. (1996) *Sld*	30	0.69	0.90 m s^{-1}
Bradley and Mulhearn (1983)	600	0.50	0.52 m s^{-1}
Perera (1981)	110	0.0	0.57 m s^{-1}

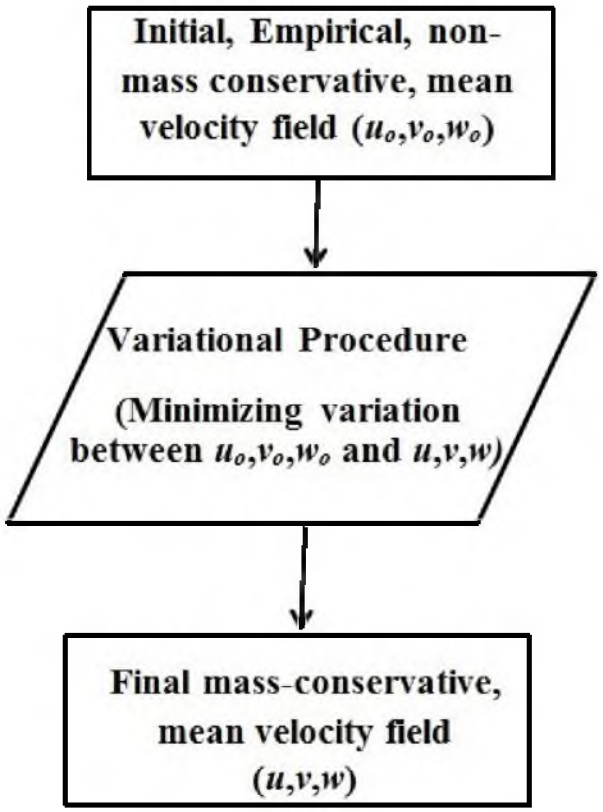

Figure 5.1. Graphic of methodology utilized in QUIC to calculate 3-D mean-velocity fields. First empirical expressions are used to define a non-mass-conservative, mean velocity field, u_o, v_o ,w_o. Subsequently, the empirical expressions have a variational procedure applied to them, resulting in a mass-conservative field, *u, v, w,* with minimal variance from u_o, v_o ,w_o results from the variational procedure.

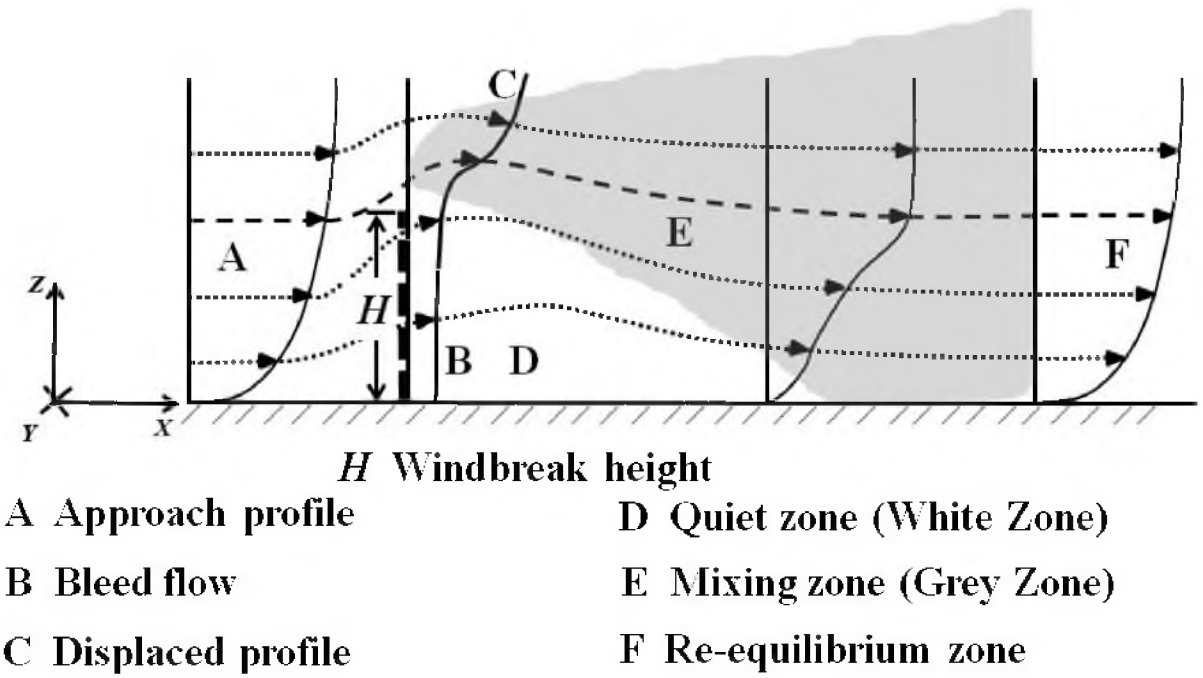

Figure 5.2. The features of a windbreak flow are shown. Different flow regimes are shown by letters (A-F) while *H* is the windbreak height. Four streamlines are included to illustrate the flow field, the bold dotted streamline indicating the center of the mixing zone. The orientation of coordinate system utilized in this work is displayed, but it is shown displaced upstream from its origin, the bottom of the windbreak. Adapted from Judd et al. (1996).

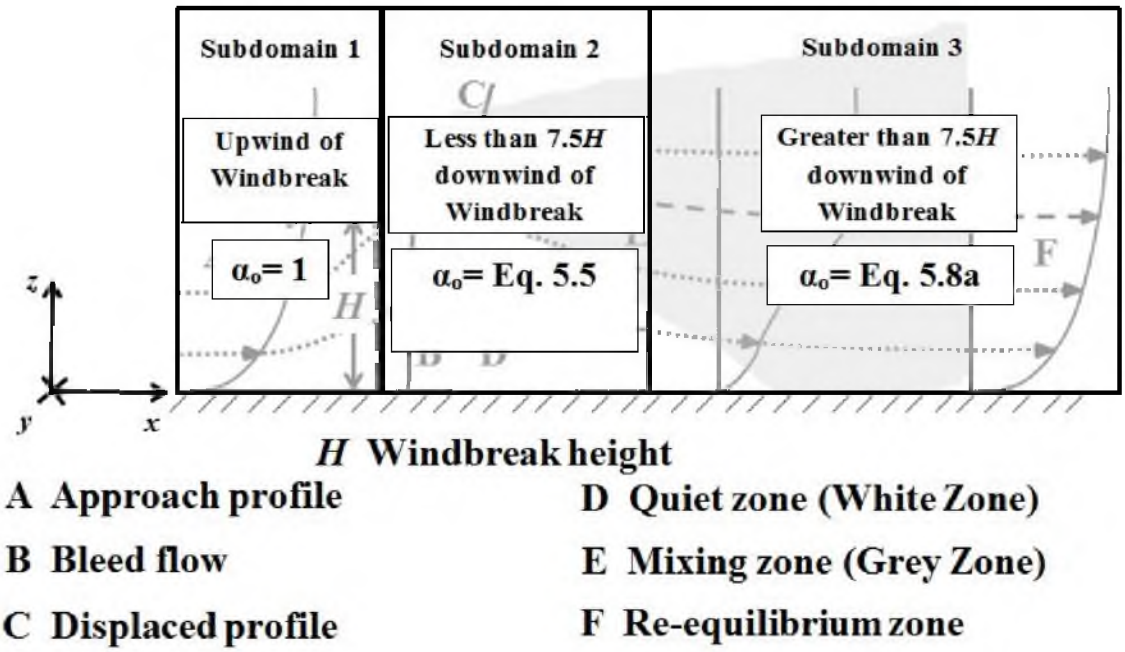

Figure 5.3. The division of the flow domain into three subdomains: Subdomain 1 the upwind side of the windbreak; Subdomain 2, less than 7.5*H* downwind of the windbreak; and Subdomain 3, greater than 7.5*H* downwind of the windbreak. The parameterization used for the aerodynamic porosity, α_o in each subdomain is shown.

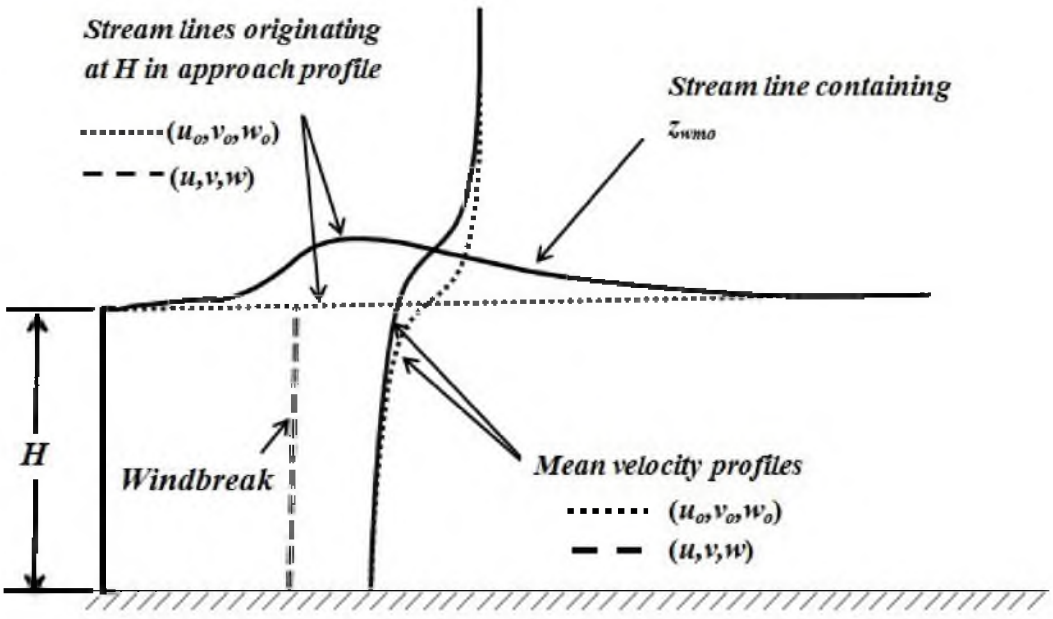

Figure 5.4. Visualization of the transformation the of the stream line containing the origin of the windbreak mixing layer, z_{wmo} from the horizontal line at height H in the (u_o, v_o, w_o) velocity field to its final form, shown in solid black in the (u, v, w) field.

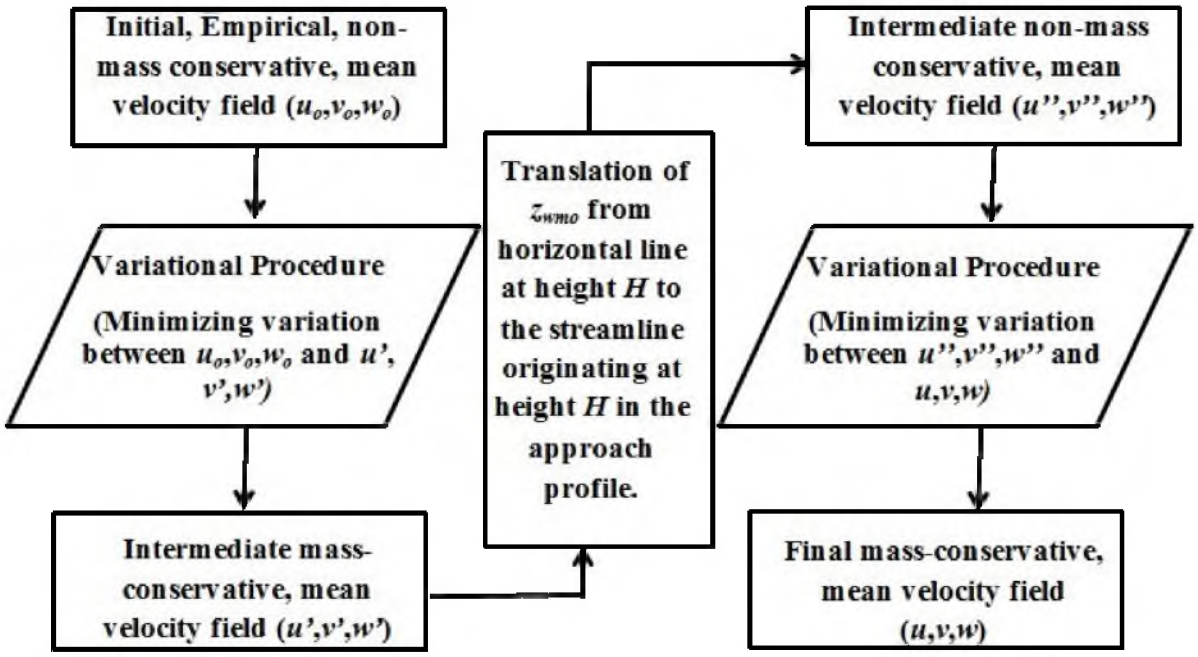

Figure 5.5. Chart showing the implementation of streamline curvature to the parameterization of z_{wmo}. The left column is the original QUIC procedure shown in Figure 5.1. where z_{wmo}= H for all downwind points. The procedures of the center and right columns calculate the streamline originating at height H within the approach profile, move z_{wmo} to this streamline, and reapply the variational procedure to insure that mass conservation is satisfied.

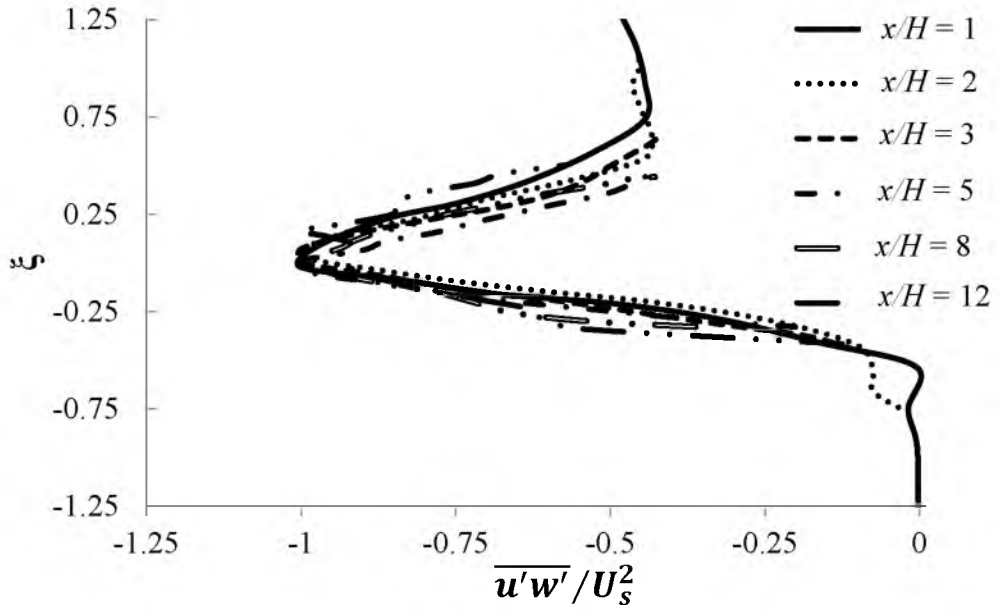

Figure 5.6. Data from Judd et al. (1996) plotted in terms of the similarity variables, ξ and $\overline{u'w'}/U_s^2$. Note the excellent collapse of data from multiple downwind distances onto a single curve. A parameterization for U_s^2 and a functional form for the similarly solution curve are currently being proposed. These data were from the Smd configuration of Judd et al. (1996).

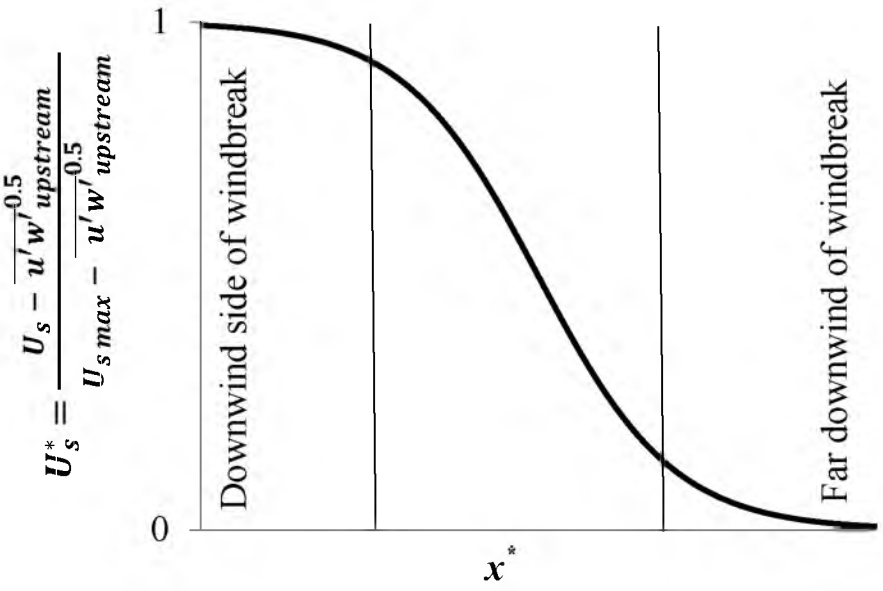

Figure 5.7. The decay of U_s, the turbulent velocity scale, from its maximum value, $U_{s\,max}$, at the windbreak on the left side of the plot to its upstream value, $\overline{u'w'}^{0.5}_{upstream}$ far downwind on the right. The decay is indicated by the variables x^* and U_s^*. ($U_s^* = 1$ when $U_s = U_{s\,max}$ and $U_s^* = 0$ when $U_s = \overline{u'w'}^{0.5}_{upstream}$). The decay is divided into three regimes (indicated by the vertical lines): the first regime exhibits asymptotic decay from$U_s^* = 1$, the second exhibits rapid decay of U_s^*, and the final exhibits U_s^*approaching 0 asymptotically.

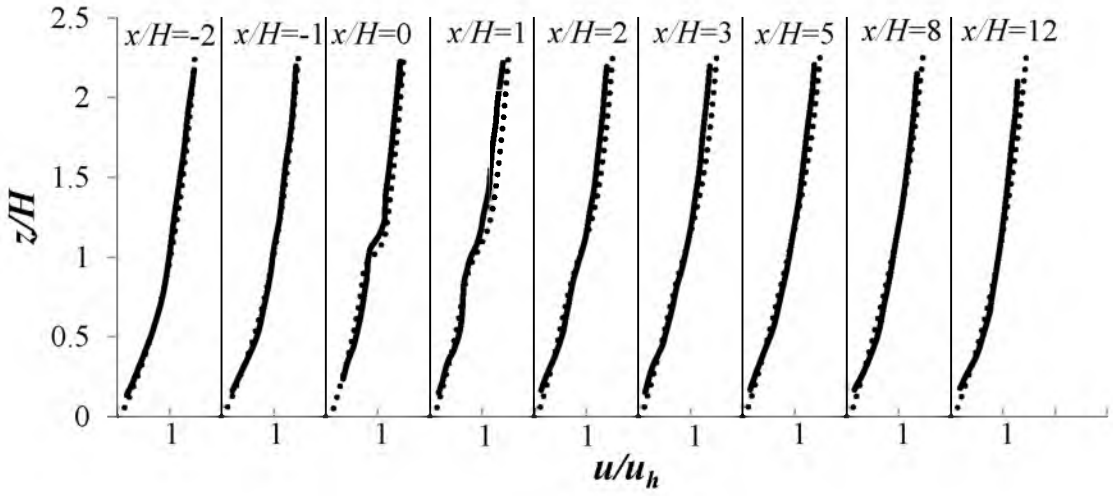

Figure 5.8. Comparison of the wind tunnel data (——) of Judd et al. (1996) for the *Sld* windbreak, β=0.69, and the QUIC simulation (·····) of the *Sld* windbreak configuration. The upstream conditions used: upstream profile is from x/H=-2 panel, $(H\text{-}d)/z_o$ =30, σ_w = 1.3 m s^{-1}.

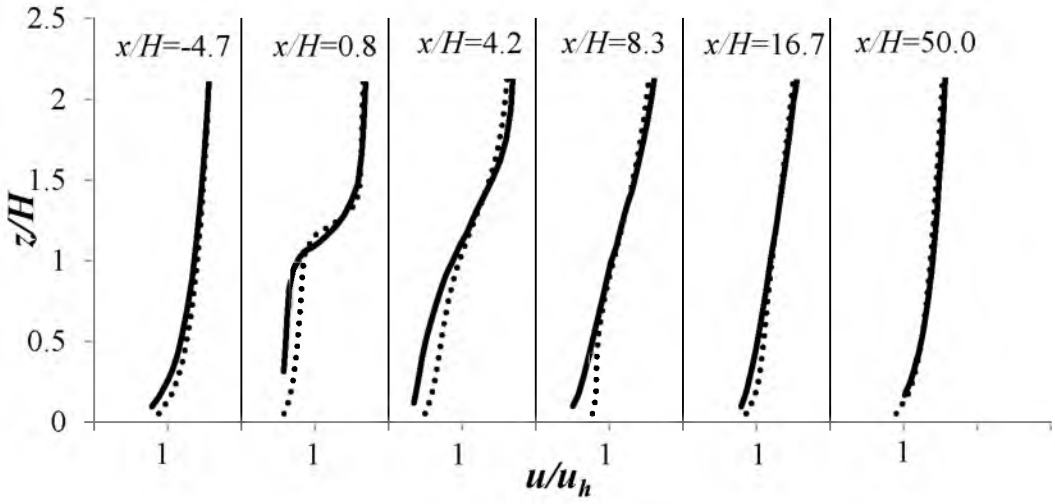

Figure 5.9. Comparison of the field data (——) of Bradley and Mulhearn (1983) for a single configuration windbreak, β=0.5, and the QUIC simulation (·····) of the windbreak. The upstream conditions used: upstream profile was parameterized as $(0.53/0.4)\ln(z/0.002)$, $(H\text{-}d)/z_o$ =600, σ_w = 1.4 m s^{-1}.

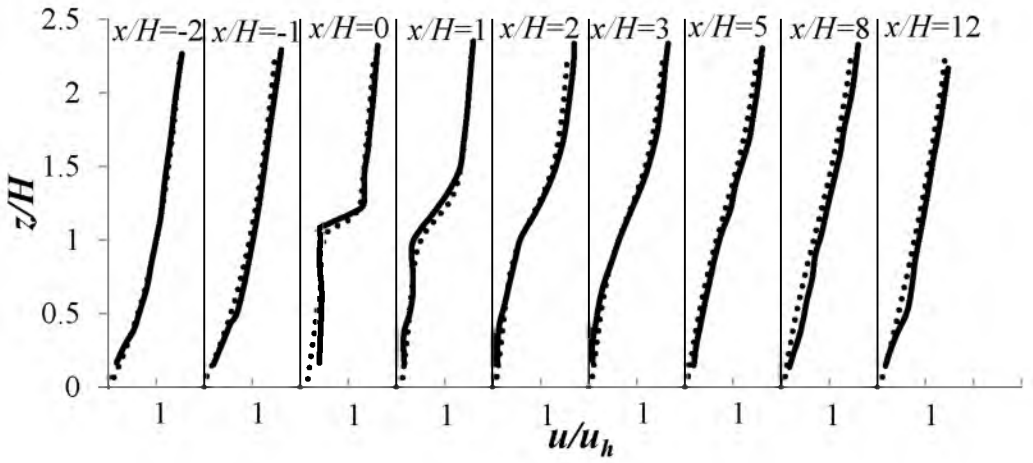

Figure 5.10. Comparison of the wind tunnel data (——) of Judd et al. (1996) for the *Shd* windbreak, β=0.3, and the QUIC simulation (·····) of the *Sld* windbreak configuration. The upstream conditions used: profile is from x/H=-2 panel, $(H\text{-}d)/z_o$ =30, σ_w = 1.3 m s^{-1}.

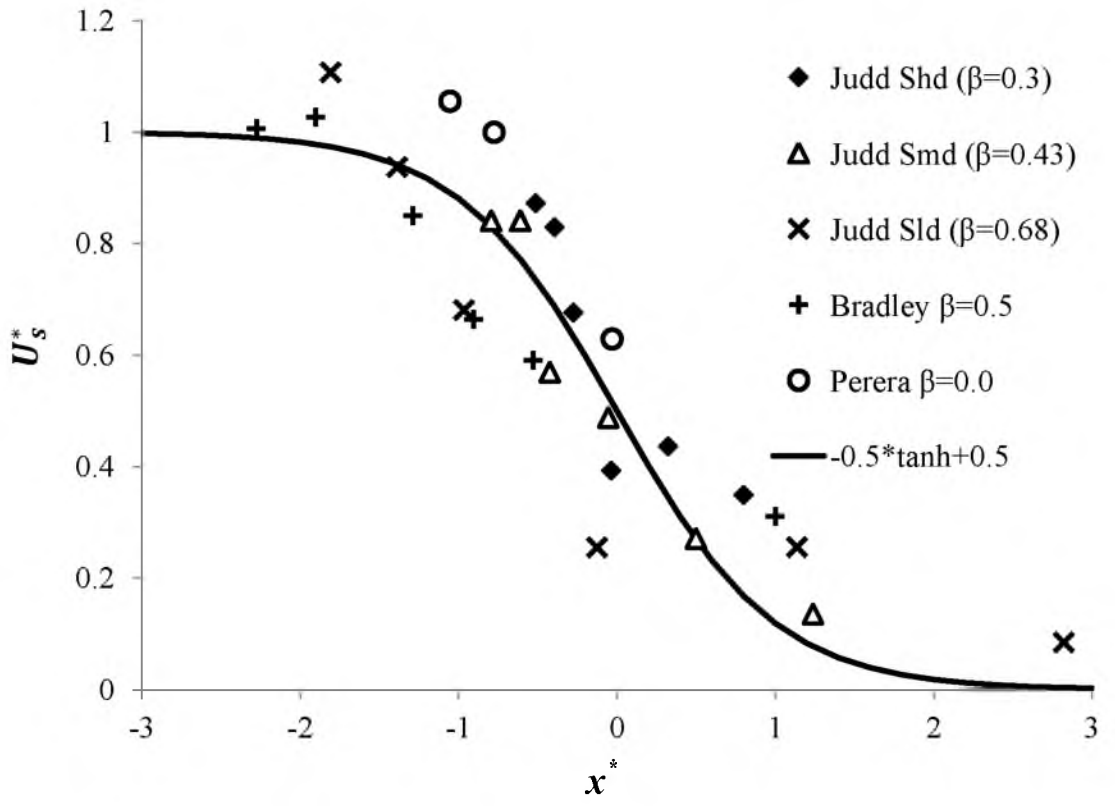

Figure 5.11. The calculation of the turbulent velocity scale, U_s, utilizing two dimensionless parameters: $U_s^*$and x^*. $x^*= \left(11.6\alpha_{obf}^{2.5}(z_o/(H-d))^{.75}+0.074\right) * (x/H - 7.9ln((H-d)/z_o)+21)$ and $U_s^* = (U_s/\overline{u'w'}_{upstream}^{0.5} - 1)/(0.22\, ln(\left(1-\alpha_{obf}\right)^2 * z_o/(H-d)) - 0.13)$, where α_{obf} is the aerodynamic porosity of the bleed flow through the windbreak. The coefficients are obtained from least square fits to data from Judd et al. (1996), Bradley and Mulhearn (1983), and Perrera (1981). $U_s^*$and $x^*$are related by: $U_s^* = -0.5 * \tanh(x^*)$ +0.5.

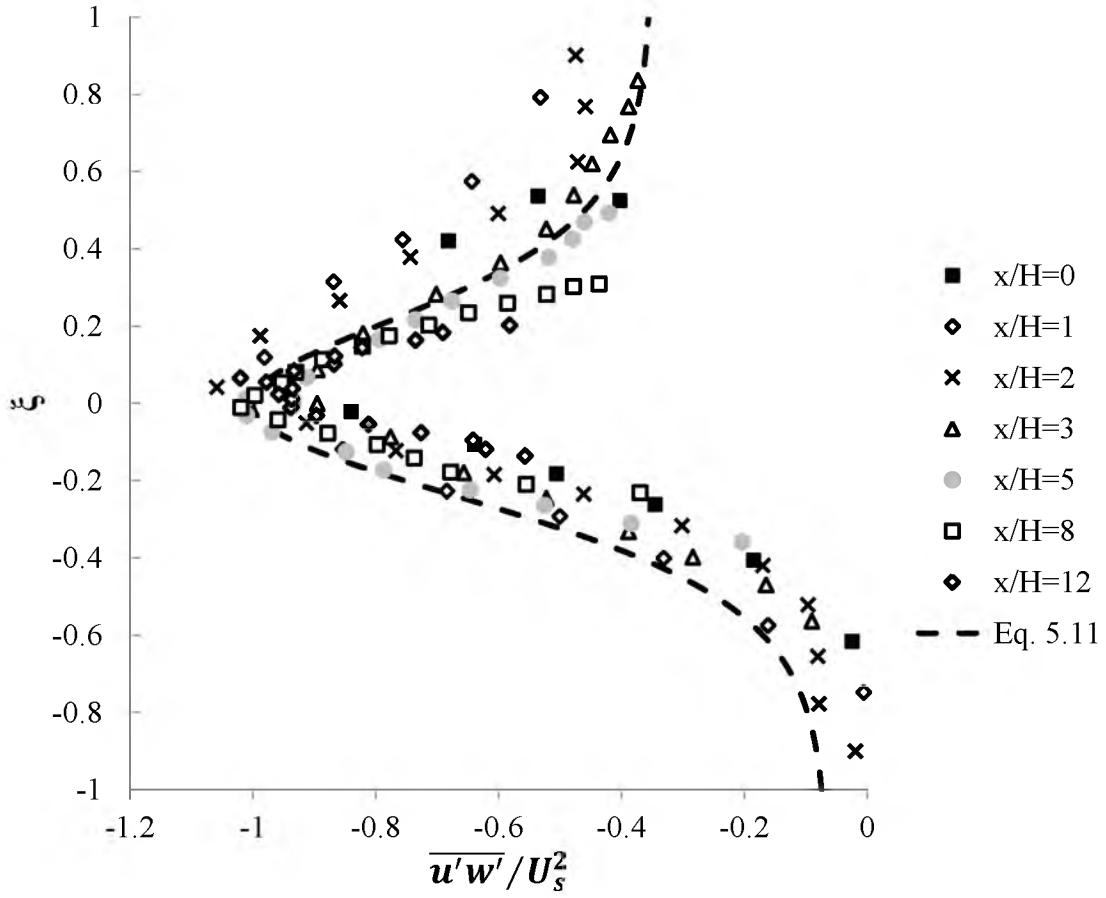

Figure 5.12. The turbulence of the *Smd* configuration of Judd et al. (1996) compared to the similarity profile for turbulence downwind of a windbreak. An incomplete form of the similarity solution was proposed by Judd et al. (1996). Parameterizations proposed in Section 5.3.4 complete the similarity solution.

5.6 References

Arya, S. P., 2001: *Introduction to micrometeorology*. Academic Press New York.

Bourdin, P., J. D. Wilson, 2008: Windbreak aerodynamics: is computational fluid dynamics reliable? *Boundary-Layer Meteorology*, **126**,181-208.

Bradley, E. F., and P. J. Mulhearn, 1983: Development of velocity and shear stress distributions in the wake of a porous shelter fence. *Journal of Industrial Aerodynamics*, **15**, 145-156.

Brown, M., A. Gowardhan, M. Nelson, M. Williams, and E. Pardyjak, QUIC Transport and Dispersion Modeling of Two Releases from the Joint Urban 2003 Field Experiment, in-press, *International Journal of Environment and Pollution*.

Cleugh H. A., 1998: Effects of windbreaks on airflow, microclimates and crop yields, *Agroforestry Systems*, **41**, 55-84.

Counihan, J.C.R., Hunt, and P.S. Jackson, 1974: Wakes behind two-dimensional surface obstacles in turbulent boundary layers. *Journal of Fluid Mechanics*, **64**,529-563.

Davis, B.N.K., M.J. Brown, A. J. Frost, T. J. Yates, and R. A. Plant, 1994: The effects of hedges on spray deposition and on the biological impact of pesticide spray drift. *Ecotoxicology and Environmental Safety*, **27**, 281–293.

Finch, S. J., 1988: Field windbreaks: design criteria. *Agriculture, Ecosystems, and Environment*, **22/23**, 215-228.

Guan, D., Y. Zhang, and T. Zhu, 2003: A wind-tunnel study of windbreak drag. *Agricultural and Forest Meteorology*, **118**, 75-84.

Iversen J. D., 1981: Comparison of wind-tunnel model and full-scale snow fence drifts. *Journal of Wind Engineering and Industrial Aerodynamics*, **8**, 231-249.

Judd M.J., M.R. Raupach, and J. J. Finnigan, 1996: A wind tunnel study of turbulent flow around single and multiple windbreaks, part1: velocity fields. *Boundary-Layer Meteorology*, **80**, 127-165.

Musick, H. B., and D. A. Gillette, 1990: Field evaluation of the relationships between a vegetation structural parameter and sheltering against wind erosion. *Land Degradation and Rehabilitation*, **2**, 87-94.

Nord, M., 1991: Shelter effects of vegetation belts- results of field measurements. *Boundary-Layer Meteorology*, **54**, 363-385.

Pardyjak, E.R., S. Speckart, F. Yin, and J. M. Veranth, 2008: Near source deposition of vehicle generated fugitive dust on vegetation and buildings: model development and theory. *Atmospheric Environment*, **42**, 6442-6452.

Patton, E. G., R. H. Shaw, M. J., Judd, and M. R. Raupach, 1998: Large-eddy simulation of windbreak flow. *Boundary Layer Meteorology*, **87**, 275-306.

Perera, M., 1981: Shelter behind two-dimensional solid and porous fences. *Journal of Wind Engineering and Industrial Aerodynamics*, **8**, 93-104.

Plate, E. J., 1971: The aerodynamics of shelterbelts. *Agricultural Meteorology*, **8**, 203-222

Pope, S.B., 2000: *Turbulent Flows*. New York, Cambridge University Press.

Press, W. H., S. A. Teukolsky, W.T. Vetterling, and B. P. Flannery, 2007: *Numerical recipes: the art of scientific computing*. Cambridge University Press, Cambridge.

Raupach, M.R., N. Woods, G. Dorr, J.F. Leys, and H.A. Cleugh, 2001: The Entrapment of Particles by Windbreaks. *Atmospheric Environment*, **35**, 3373-3383.

Röckle, R., 1990: *Bestimmung der strömungsverhältnisse im bereich komplexer bebauungsstrukturen*. Ph.D. thesis, Vom Fachbereich Mechanik, der Technischen Hochschule Darmstadt, Germany.

Schlichting, H., 1968: *Boundary Layer Theory*. McGraw-Hill, New York.

Singh, B., B. S. Hansen, M. J. Brown, and E. R. Pardyjak, 2008: Evaluation of the QUIC-URB fast response urban wind model for a cubical building array and wide building street canyon. *Environmental Fluid Mechanics*, **8**, 281-312.

Singh, B., E. R. Pardyjak, A. Norgren, and P. Willemsen, 2011: Accelerating urban fast response Lagrangain dispersion simulations using inexpensive graphics processor parallelism. *Environmental Modeling and Software*, **26**,739-750.

Tabler, R.D., 1991: Snow fence guide. Report: SHRP-W/FR-91-106. Strategic Highway Research Program, National Research Council. Washington.

Williams, M. D., M. J. Brown, B. Singh, and D. Boswell, 2004: QUIC-PLUME Theory Guide. http://www.lanl.gov/projects/quic/open_files/QUICPLUME_theory.pdf

Wilson, J. D., 1985: Numerical Studies of Flow through a Windbreak. *Journal of wind engineering and industrial aerodynamics*, **21**, 119-154.

Wilson, J. D., G. E. Swaters, and F. Ustina, 1990: A perturbation analysis of turbulent flow through a porous barrier. *Quarterly Journal of the Royal Meteorological Society*, **116**, 989-1004.

Wilson, J. D., 2004: Oblique stratified winds about a shelter fence, Part 1. *Journal of Applied Metrology*, **43**, 1149-1167.

CHAPTER 6

CONCLUSIONS

6.1 Summary

The experimental and modeling results presented in this dissertation contribute to an improved understanding of transport and removal of vehicle-generated PM_{10} within the first hundred meters downwind of unpaved roads. Understanding the transport and removal of PM_{10} downwind of unpaved roads is critical for accurate estimation of net-emission factors utilized in regional-scale air quality monitoring (Countess, 2001). For field conditions where vegetation is uniformly distributed, such as in a vegetative canopy, field data were utilized together with numerical simulations (Atmospheric Diffusion Equation (ADE) and Lagrangian dispersion models) to obtain a simple formula relating vegetative height, vegetative thickness, and atmospheric stability to the transmitted fraction, *TF*, of roadside PM_{10} that reaches distances greater than 100 m downwind. The formula was:

$$TF = (1 - \exp(-2.8H^*)) \exp(-2.0T_m^{*0.64}) + \exp(-2.8H^*),$$

where H^* and T_m^* parameterize site roughness and meteorological conditions. For computer simulation purposes, simple models of the transport phenomenon of horizontal advection and turbulent diffusion within canopies were developed. The canopy transport models were applicable for canopies of intermediate to high density and utilized simple, easily obtained inputs such as Leaf Area Index (LAI). Capabilities of modeling

horizontal advection and turbulent diffusion were extended to conditions where the vegetation was present in a few rows (less than three or four), such as a windbreak. The simple windbreak model was applicable for the transport fields, upwind, within, and downwind of windbreaks and utilized easily obtained inputs such as optical porosity, β. A simple formula for the TF of roadside PM_{10} transported through windbreaks was not developed.

This dissertation commenced, in Chapter 2, with the documentation of a field study that measured roadside PM_{10} transport and removal within 100 m downwind of an unpaved road in an area of New Mexico which featured a vegetative canopy typical of the arid southwestern United States. The results of the field study together with results from two previous field studies (Etyemezian et al., 2004; Veranth et al., 2003) suggested that vegetative height, vegetative thickness, and atmospheric stability were important parameters determining the removal of roadside PM_{10}.

Chapter 3 examined the transport of PM_{10} 100 m downwind of unpaved roads within vegetative canopies by utilizing an Atmospheric Diffusion Equation (ADE) model. To develop the ADE model, simple parameterizations were introduced for the transport phenomenon of horizontal advection and turbulent diffusion within canopies of intermediate to high density. The models were found to have good agreement, less than 10% relative error, with data for canopies of varying density. The simulation results for PM_{10} suggested that PM_{10} removal within canopies was governed by two dimensionless parameters: H^* (the ratio of canopy height to initial plume height) and T^* (the ratio of the probability of PM_{10} within the canopy to deposit to the probability to be transported out

of the canopy). The introduction of H^* and T^* greatly simplified the analysis of the removal PM_{10} removal within 100 m downwind of the unpaved road.

Chapter 4 utilized the field data for PM_{10} removal within a desert canopy from Chapter 2, field data published in Etyemezian et al. (2004) and Veranth et al. (2003), and simulation results from the Los Alamos National Laboratory's (LANL) Quick Urban and Industrial Complex (QUIC) Lagrangian dispersion model to develop the formula:

$$TF = (1 - \exp(-2.8H^*)) \exp(-2.0T_m^{*0.64}) + \exp(-2.8H^*).$$

Chapter 4 introduced T_m^* to be used in place of T^* because of the difficulty of parameterizing T^* for given site conditions. Chapter 4 also incorporated the canopy transport models to QUIC and used the deposition model of Judd et al. (2001) to model PM_{10} removal in QUIC. The field results from Chapter 2, (Etyemezian et al., 2004; Veranth et al., 2003) together with the QUIC simulations indicated that a characteristic vegetative element size of 50 μm (on the order of the smallest vegetative elements) was necessary for the simulations to match the removal measured in the field.

Chapter 5 extended the use of QUIC from modeling horizontal advection and turbulent diffusion within canopies to modeling horizontal advection and turbulent diffusion upwind, within, and downwind of windbreaks. No results were presented for PM_{10} removal; however, the windbreak model results showed very good agreement, within 10% relative difference, with experimental windbreak data for horizontal advection and turbulent diffusion taken in the field and in wind tunnels. The QUIC windbreak model was found to be applicable for windbreaks of porosities varying from 0 to 0.9 and varying windbreak heights of 30 to 600 compared to upstream aerodynamic roughness, z_o.

6.2 Future Work

Despite the accomplishments of the current work, there is room for future progress. A comprehensive model describing dry deposition by impaction in the near-source zone within vegetation would be an improvement over the Raupach et al. (2001) model used in this current work. The 50 μm characteristic vegetative element size is extremely small in relation to realistic vegetative element sizes. Results presented in (Moran et al., 2013) suggest that turbulence enhances deposition. Models such as Raupach et al. (2001) neglect the effects of turbulence upon deposition. Incorporating a turbulent deposition model, such as the model presented in (Moran et al., 2013), into QUIC would likely result in the simulation removal matching the field data while utilizing a more realistic vegetative element size in the Raupach et al. (2001) model.

Vegetative and anthropogenic roughness elements come in an array of sizes, not just the single size assumed in Chapter 4. Canopy models with distributions of elements sizes (Petroff et al., 2008) are advancing this topic.

Field data for the removal of roadside PM_{10} within windbreaks would be greatly beneficial to validate dispersion models estimate for the transmitted fraction when windbreaks are located downwind of unpaved roads. Data are published for larger particles (Raupach et al., 2001) but according to the author's knowledge have yet to be published for PM_{10}. With additional data, it would be likely possible to develop a simple equation relating windbreak height, density, and fetch depth to roadside PM_{10} *TF* through downwind windbreaks.

6.3 References

Countess, R., 2001: Methodology for estimating fugitive windblown and mechanically resuspended road dust emissions applicable for regional scale air quality modeling. Western Governors Association by Countess Environmental: Westlake Village, CA.

Etyemezian, V., S. Ahonen, D. Nikolic, J. Gillies, H. Kuhns, D. Gillette, and J. Veranth, 2004: Deposition and removal of fugitive dust in the arid southwestern United States: measurements and model results. *Journal of the Air and Waste Management Association,* **54**, 1099-1111.

Petroff, A., A. Mailliat, M. Amielh, and F. Anselmet, 2008: Aerosol dry deposition on vegetative canopies. Part I: review of present knowledge. *Atmospheric Environment*, **42**, 3625-3653.

Moran, S.M., E. R. Pardyjak, and J. M. Veranth, The role of turbulence in enhancing particle deposition. Article in press in the journal *Physics of Fluids*.

Raupach, M.R., N. Woods, G. Dorr, J.F. Leys, and H.A. Cleugh, 2001: The entrapment of particles by windbreaks. *Atmospheric Environment*, **35**,3373–3383.

Veranth, J.M., G. Seshadri, and E. R. Pardyjak, 2003: Vehicle-generated fugitive dust transport: analytic models and field study. *Atmospheric Environment*, **37**, 2295-2303.